INFORMATION TO USERS

NOTE TO USERS

Page(s) not included in the original manuscript are unavailable from the author or university. The manuscript was microfilmed as received.

42 - 45

This reproduction is the best copy available.

UMI

A New Technique to Reduce Phase Distortion of Recursive Filters for Video and Image Processing

Leon C. K. Lee

A Thesis
in
the Department
of
Electrical & Computer Engineering

Presented in Partial Fulfillment of the Requirements

for the degree of Master of Applied Science at

Concordia University

Montreal, Quebec, Canada

October, 1997

Your file Votre référence

Our file Notre référence

0-612-39980-X

Canada

ABSTRACT

A New Technique to Reduce Phase Distortion of Recursive Filters for Video and Image Processing

Leon C. K. Lee

IIR filters require less multiplication and less memory to perform filtering than their FIR counterparts. On the other hand, IIR filters have nonlinear phase response as a side effect. This is a major concern in applications such as video and image processing. In this thesis, a new method of preventing artifacts caused by nonlinear phase filtering is introduced. The proposed method, called State Value Updating technique, will remove frequency components of a picture that are shifted nonlinearly due to the nonlinear phase response of recursive filters. This thesis will provide a method of finding the proper new state values and decision algorithms to reduce the artifacts. Simulations for sampling structure conversions, video deinterlacing and 3-D Y-C separation are performed in this thesis. The resulting picture quality is at least as the one using nearly-linear-phase recursive filters alone, and close to that achieved with more complex algorithms. The timing overhead and complexity of the new method are low so that video and imaging systems could benefit.

ACKNOWLEDGEMENT

Table of Contents

List of Figures

List of Tables

1 Introduction

Since the first introduction of color television, video-broadcasting technology has changed only a little. Today a number of digital technologies are making new video services more feasible. Generally, there are two types of improvement that can be considered:

1) The first type of improvement is to use a new form of television signal. The new television will have higher picture quality and higher resolution. However, it may not be compatible with existing TV sets and may require a new transmission media due to the increased bandwidth. This type of television is generally called High Definition Television (HDTV).

2) Another type of improvement is based on the existing video signal. By using advanced digital video technologies on both the transmitter and the receivers, picture quality can be improved significantly. Moreover, because this method uses the traditional video signal standard, compatibility is guaranteed. This type of system is known as Improved Definition Television (IDTV).

One should notice that TV sets are very price sensitive. Although the picture quality of advanced TV systems is much better than the traditional TV systems, the popular success of any advanced system is still unlikely if the TV sets are too expensive. To increase the acceptance of a new TV standard, we need to reduce the cost by simplifying the components of the advanced TV sets whenever possible. Filtering is one of the most

important operations in advanced TV systems. Therefore, the complexity of the filters will directly affect the price of the TV receivers.

FIR filters are commonly considered as the first choice for digital video processing because of their linear phase response and guaranteed stability. On the other hand, IIR filters are more efficient than their FIR counterparts in terms of storage and computation. Their simple structures make IIR filters a potential substitute for FIR filters to reduce cost.

However, IIR filters still have their own problems, such as stability and nonlinear phase. These problems discourage the use of IIR filters in video and image applications. Recently, the introduction of the 2-D lattice wave digital filters (WDF) [1] has solved the stability problems and has thus made recursive filtering more realistic for video applications. In some of our previous work, we have applied IIR filters using WDF structures to several video and image processing applications [2-4]. Because of the WDF structures, stability is guaranteed and the multiplierless WDF structures are very efficient. Although attempts to reduce nonlinear phase by using some special filter structures have been made [2], nonlinear phase is still noticeable in the results under certain conditions. Therefore, to make IIR filters truly practical for video and image processing, we still need to further reduce nonlinear phase error. This is the purpose of this thesis.

There are different approaches to reducing nonlinear phase error without using an all-pass phase compensation filter. One way is by anticausal filtering in the reverse direction after the first causal filtering by the same filter. This method is particularly useful for a sampling structure conversion process, because an interpolation filtering process follows an antialias filtering process. In addition, the anticausal nature of the filter introduces overshoots right before and after the transitions. The overshoots enhance the Mach-Band effect [5] [6] and result in a sharper filtered image. However, anticausal filtering is only practical in the spatial domain. If a filtering process is in the time domain, anticausal filtering is not a proper solution.

2

A new approach to suppress ringing caused by phase error is proposed in this thesis. This technique is called *state value updating* (SVU). The basic idea of SVU is to eliminate the phase distorted high frequency components in order to reduce phase distortions. Some waveforms such as a step function contain both high and low frequency components. If an IIR filter is applied to a step function, some of the shifted high frequency components will appear after the step as a form of ringing. During normal operations, an SVU filter operates as an ordinary recursive filter. However, if a step is detected, the state values of the filter will be set to new values so that the phase distorted and shifted high frequency components will not appear at all. Thus, there will be no ringing caused by phase distortion.

In this thesis, the SVU algorithm is used with some special WDFs designed for video and image applications. An SVU WDF requires additional logical operations, but the overall structure is still simple. In addition, most of the logical operations can be operated in parallel. Therefore, SVU WDFs are still much faster and simpler than the FIR filters, and can be used to reduce system cost by replacing the FIR filters.

Since some special WDFs will be used in this thesis, their structures and the design methods are discussed in Chapter 2. In the same chapter, 1-D bireciprocal WDF structures are discussed because the 1-D filters can be used as 2-D lowpass filters if they are applied in the 2-D plane. Furthermore, a 1-D lowpass filter can be transformed into a 2-D diamond filter, which is another frequently used 2-D filter. The design technique and the determination of the parameters to obtain filter structures for better picture quality are also discussed.

In Chapter 3, a desired step response is used as a reference. It will be shown that by changing the state values of a WDF, the desired step response can be obtained without endangering the stability of the WDF. Since SVU is developed for a desired step response, one may doubt its filtering capability if waveforms other than step functions are used. Therefore, various waveforms are also filtered by SVU WDFs to ensure that the SVU filtering does not seriously distort some commonly used waveforms. Since the SVU technique is believed to have potential use in image and video applications, this thesis

dedicates three chapters to discuss the use of SVU in some image and video processing applications. Due to the nature of different applications, a specific decision algorithm will be developed for each application.

In Chapter 4, sampling structure conversions using SVU is discussed. Sampling structure conversions are commonly used in image and video applications. Applications such as television aspect ratio and resolution changing [7], wavelet coding [8-17], subband coding [12] [13], spatial and temporal resolution exchange in television coding [14-17] and video deinterlacing, require sampling structure conversions. The theory of sampling structure conversion is well studied [18-28] but the implementations are still somewhat limited to FIR filters only [23-27]. Since each conversion process requires repeating lowpass filtering for interpolation and antialiasing, the use of FIR filters increases the complexity of the system substantially. Therefore, it is of interest to show that SVU WDFs can produce comparable or better quality results than FIR filters.

Another application that will be discussed in this thesis is video deinterlacing. The interlaced video signal is an integral part of NTSC and PAL standards. Because some of the proposed advanced TV systems employ progressive scanning displays, deinterlacing may become an important tool to make advanced systems compatible with the traditional TV signals. Moreover, due to the improved quality of progressive scanning, noninterlace TVs for NTSC are already available [20] [21].

For a deinterlacing system, the huge amount of video data demands an efficient algorithm. If the algorithm is complicated, the increased price may lower public acceptance of the system. Therefore, in Chapter 5, we will try to find a simple, yet well performing, deinterlacing method. The WDF deinterlacing technique [3] is an attempt to provide a reasonable solution using a simple method. In view of the phase distortion, another attempt is made using the SVU technique to show that it can produce deinterlaced results comparable to those generated by more complex algorithms.

In Chapter 6, 3-D luminance and chrominance (Y-C) processing will be discussed. Because of the advancements in NTSC processing [24] [25], new ways of Y-C separation

and encoding are now possible. The traditional 1-D Y-C processing cannot separate the Y and C signals effectively. Cross-colors and cross-luminance are the most noticeable artifacts. Moreover, much of the bandwidth is wasted if the signal is processed in a 1-D domain during the encoding process. Digital 3-D processing is the answer to provide better Y-C separation and encoding. Again, FIR filters are the main components of the proposed 3-D processing TVs [32-35]. To simplify the TV sets, WDFs could be used. However, phase distortion remains a problem because phase compensation using anticausal filtering is not possible. So, in this chapter, we demonstrate the SVU's ability to perform Y-C processing. Simulations of Y-C processing are presented. Lastly, combined SVU deinterlacing and SVU Y-C processing simulations are shown to demonstrate an Improved Definition Television (IDTV) coding and decoding.

Finally, Chapter 7 contains conclusions and mentions some possible directions for future research.

References

[1]   Q. Gu and M.N.S. Swamy, "On the design of a Broad Class of 2-D Recursive Digital Filters with Fan, Diamond and Elliptical Response," *IEEE Transactions on CAS*, Part II vol. 39, Sept. 1994, pp. 603-614

[2]   Q. Gu, C. K. L. Lee, M. N. S. Swamy, "Multidimensional IIR digital filters for video signal   processing," Int. Conf. on Signal Processing, Beijing, China, 1993.

[3]   Q. Gu, C. K. L. Lee, M. N. S. Swamy, "2D digital filters for deinterlacing of video signals," CCECE, Vancouver, Canada, Sept., 1993.

[4]   Q. Gu, C. K. L. Lee, M. N. S. Swamy, "2D IIR digital filters for sampling structure conversion of video signal," submitted to IEEE Trans. on CAS for Video Tech.

[6]   W. F. Schreiber, "Image Processing for Quality Improvement," *Proc. of the IEEE*, VOL. 66, NO. 12, pp. 1640 - 1651. Dec. 1978.

[7]   T. G. Stockham, JR., "Image Processing in the context of a visual model, " *Proc. IEEE*, VOL., 60, NO. 7, pp. 828-841. July 1972.

[8]   H. Ito, T. Kurashita, M. Ishizuka and N. Yamaguchi "A decoder for a letter-box-type wide-aspect EDTV system," " *Jour. SMPT*, pp. 790 - 796, Nov. 92.

[9]   G. J. Tonge, "The sampling of television images, " *IBA Report* 112/81.

[10]   G. J. Tonge, "Three-dimensional filter for television sampling," *IBA Report* 117/82.

[11]   G. Schamel, "Pre- and postfiltering of HDTV signals for sampling rate reduction and displayup-conversion," *IEEE* Trans. CAS, VOL. CAS-34, no. 11, pp. 1432-1439, NOV. 1987.

[12]   R. F. W. Pease, J. O. Limb, "Exchange of spatial and temporal resolution in television coding," *The BELL sys. Tech. Jour.* pp. 191-199, January 1971.

[13]   D. P. Petersen and D. Middleton, "Sampling and reconstruction of wave-number-limited functions in N-dimensional Euclidean space", *Information and Control.*, vol. 5, pp. 279-323.

[14]   R. M. Mersereau, "The processing of hexagonally sampled two-dimensional signals, " *Proc. IEEE*, vol. 67, pp. 930-949, May 1979.

[15]   R. M. Mersereau and T. C. Speake, "The processing of periodically sampled multidimensional signals, " *IEEE Trans.ASSP.*, vol. ASSP-31, NO. 1, February 1983.

[16]   N. T. Gaarder, "A note on the multidimensional sampling theorem," *Proc. IEEE*, pp. 247-248, Feb. 1972.

[17]   E. Dubois, "The sampling and reconstruction of time-varying imagery with application in video systems", *Proc. IEEE*, VOL. 73, NO.4, pp 502-522, April 1985.

[18]   P. Siohan, "2D FIR filter design for sampling structure conversion," *Trans. CAS. for VideoTech.*, Vol. 1, NO. 4, pp. 337-350, Dec., 1991.

[19]   E. Viscito and J. P. Allebach, "The analysis and design of multidimentional FIR perfect reconstruction filter banks for arbitrary sampling lattices," *IEEE Trans. CAS*, VOL. 38, NO. 1, pp. 29-39, Jan. 1991.

[20]   L. Banzato, N. Benvenuto and G. M. Cortelazzo, "A design technique for two-dimensional multiplierless FIR filters for video applications," *IEEE CAS for Video Tech.* pp. 273-284, Sept. 1992.

[21]   Y. Araki *et al.*, "Experiment with second generation EDTV system," presented at the 131st. SMPTE Technical Conference, LA. Calif., 1989.

[22]   H. Kurashita, M. Ishizuka, and N. Yamaguchi, "A decoder for a letter-box-type wide-aspect EDTV system," *Jour. SMPT*, pp. 790 - 796, Nov. 92.

[23]   Y. Neuvo, "Scan rate up-conversion in television receivers", *UCSB/CIPR* Santa Barbara, CA. 1992.

[24]   D. Pele, B. Choquet, and P.Siohan, "Field rate conversion by motion Estimation/Compensation, " in *Proc. 2nd Int. Workshop on Signal Processing of HDTV*, l'Aquila, Italy, VOL. 2, Feb. 1988, pp.3-12.

[25]   E. Dubois, M. N. S. Sabri and J. Y. Ouellet, "Three-dimensional spectrum and processing of digital NTSC signals," *SMPTE Jour.*, pp. 372 - 378, April 1982.

[26]   E. Dubois and W. Schreiber, "Improvements to NTSC by multidimensional filtering," *SMPTE Jour.*, Vol. 97, pp. 446 - 463, June 1988.

[27]   C. H. Strolle, "Cooperative processing for improved NTSC chrominance/luminance separation," *SMPTE Jour.* pp. 782 - 787, August 1986.

[28]   T. Fukinuki and N. Suzuki, "Multidimensional signal processing for NTSC," *IEICE Trans. Fundamentals*, VOL. E75-A, NO. 7, July 1992.

[29]   J. O. Drewery, "The filtering of luminance and chrominance signals to avoid cross-colour in a PAL color system, " *BBC Report BBC RD*, 1975, /36.

[30]   C. K. P. Clarke, "PAL decoding: Multi-dimensional filter design for chrominance-luminance separation," *BBC Report BBC RD* 1988/11.

2 A Two Dimensional Wave Digital Filter Design Technique for Image and Video Processing

2.1 Introduction

SVU technique uses a decision algorithm to control the state values of a lowpass filter. The thesis uses two specially designed 2-D WDFs suggested by Gu *et al* [1], [2], [3]. These filters will be discussed in this chapter and eventually used in the following chapters and simulations. Before we synthesize the 2-D lattice WDFs, we will give a brief review of WDF [4], [5].

2.2 Wave Network Realization

2.2.1 Wave Network Characterization
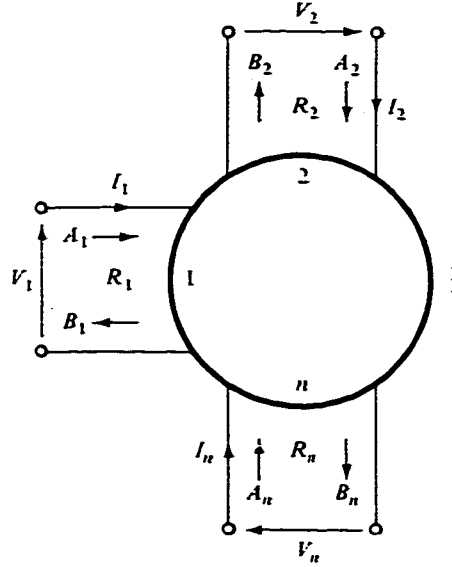
Figure 1. Analog n-port network

An analog n-port network Figure 1 can be represented by the following equations.

$$A_k = V_k + R_k I_k \tag{2.0a}$$

$$B_k = V_k - R_k I_k \tag{2.0b}$$

The variable A_k and B_k are the incident wave and reflected wave quantities respectively. The variable R_k is the port resistance.

If we cascade two n-port networks as shown in Figure 2, We have $A_k = B_j$ and $A_j = B_k$. Hence the port resistances R_j and R_k need to have the same value and this common resistance will maintain the continuity in the wave flow.

The wave digital filter realization of an LC filter can be realized by using the source, impedance, and the connections shown in Figure 3.

9
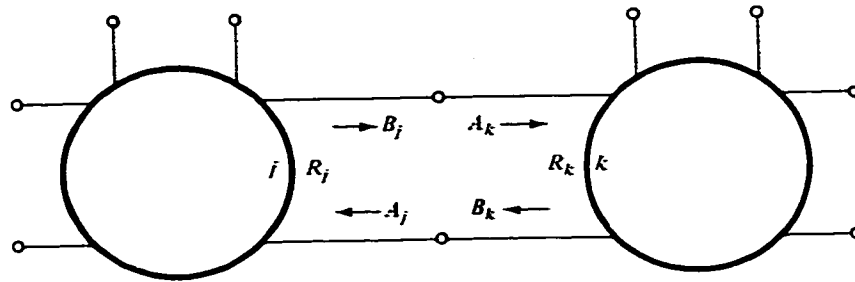
Figure 2. Cascaded n-ports
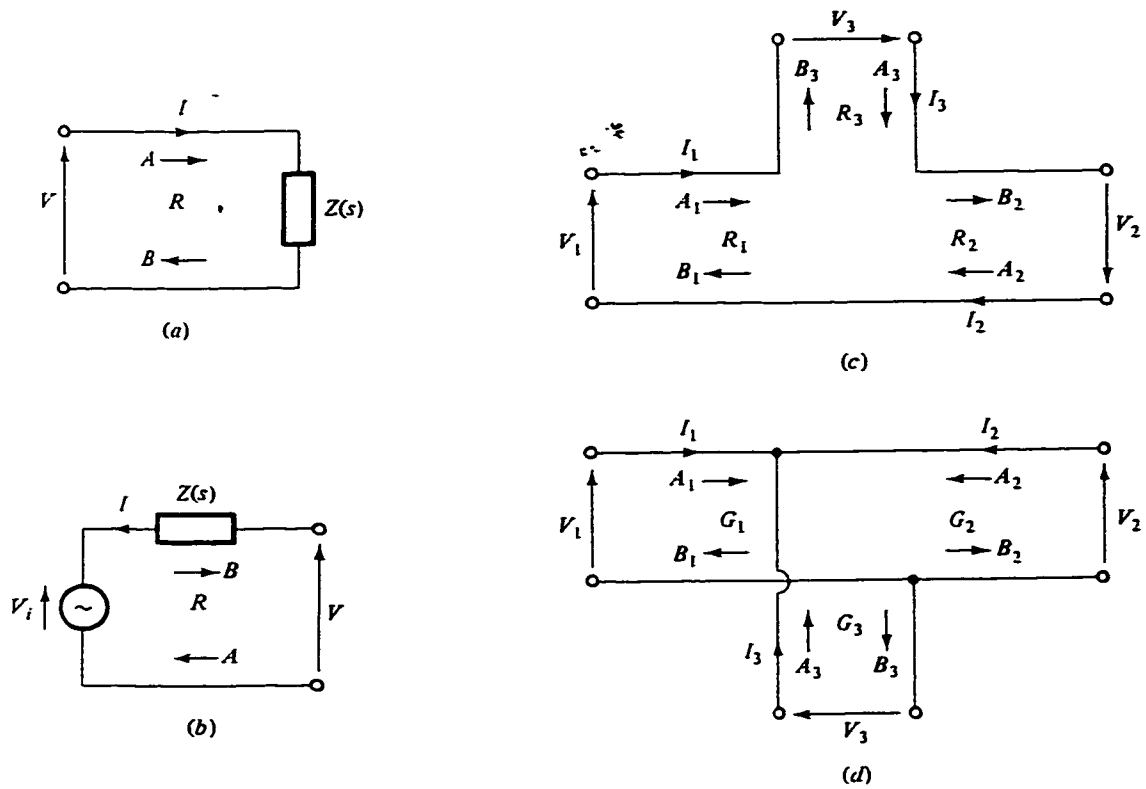
Figure 3. (a)Impedance (b) voltage (c) series wire interconnection, (d) parallel wire interconnection

10

2.3 Element Realization

To obtain the digital realization from an analog network, one can follow the following derivation procedure:

1) Characterize the analog element into wave quanties.

2) Eliminate V and I using the loop and node equations and use the bilinear transformation $s = \dfrac{2z-1}{Tz+1}$.

3) Express the reflected wave quantities as function of the incident wave quanties.

4) Realize the resulting set of equations by using adders, delays and multipliers.

2.3.1 Impedances

An impedance $Z(s) = s^{\lambda}R_x$, where $R_x > 0$ is a capacitance if $\lambda=-1$. It is resistive if $\lambda=0$, and is inductive if $\lambda=1$. This impedance could be used in Figure 3a and leads to the equations

$$A = V + IR$$
$$B = V - IR$$

where $V = IZ(s)$.

If we now apply the bilinear transformation and eliminate V and I, we get

$$B = f(z)A$$

where
$$f(s) = \left. \frac{Z(s) - R}{Z(s) + R} \right|_{s = \frac{2}{T}\frac{z-1}{Tz+1}} .$$
(2.1)

Since $R = \left(\dfrac{2}{T}\right)^{\lambda} R_x$, Equation 2.1 becomes

$$f(z) = \begin{cases} z^{-1} & \lambda = -1 \\ 0 & \lambda = 0 \\ -z^{-1} & \lambda = 1 \end{cases}.$$

These results imply that a resistance will translate into a digital sink, a capacitance into a unit delay, and an inductance into a unit delay in cascade with an inverter as shown in Figure 4.
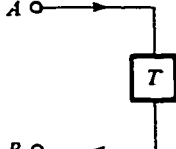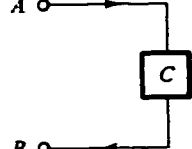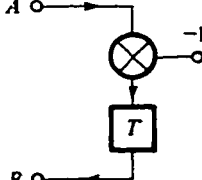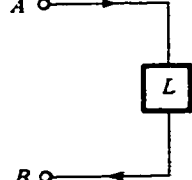
Element	R	Realization	Symbol

Figure 4. Digital Realization of Impedances

2.3.2 Voltage Source

For the voltage source and the impedance $Z(s)$ in Figure 3b, we can write

$$A = V + IR$$
$$B = V - IR$$
$$V = IZ(s) + V_1$$

12

Again, using bilinear transformation and eliminating V and I, we get

$$B = f_1(z)V_i + f_2(z)A \qquad \text{where}$$

$$f_1(z) = \left.\frac{2R}{R+Z(s)}\right|_{s=\frac{2}{T}\frac{z-1}{z+1}} \quad \text{and} \quad f_2(z) = \left.\frac{Z(s)-R}{Z(s)+R}\right|_{s=\frac{2}{T}\frac{z-1}{z+1}}$$

with $\quad R = \left(\dfrac{2}{T}\right)^{\lambda} R_x$. $f_1(z)$ and $f_2(z)$ can be simplified to

$$f_1(z) = \begin{cases} 1-z^{-1} & \lambda=-1 \\ 1 & \lambda=0 \\ 1+z^{-1} & \lambda=1 \end{cases} \quad \text{and} \quad f_2(z) = \begin{cases} z^{-1} & \lambda=-1 \\ 0 & \lambda=0 \\ -z^{-1} & \lambda=1 \end{cases}.$$

The realization of the capacitive, resistive and inductive sources are shown in Figure 5.
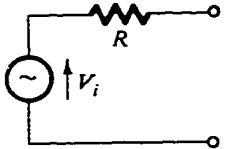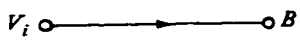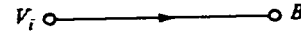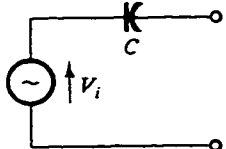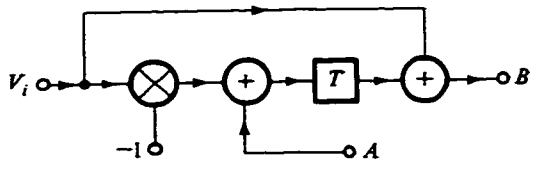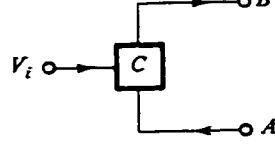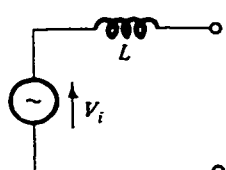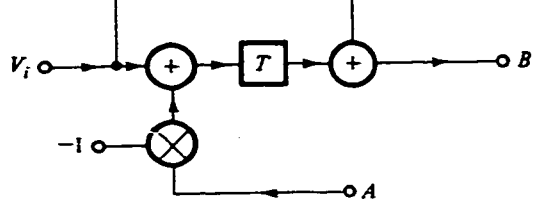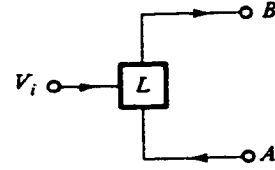
Figure 5. Digital relization of voltage sources

Therefore, the classic one-port can be characterized by the two wave quantities.

13

2.3.3 Series Wire Interconnection

From Figure 3c and the constraints $V_1 = V_2 = V_3$ and $I_1 + I_2 + I_3 = 0$, one could use the realization techniques from previous sections and obtain

$$\mathbf{B} = (\mathbf{I} - \mathbf{M}_s)\mathbf{A} \tag{2.2}$$

where

$$\mathbf{M}_s = \begin{bmatrix} m_{s1} & m_{s1} & m_{s1} \\ m_{s2} & m_{s2} & m_{s2} \\ m_{s3} & m_{s3} & m_{s3} \end{bmatrix} \qquad m_{s3} = 2 - m_{s1} - m_{s2} \tag{2.3}$$

and $\quad m_{sk} = \dfrac{2R_k}{R_1 + R_2 + R_3}. \tag{2.4}$

A realization of Equation 2.2 is shown in Figure 6. This type of connection is referred as S2 (Series 2-multiplier) adaptor.
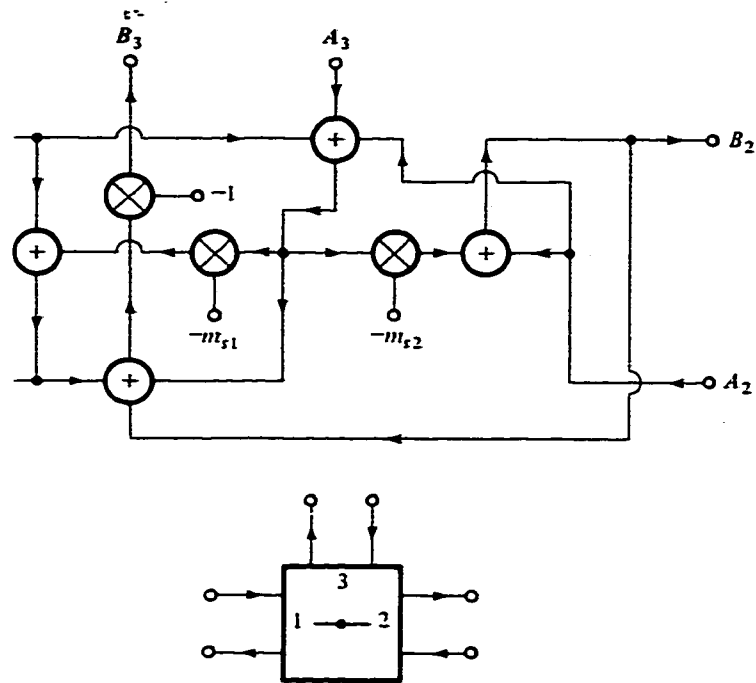
Figure 6. Type S2 Adaptor
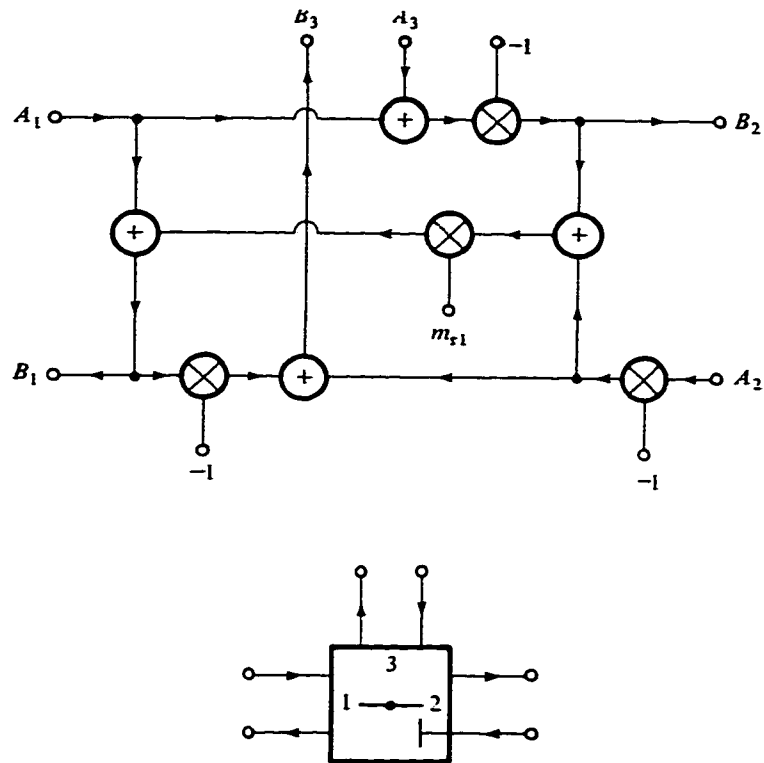
Figure 7. Type S1 Adaptor

Since R_2 is not specified, we can choose $R_2 = R_1 + R_3$ so that

$$m_{s1} = \frac{R_1}{R_2} \qquad m_{s2} = 1.$$

According to Equation 2.4, the S2 adaptor can be simplified as the series 1-multiplier adaptor (type S1) as shown in Figure 7.

2.3.4 Parallel Interconnection

With Figure 3d and the constraints $V_1 = V_2 = V_3$ and $I_1 + I_2 + I_3 = 0$, one could similarly obtains

$$\mathbf{B} = (\mathbf{M}_p - \mathbf{I})\mathbf{A} \tag{2.5}$$

where

$$\mathbf{M}_s = \begin{bmatrix} m_{p1} & m_{p2} & m_{p3} \\ m_{p1} & m_{p2} & m_{p3} \\ m_{p1} & m_{p2} & m_{p3} \end{bmatrix} \qquad m_{p3} = 2 - m_{p1} - m_{p2} \tag{2.6}$$

and $\quad m_{pk} = \dfrac{2G_k}{G_1 + G_2 + G_3}.$ \hfill (2.7)

The interconnection can be realized as in Figure 8.
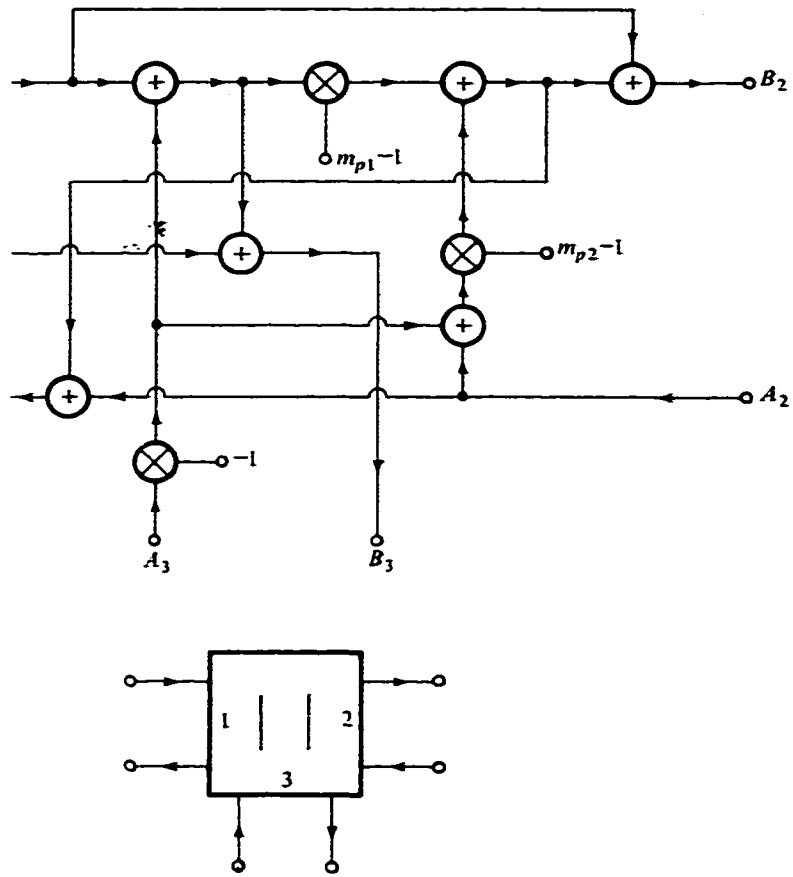
Figure 8. Type P2 Adaptor

By Choosing conductance $G_2 = G_1 + G_3$,

$$m_{p1} = \frac{G_1}{G_2} \qquad m_{p2} = 1.$$

we obtain a 1-multiplier realization (P1 adaptor) as shown in Figure 9
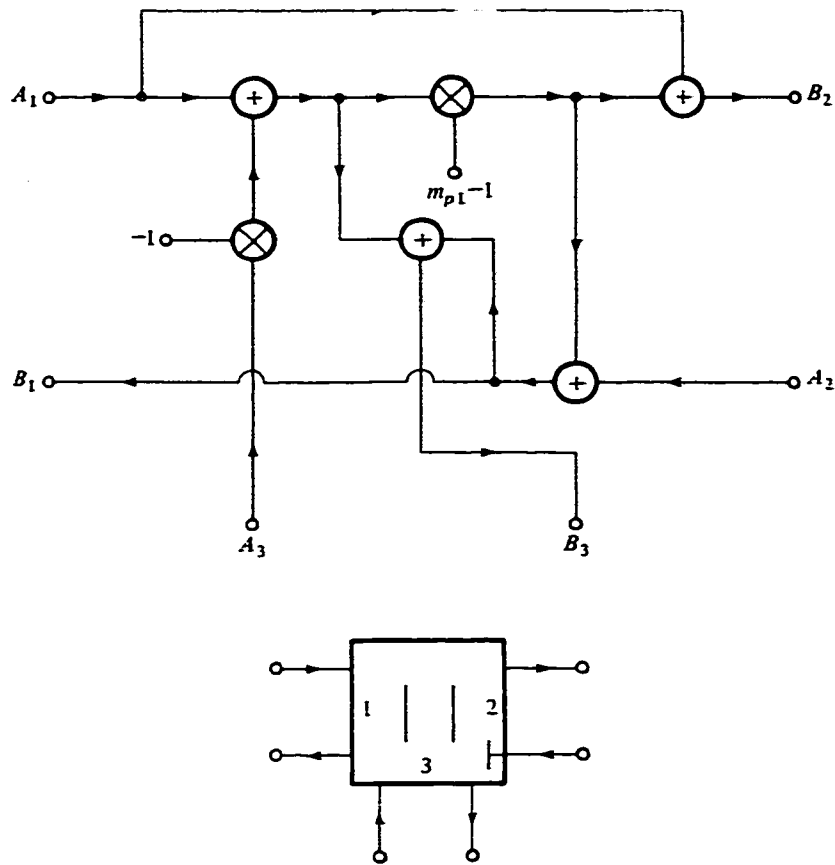
Figure 9. Type P1 Adaptor

2.3.5 Lattice Reference Filter

A classical symmetric lattice filter can also be represented using the wave quantities. Consequently, the lattice filter serves as a reference filter for a WDF. The resulting WDF is one of the most attractive structures available [4]. Consider a lattice reference filter with equal resistance with Z' and Z" as the lattice impedance (see Figure 10).
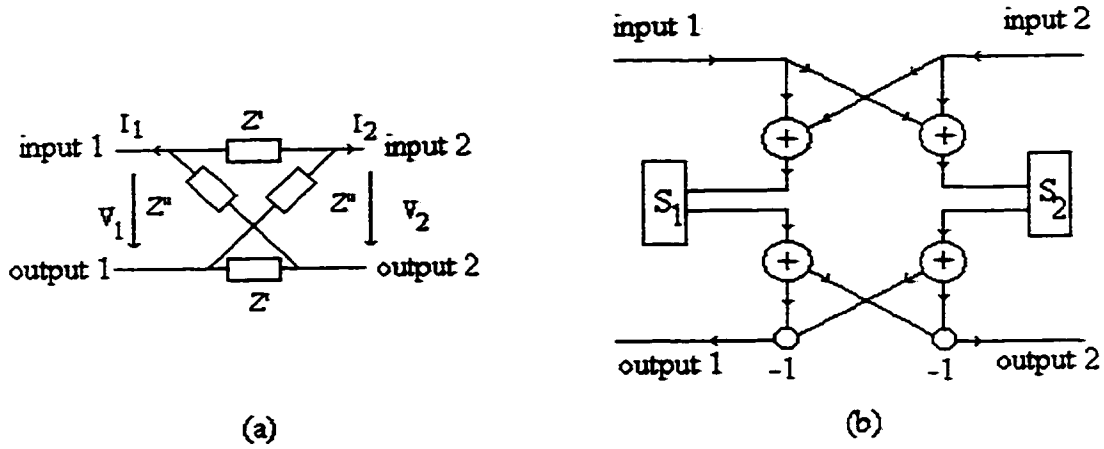
Figure 10. Classical Lattice circuit and Wave flow diagram

(a) classical lattice circuit and (b) its corresponding WDF wave flow diagram.

The reflectances of the reactances of both lattice branches can be written as [5]

$$S_1 = \frac{g_1(-\psi)}{g_1(\psi)} \quad \text{and} \quad S_2 = \frac{g_2(-\psi)}{g_2(\psi)}. \tag{2.8}$$

in which $g_1(\psi)$ and $g_2(\psi)$ are Hurwitz polynomials of degree N_1 and N_2 respectively.

The transfer functions S_{11} and S_{22} are known as

$$S_{11} = S_{22} = \frac{S_1 + S_2}{2} = \frac{h(\psi)}{g(\psi)} \quad \text{and}$$
$$S_{21} = S_{12} = \frac{S_2 - S_1}{2} = \frac{f(\psi)}{g(\psi)}. \tag{2.9}$$

$h(\psi), f(\psi)$ and $g(\psi)$ are the canonic polynomials. The characteristic function is defined as

$$C(\psi) = \frac{S_{11}(\psi)}{S_{21}(\psi)} = \frac{h(\psi)}{f(\psi)}. \tag{2.10}$$

19

The reflectance of a first order all-pass section can be written in the form [5]

$$S = \frac{-\psi + B_0}{\psi + B_0}$$ (2.11)

and the corresponding wave flow diagram is shown in Figure 11. All-pass functions(a) with $\gamma_0 = C$.
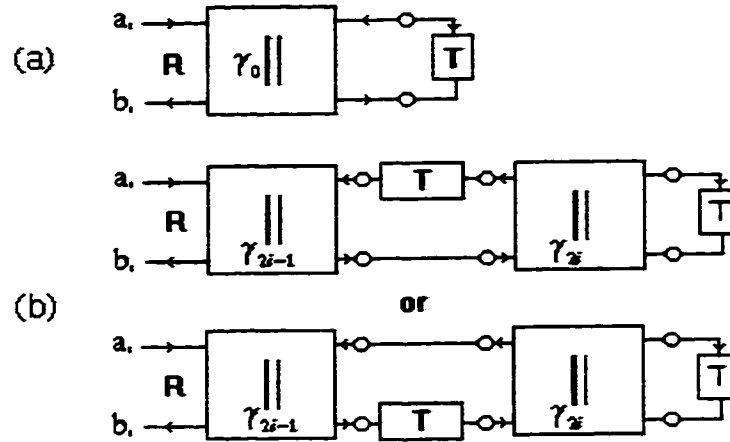
Figure 11. All-pass functions

(a) The Wave flow diagram of a first order filter (b) and two forms of second order (B) all-pass functions

The reflectance of a second order all-pass section is known as [5]

$$S = \frac{\psi^2 - A_i + B_i}{\psi^2 + A_i + B_i}$$ (2.12)

and the corresponding wave flow diagram is shown in Figure 11(b). The adapter coefficients are given as [5]

$$\gamma_{2i-1} = \frac{A_i - B_i - 1}{A_i + B_i + 1} \quad \text{and} \quad \gamma_{2i} = \frac{1 - B_i}{1 + B_i}.$$ (2.13)

20

One may use the first and second order all-pass structures to construct the lattice WDF. The resulting lattice WDF using only cascaded first and second order all-pass sections and two port adapters [4] is shown in Figure 12 [5].
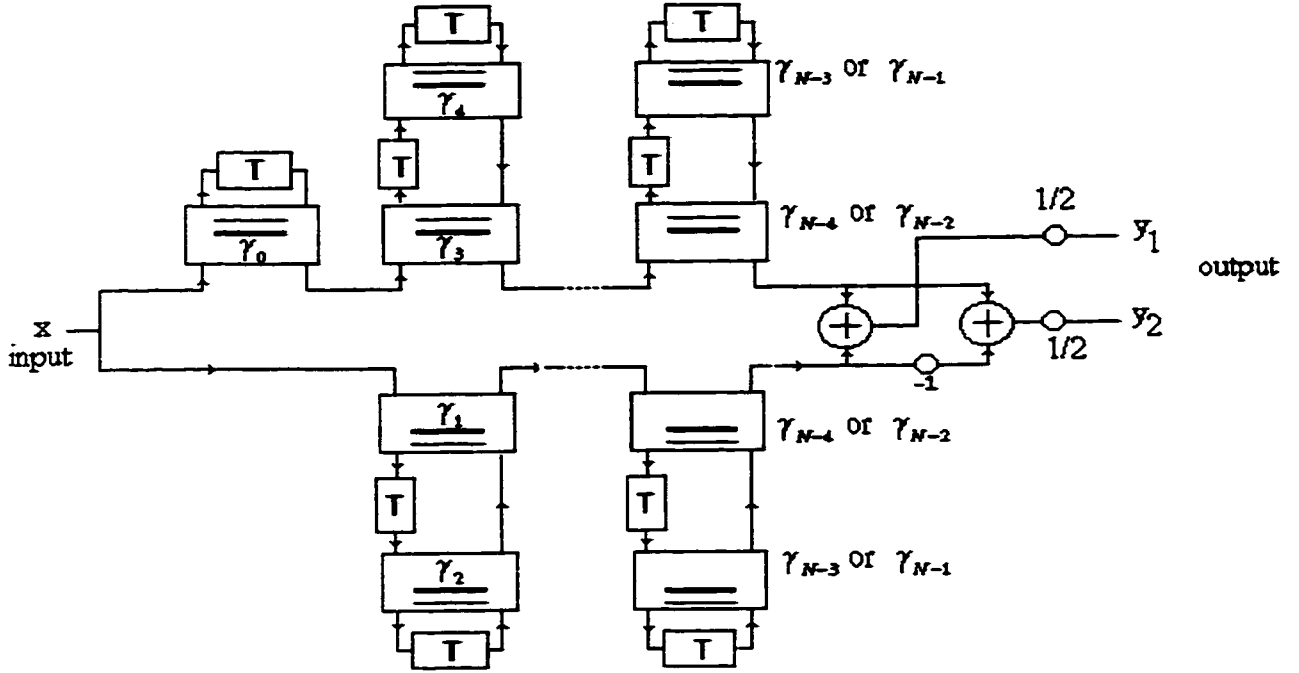
Figure 12. Block Diagram of the lattice WDF with Cascaded All-pass Structure

2.3.6 Explicit Formulas for Designing Bireciprocal Lattice WDFs

A special class of lattice WDFs have self-reciprocal characteristic functions. The characteristic functions have the form

$$C(\psi) = \frac{1}{C(1/\psi)}.$$

For a lattice WDF having the bireciprocal characteristic function is known as a bireciprocal lattice WDF. The bireciprocal filters will have some useful properties.

21

Firstly, the bireciprocal filter has (N-1)/2 adapters only, which is less than a half of a usual lattice filter (see Figure 13) [5].
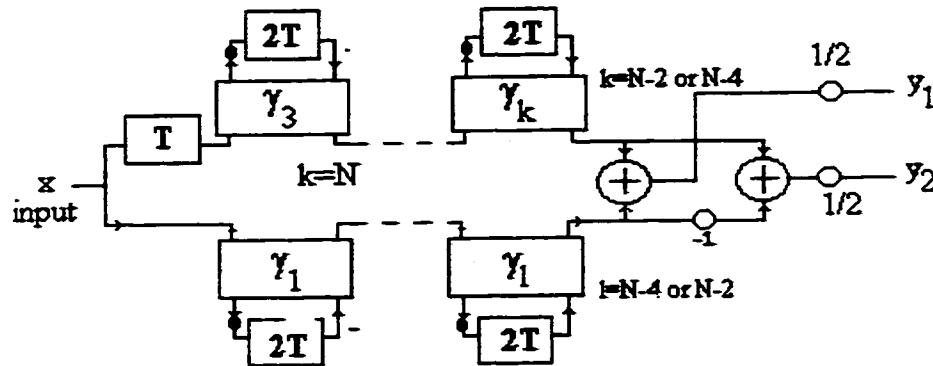
Figure 13. Block Diagram of a Bireciprocal Halfband Lattice WDF

The filters with the structure as shown in Figure 13 will have their 3dB cutoff at ¼ of their sampling frequency. The halfband lowpass characteristic is especially attractive for certain applications such as sampling rate conversion. For those who may be interested in cutoffs at 1/6, 1/7 or other fractions of sampling frequency, a polyphase filter or a combination of polyphase filters can be used to obtain cutoff at a rational fraction of the sampling frequency [6], [7].

The design of a bireciprocal lattice WDF can be done by using the explicit formulas given by Gazsi[5]. The explicit formulas can be summarized in the following:
The specifications of a lowpass filter design specification are

a_s minimum attenuation in the stopband in decibels.

a_p Maximum attenuation on passband in decibels.

f_s lower edge frequency of the stopband.

f_p upper edge frequency of the passband.

F sampling frequency.

One may calculate the ripple factors

$$\varepsilon_s = \sqrt{10^{a_s/10} - 1}.$$
$$\varepsilon_p = \sqrt{10^{a_p/10} - 1}.$$

(2.14)

where ε_s and ε_p are the ripple factors for the stopband and passband respectively. The transformed frequencies φ_s and φ_p are obtained by using the lower edge frequency of the stopband and upper edge frequency of the passband.

$$\varphi_s = \tan(\pi f_s / F)$$
$$\varphi_s = \tan(\pi f_s / F).$$

(2.15)

With the parameters calculated, the minimum order n_{min} of the filter can be estimated by using the results obtained previously.

$$n_{min} = \left\lceil \frac{c_1 \ln(c_2 \varepsilon_s / \varepsilon_p)}{\ln(c_3)} \right\rceil.$$

(2.16)

Note that the minimum order should be an odd number. If an estimated order is an even number, simply round it up to the nearest odd number. The values of c_1, c_2 and c_3 are given in Table 2.1 and the factor k can be calculated as

$$k_0 = \sqrt{\varphi_s / \varphi_p}$$
and
$$k_{i+1} = k_i^2 + \sqrt{k_i^4 - 1}, \text{ for } i = 0,1,2,3.$$

(2.17)

Table 1 Parameters for the Degree Estimation

Filter Type	c_1	c_2	c_3
Butterworth	1	1	k_0^2
Elliptic	8	4	$2k_4$

To determine the parameters of the Butterworth filters

$$\gamma_0 = 0, \quad \gamma_{2i-1} = -\tan^2\left(\frac{\pi i}{2N}\right), \quad \gamma_{2i} = 0 \quad \text{for } i = 1,2,\dots,(N-1)/2.$$

(2.18)

For the elliptic filters, the parameters are determined by first choosing the actual stopband frequency f_s^*, and $f_{s\min} \geq f_s^* \geq f_s$, and

$$\varphi_s^* = \tan(\pi f_s^* / F)$$
and
$$q_0 = \sqrt{\varphi_s^* / \varphi_s}.$$

(2.19)

The other values of q_{i+1} can be calculated as:

$$q_{i+1} = q_i^2 + \sqrt{q_i^4 - 1} \quad \text{for } i = 0,1,2,3.$$

(2.20)

Furthermore, by using q_i, various of $c_{j,i}$ can be determined by first obtaining

24

$$c_{4,i} = \frac{q_4}{\sin \dfrac{i\pi}{N}}$$

(2.21)

and

and

$$y_i = \frac{1}{c_{0,i}}.$$

(2.22)

then for $j = 4,3,2,1$

$$c_{j-1,i} = \frac{1}{2q_{j-1}}\left(c_{j,i} + \frac{1}{c_{j,i}}\right).$$

(2.23)

One must first calculate the values of A_i and B_i to get the filter coefficients

$$B_i = 1,$$
$$A_i = \frac{2}{1+y_i^2}\sqrt{1-\left(q_0^2 + \frac{1}{q_0^2} - y_i^2\right)}.$$

(2.24)

Finally, the adapter coefficients γ can be found as

$$\gamma_{2i-1} = \frac{A_i - 2}{A_i + 2}$$

and

$$\gamma_{2i} = 0.$$

For i=1,2,...(N-1)/2.   (2.25)

With the formulas above, one may easily design any halfband bireciprocal filter.

2.3.7 A 2-D Bireciprocal Lattice Filter Design

With the development of the 1-D bireciprocal lattice WDF, the design of 2-D bireciprocal lattice WDFs can be easily obtained by using suitable transformations [1], [2], [3]. Let $H_1(Z)$ be a 1-D lowpass filter with a cut off at ¼ of its sampling frequency. A 2-D lowpass filter $H(Z_1, Z_2)$ using the 1-D filter on both of the x and y directions can be written as $H(Z_1, Z_2) = H_1(Z_1)H_2(Z_2)$. By transforming Z_1 and Z_2 as

$$Z_1 \rightarrow Z_1 e^{j\pi/2} = jZ_1$$
$$Z_2 \rightarrow Z_2 e^{j\pi/2} = jZ_2 ,$$

(2.26)

we obtain a first quadrant filter.

$$G(Z_1, Z_2) = H(jZ_1, jZ_2) = H_1(jZ_1)H_2(jZ_2)$$

(2.27)

On the other hand, $G(-Z_1, -Z_2)$ corresponds to the third quadrant pass filter. Thus, one may combine both the first and third quadrant filters as:

$$G_{1,3}(Z_1, Z_2) = G(Z_1, Z_2) + G(-Z_1, -Z_2)$$
$$= H(jZ_1)H(jZ_2) + H(-jZ_1)H(-jZ_2).$$

(2.28a)

Similarly, the second and fourth quadrant filters are:

$$G_{2,4}(Z_1, Z_2) = H(-jZ_1)H(jZ_2) + H(jZ_1)H(-jZ_2).$$

(2.28b)

26

For a special class of the transfer function, in which $H_1(Z) = Z^{-1}H_a(Z^2) + H_b(Z^2)$, the transfer function G can be rewritten as

$$G_{1,3}(Z_1, Z_2) = 2[H_b(-Z_1^2)H_b(-Z_2^2) - Z_1^{-1}Z_2^{-1}H_a(Z_1^2)H_a(Z_2^2)]. \qquad (2.29a)$$

and

$$G_{2,4}(Z_1, Z_2) = 2[H_b(-Z_1^2)H_b(-Z_2^2) + Z_1^{-1}Z_2^{-1}H_a(Z_1^2)H_a(Z_2^2)]. \qquad (2.29b)$$

The filter structure is shown in Figure 14.
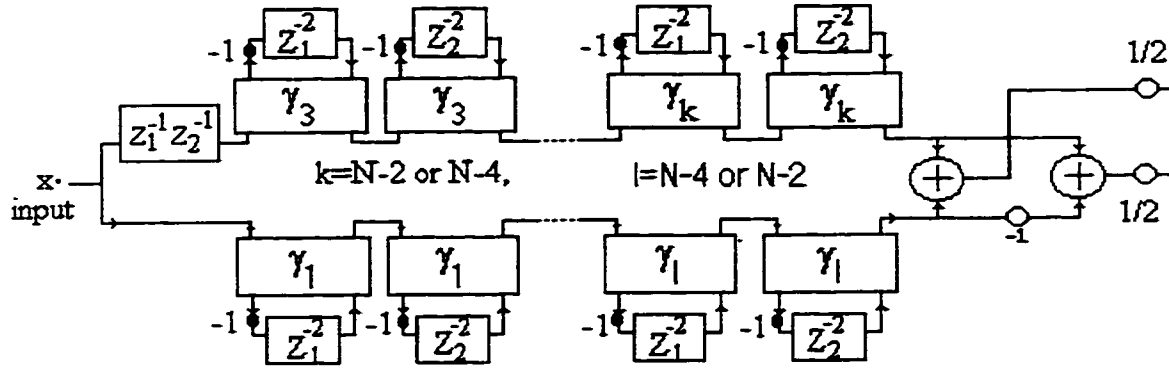
Figure 14. The Quadrant Filter Derived from a 1-D Lattice

From the quadrant filter, both $\pm 45°$ fan and diamond filters can be obtained through transformations [2]. The transformations of a fan filter are:

$$Z_1 \rightarrow \sqrt{Z_1^{-1}Z_2}, \qquad Z_2 \rightarrow \sqrt{Z_1 Z_2}. \qquad (2.30)$$

The structure of the resulting fan filter is shown in Figure 15.

27

$$Z_3^{-1} = Z_1 \ Z_2^{-1} \qquad\qquad Z_4^{-1} = Z_1^{-1} \ Z_2^{-1}$$
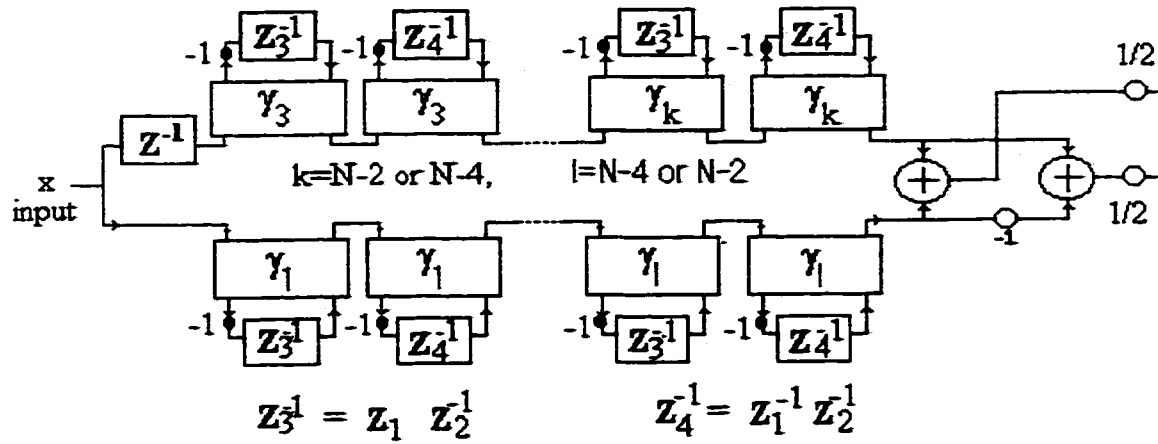
Figure 15. The Fan Filter Derived from a 2-D Quadrant Filter

Moreover, an additional transformation from the ± 45° fan filter will lead to a full-plane diamond filter by letting

$$Z_1 \rightarrow Z_1, \qquad Z_2 \rightarrow -Z_2 \qquad \text{or} \qquad (2.31a)$$

$$Z_1 \rightarrow -Z_1, \qquad Z_2 \rightarrow Z_2. \qquad\qquad\qquad (2.31b)$$

Finally, the full-plane diamond filters have the structure shown in Figure 16.

28

$$Z_3^{-1} = Z_1 \, Z_2^{-1} \qquad\qquad Z_4^{-1} = Z_1^{-1} \, Z_2^{-1}$$
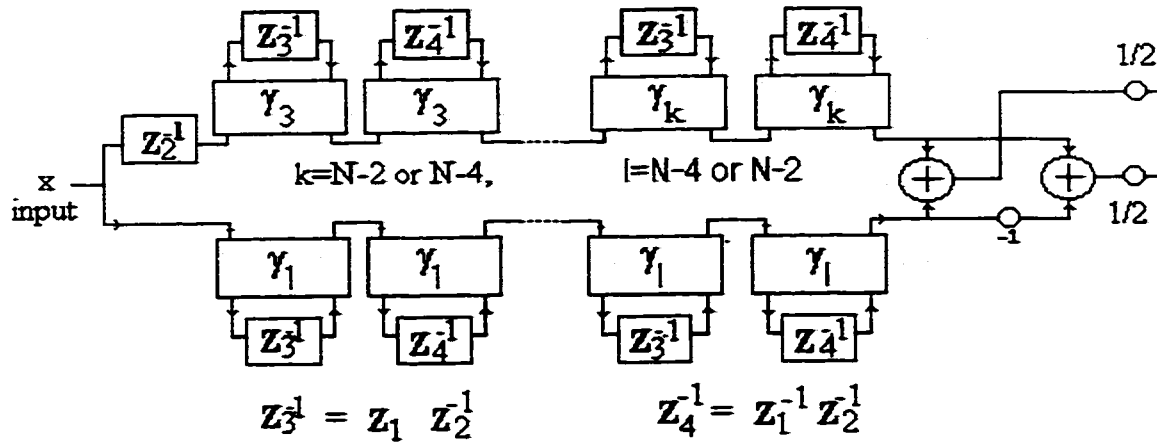
Figure 16. The Full-plane Diamond Filter Derived from Fan Filter

The adapter coefficients γ_k can be determined by using the explicit formulae given in the previous section.

To illustrate the full-plane diamond filter with the structure in Figure 16, we use the adapter sections containing γ_1, and substitute the rest of the adapters by short circuits (see Figure 18). The coefficient is $\gamma_1 = 0.5$. The corresponding diamond filter will have a frequency response shown in Figure 17.
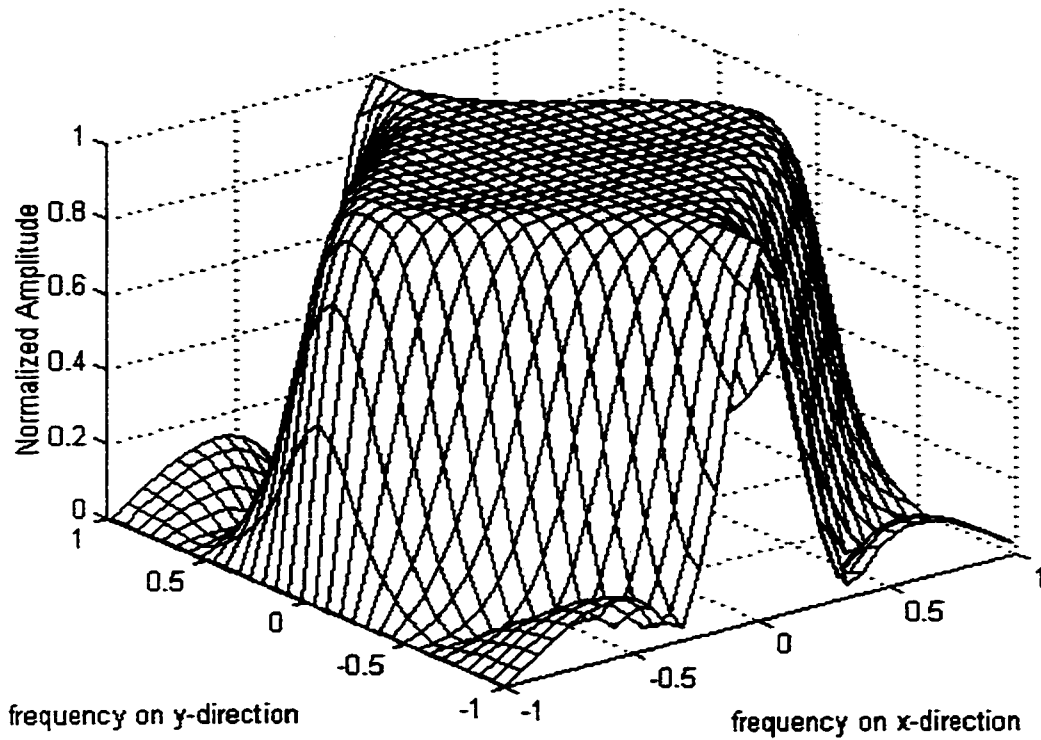
Figure 17. Frequency response of the Full-plane Diamond WDF with $\gamma_1 = 0.5$.

The full-plane diamond filter is also called a (1,1) diamond filter because it has the spectrum of a (1,1) quincunx structure. Similarly, a (2,2) diamond filter is so named because it has the spectrum of a (2,2) quincunx structure.

If a (2,2) diamond filter is needed, one may use two 1-D halfband filters and one 2-D (1,1) diamond filter to form a (2,2) diamond filter. The frequency response of a (2,2) diamond filter is shown in Figure 21.

30
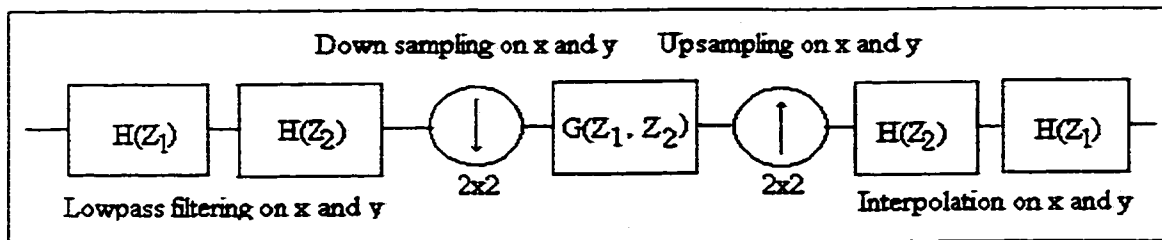
Figure 18. The Block Diagram of a (2,2) Diamond Filter.
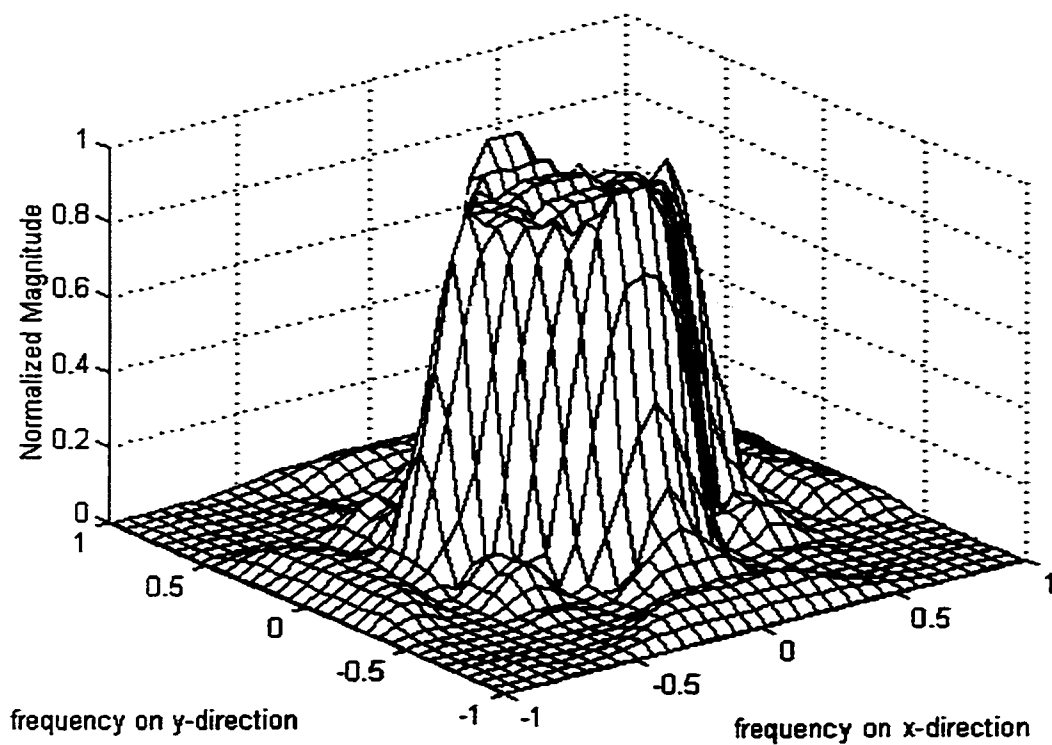
Figure 19. The Spectrum of a (2,2) Diamond Filter

2.4 Some Related Visual Effects and Properties for the Filter Structures

2.4.1 Parameters of a filter and its visual effects.

Neither 1-D nor 2-D bireciprocal lattice WDFs are ideal filters. To achieve the best possible result, certain design parameters are usually needed. Some common design parameters are:

1) Passband ripple.

2) stopband loss

3) transition bandwidth

4) phase distortion.

If complexity is not a concern, filters are preferred to have a response as ideal as possible. An ideal response implies minimum passband ripple, infinite stopband loss, very narrow transition band and exact zero phase or linear phase. However, for video and image processing, the design parameters may be weighted differently due to the nature of the application.

Passband ripple: It is known that very small passband ripple does not have significant impact on image quality[3], except that the DC component must be preserved. Therefore, passband ripple is not an important factor.

Stopband loss: Due to the nature of video and image signals, their DC components are very pronounced. During an interpolation process, repetitive DC components will be aliased into the spectrum if the DC components are not properly suppressed. Except for the DC component, 20dB stopband attenuation is good enough for image and video applications [3].

Transition bandwidth: If the transition region is very narrow, a spatially filtered image will have rings formed around boundaries. If temporally filtered, ghosts will form behind moving objects. On the other hand, if the transition is too wide, there will be a loss of resolution or aliasing or both. Therefore, there is a tradeoff to be made in choosing the transition bandwidth.

Phase Distortion: It is known that the human eye is very sensitive to phase distortion [8]. Although IIR filters have nonlinear phase response, using a third order of IIR filter with a small coefficient can provide a nearly linear phase response. Furthermore, the reciprocal lattice WDF can made to achieve a linear phase response by cascading an anticausal filter to the output of a causal filter. However, it is difficult to perform anticausal operations during temporal filtering and the nearly linear phase filter is therefore the only choice.

2.4.2 A Special Class of Filters for Sampling Structure Conversion

There are several filters that are especially useful for image and video applications related to sampling structure conversion. They are 1-D halfband filters, Nth band filters and full-plane diamond filters. Using them, we can obtain almost all (L,K) rectangular and (L,K) diamond filters useful for practical applications[3]. In this thesis we will only use the 1-D halfband filter and the full-plane diamond filter.

1-D Halfband Filter:

The transfer function of the 1-D filter is given as:

$$H(Z) = \frac{1}{2}\left(Z^{-1} + \frac{Z^{-2} + \gamma}{1 + \gamma Z^{-2}}\right)$$

(2.32)

The adapter coefficient γ has the range of $0 \leq \gamma \leq 1$ and is responsible for controlling the frequency response of the filter. As γ increases, passband ripple will increase and the transition bandwidth, stopband loss and phase linearity will decrease. The block diagram of the filter is shown in Figure 20

33
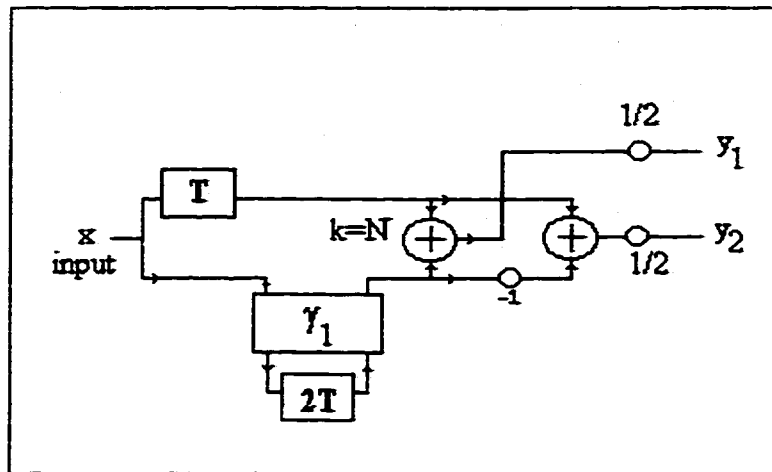
Figure 20. Nearly-Linear-Phase Halfband 1-D WDF

The frequency response and the phase response of the nearly linear phase halfband filter are shown in Figure 21 and Figure 22.
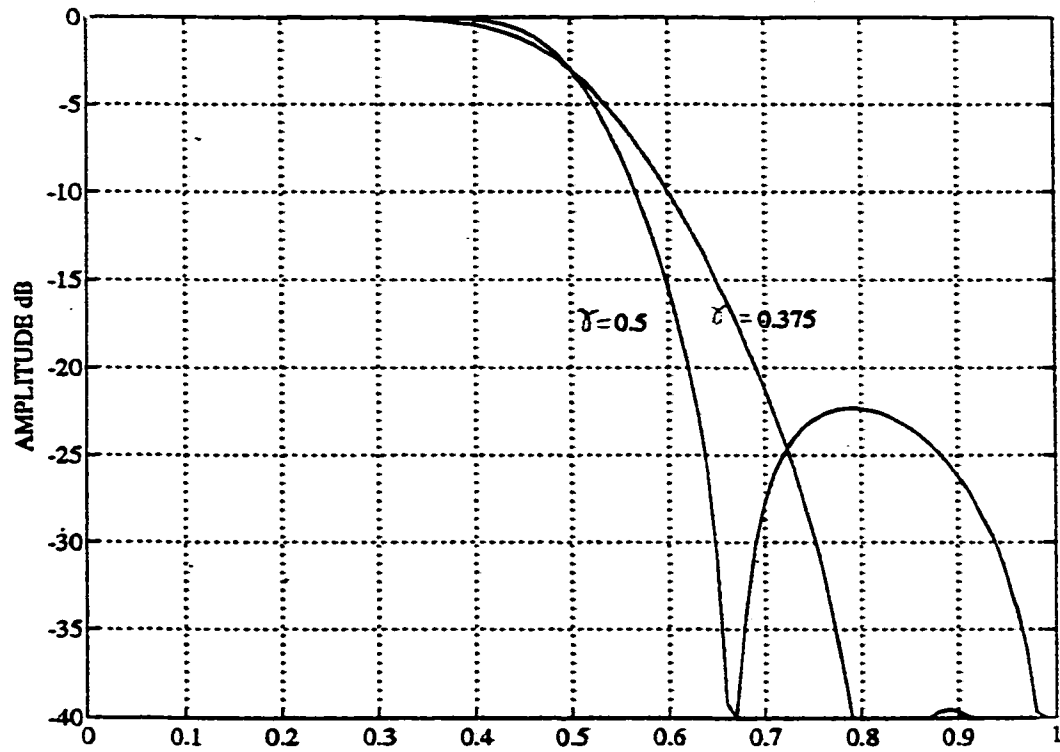
Figure 21. Frequency Response of the Nearly-Linear-Phase 1-D WDF
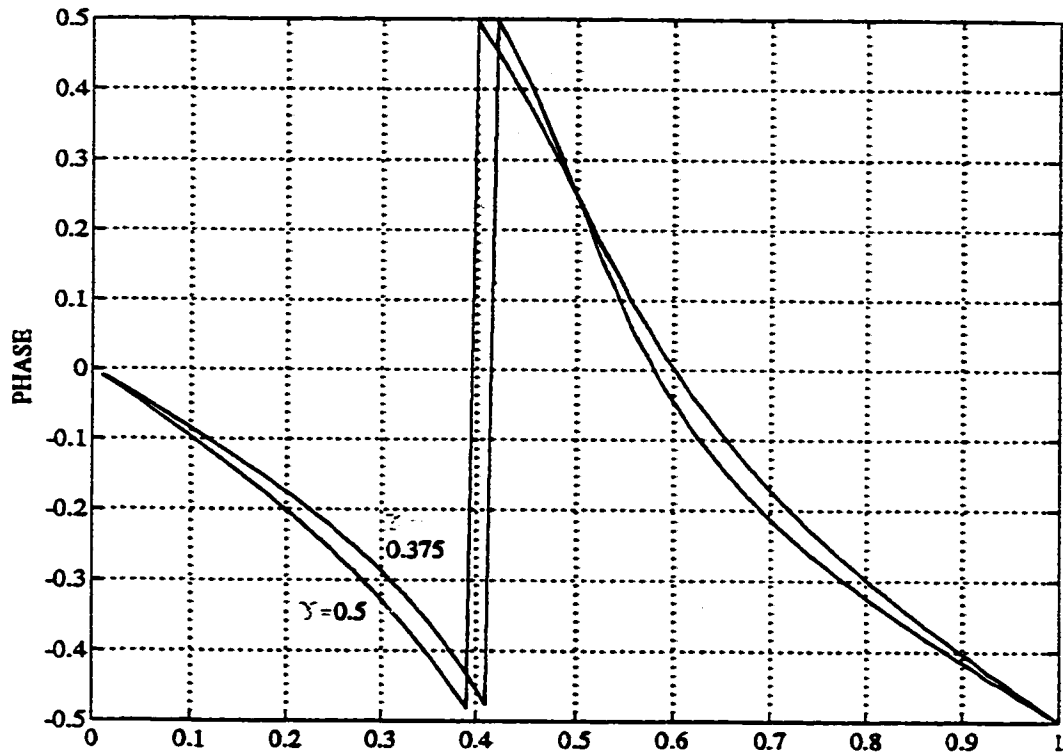
Figure 22. Phase Response of the Nearly-Linear-Phase 1-D WDF

Because of the good frequency response of the WDF, the suggested filter has a simple structure. Moreover, it consists of only a single multiplier γ_1, and hence only low computational power is needed. To further reduce the computational requirement, the value of γ can be chosen to be a power-of-two or a sum of powers-of-twos (0.75, 0.625, 0.5, 0.375 and 0.25). The powers-of-two values can eliminate the multiplication by shifts or shifts-and-adding operations. Furthermore, for practical use, the coefficient γ_k should be either 0.5 or 0.375[3], depending on the frequency content of the picture. This is because values other than the suggested 0.5 or 0.375 will either create excessive ringing ($\gamma > 0.5$), or visible aliasing ($\gamma < 0.375$), after up and down sampling.

36

Full-Plane Diamond Filter: Another suggested filter is a nearly linear phase (1,1) full-plane diamond filter with the transfer function given as:

$$H(Z_1, Z_2) = \frac{1}{2}\left(Z_2^{-1} + \frac{Z_1^{-1}Z_2^{-1} + \gamma}{1 + \gamma Z_1^{-1}Z_2^{-1}} \frac{Z_1 Z_2^{-1} + \gamma}{1 + \gamma Z_1 Z_2^{-1}}\right)$$

(2.33)

where $0 \leq \gamma \leq 1$. Note that the (1,1) diamond is derived from the halfband filter using the transformation. Therefore, the coefficient γ and all the properties are the same as the 1-D halfband filter. The block diagram of the filter is given in Figure 23.
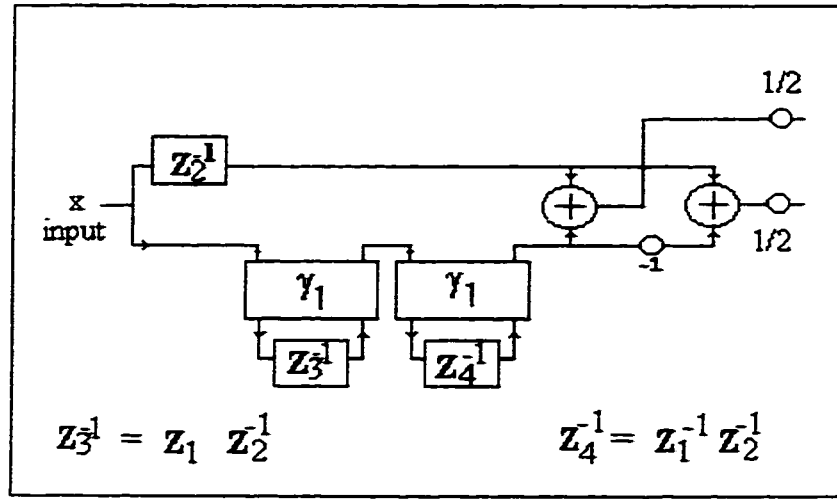
Figure 23. Nearly-Linear-Phase (1,1) Diamond Filter

The structure of the nearly-linear-phase (1,1) diamond filter has a pure delay element in one of the branches. Similar to the 1-D halfband filter, with the power-of-two coefficients, the computation requirement is very low. Figure 21 and Figure 24 respectively show the Magnitude and the phase responses using the coefficient $\gamma_1 = 0.5$.
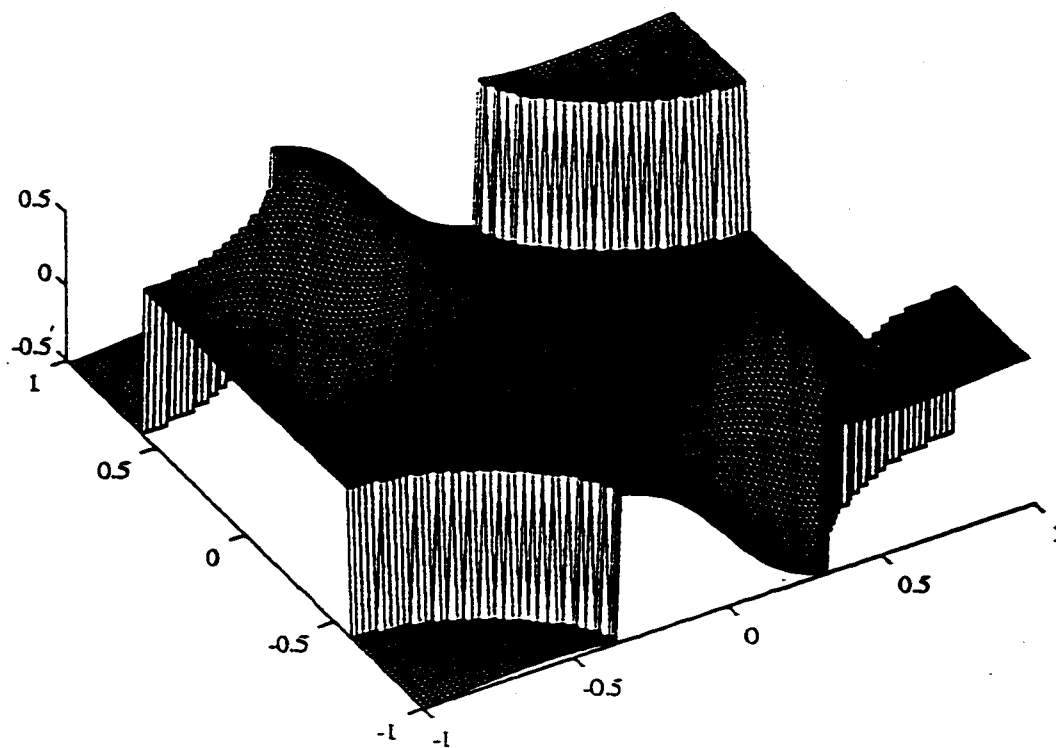
Figure 24. The Phase Response of the Nearly Linear Phase Full-plane Diamond

2.5 Summary

This chapter has presented two specially designed WDFs: 1-D halfband filter and a 2-D (1,1) diamond filter. The 1-D halfband filter is designed using explicit formulas [5], and the (1,1) diamond filter is obtained using transformations based on the 1-D halfband WDF [1], [2], [3]. The parameters of the filter design are chosen to have low visual degradation and high computational efficiency, so that the filters will have one pure delay section and require no multiplication.

Reference

[1]   Q. Gu and X. Du, "2D lattice structure and explicit formulas for the design of 2-D digital fan filters," *IEEE ISCAS Proc.*, May 1990, USA.

[2]   Q. Gu and M.N.S. Swamy, "On the design of a Broad Class of 2-D Recursive Digital Filters with Fan, Diamond and Elliptical Response," submitted to *IEEE CAS.*

[3]   Q. Gu, L. Lee and M. N. S. Swamy, "2D IIR digital filters for sampling structure conversion for video signals, " submitted to *IEEE CAS.*

[4]   A. Fettweis, "Wave digital filters: Theory and practice," *Proc. IEEE,* VOL. 74, NO. 2, pp. 270-326. February, 1986.

[5]   L. Gazsi, "Explicit Formulas for Lattice Wave Digital Filters, " *IEEE Transaction on Circuit and Systems*, VOL. CAS-32, NO.1, January 1985.

[6]   M. Renfors, "Recursive N th-band digital filters - Part I: Design and properties," *IEEE Trans. On CAS,* VOL. CAS-34, NO. 1, pp. 24 - 39, January 1987.

[7]   M. Renfors, "Recursive N th-band digital filters - Part I: Design of multistage decimators and Interpolators," *IEEE Trans. on CAS,* VOL. CAS-34, NO. 1, pp. 40 - 51, January 1987.

[8]   D. E. Pearson, *Transmission and Display of Pictorial Information*, Pentech Press, London, 1975.

3 State Value Updating Technique

3.1 Introduction

In the previous chapter, we have seen that simple WDF structures make filtering efficient and have low hardware requirements. On the aspect of phase distortion, although the nearly linear phase response of the filters do not cause significant phase distortion, some amount of phase distortion is still there. Consequently, if an image is being filtered repeatedly, the phase distortion can accumulate and the final filtered image may be distorted heavily.

To eliminate the accumulating phase distortion, one can add anticausal filtering to compensate the phase distortion. Ideally, the combined filter should have no phase distortion at all. But it is not the case if a non-ideal filter is used. For a sampling structure conversion process, the frequency content of the image being filtered for antialiasing, and the image being filtered for interpolation, are different. Although both passband signals are the same, the stopband spectra are not. If an ideal filter is used, the difference in the stop band has no effect since the frequency components will be attenuated in any case. If the filter has an imperfect stopband, however, the high frquency signal will leak through during anticausal filtering. The interpolation filtering cannot compensate for the extra phase distortion, because the signal being interpolated does not have the frequency

NOTE TO USERS

Page(s) not included in the original manuscript
are unavailable from the author or university. The
manuscript was microfilmed as received.

42 - 45

This reproduction is the best copy available.

UMI

The variables q_1, q_2 and q_3 are the state variables defined for the filter. During normal operations, the state values will combine with the input x to produce the output. At the same time, the new state values will be generated for the next calculation. For the suggested 2-D diamond filter, the state variables are defined in Figure 29. Both of the state variable assignments in Figure 27 and Figure 29 will be used for the entire thesis.

Since the state values determine the condition of the filter, it is obvious that if one wants to change the condition of a filter, changing the state values is an effective way. In our situation, when we want to force the 1-D WDF filter to operate in its steady state, we may change the state value q_1 of the filter to the steady-state value. The implementation is shown in Figure 28.
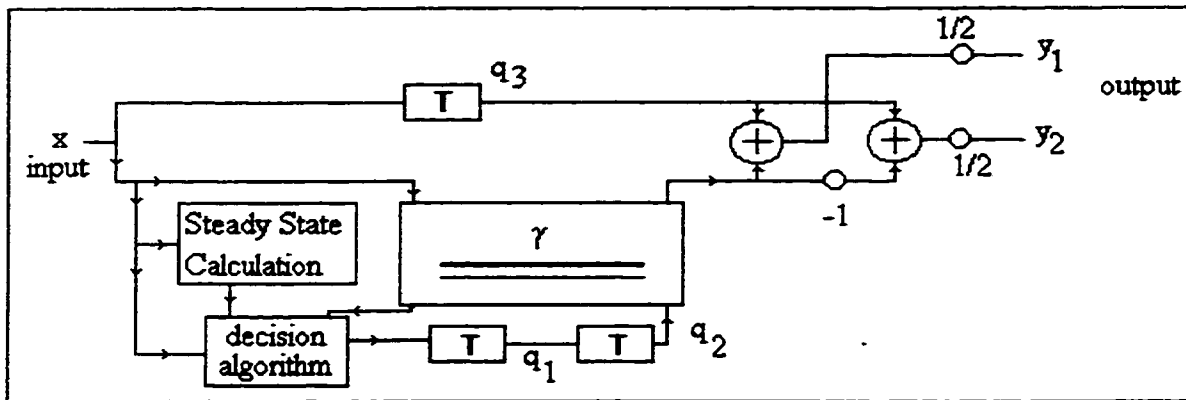
Figure 28. The State Value Updating Implementation for the Suggested 1-D WDFs

The steady-state calculation module gets the steady-state value by either using a look-up table or calculations. Both the state values from the filter and the steady-state calculations go into the decision algorithm. The decision algorithm then chooses either the state value from the filter (if no adaptation is needed) or from the steady-state calculation module (if a large discontinuity is found), based on the previous and current inputs.

To find the state values during the steady state, one may use the Final Value theorem and the transfer function of the filter suggested in [1]. An alternative method to find the value is by iterating the state variables with an infinite long constant input k. For the 1-D WDFs suggested in Chapter 2 with the states defined in Figure 27, we can calculate the state

values $q_1(n)$, $q_2(n)$ and $q_3(n)$. Using the adapter structure given in [4] and assuming the coefficient is $|\gamma|$, then

$$Eq_1(n) = \gamma[x(n) - q_2(n)] - x(n). \tag{3.1}$$

$$Eq_2(n) = q_1(n) \tag{3.2}$$

$$Eq_3(n) = x(n). \tag{3.3}$$

where E is the delay operation and $x(n)$ is the input at time n.

The output y can be expressed as:

$$y(n) = (q_3(n) - \gamma[x(n) - q_2(n)] - q_2(n))/2 \tag{3.4}$$

Since the output y is independent from (3.1), to calculate the steady-state value of q_1, only equation (3.1) and (3.2) are needed. From (3.1):

$Eq_1(n) = \gamma[x(n) - q_2(n)] - x(n)$, then

$$q_1(n) = \gamma[x(n-1) - q_2(n-1)] - x(n-1). \tag{3.5}$$

since $q_2(n) = q_1(n-1)$ if the inputs $x(n) = k$ for all n, and k is a constant, equation (3.5) can be rewritten as:

$$q_1(n) = \gamma[k - q_1(n-2)] - k = k(\gamma - 1) - \gamma q_1(n-2) \tag{3.6}$$

For the state value q_1 at n-2 and n-4:

$$q_1(n-2) = \gamma[k - q_1(n-4)] - k = k(\gamma - 1) - \gamma q_1(n-4) \qquad \text{and}$$

$$q_1(n-4) = \gamma[k - q_1(n-6)] - k = k(\gamma - 1) - \gamma q_1(n-6)$$

and one may obtain the state value q_t at any time delay in a similar fashion.

Substituting all previous state values into (3.1) recursively, the state value becomes

$$q_1(n) = k(\gamma - 1) - \gamma\{k(\gamma - 1) - \gamma[k(\gamma - 1) - \gamma(k(\gamma - 1) + ...$$

$$= k(\gamma - 1) - \gamma k(\gamma - 1) + \gamma^2 k(\gamma - 1) - \gamma^3 k(\gamma - 1) + ...$$

$$= k(\gamma - 1)\sum_{i=0}^{\infty}(-1)^i\gamma^i \qquad (3.7)$$

Since $0 \leq |\gamma| < 1$, the sum of the alternating sign exponential series in (3.11) converges and becomes:

$$q_1(n) = k(\gamma - 1)\frac{1}{1 + \gamma} \qquad (3.8)$$

or

$$q_1(n) = k\frac{\gamma - 1}{\gamma + 1}. \qquad (3.9)$$

Finally, by dividing the output state value q_1 by the constant input k, the factor to determine the state value during steady state becomes

$$\Gamma = \frac{\gamma - 1}{\gamma + 1}. \qquad (3.10)$$

Therefore, to find the steady-state register value q_1 for an dc input value k, one may simply multiply the input value k with the factor Γ to obtain the steady state $q_1(n)$.

The steady-state factor for the diamond filter can similarly obtained. For the diamond filter, the state variable assignments are given in Figure 29.
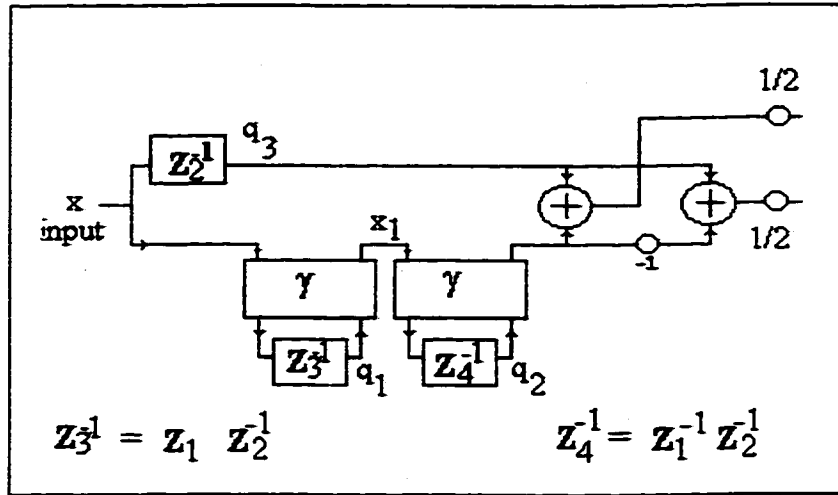
Figure 29. The State Variable Assignments for the Suggested 2-D Diamond WDF

The values q_1, q_2 and q_3 are the defined state variables for the diamond filter. The value x_1 is a label to identify the input of the second adapter. For the 2-D WDF, one may properly control the condition of the filter by changing the value of q_1 and q_2. The implementation of the state value updating technique for the diamond filter is shown in Figure 30.
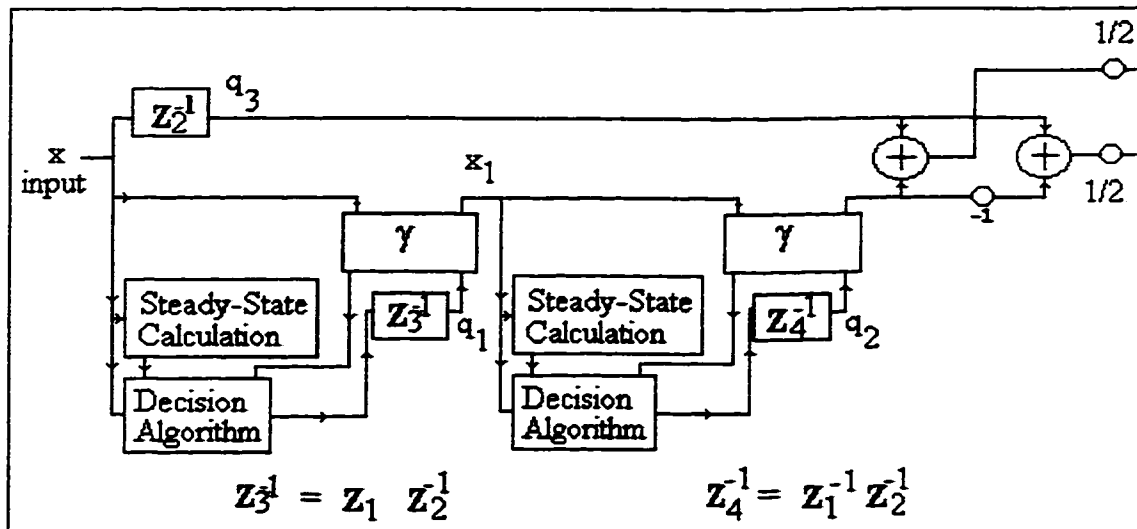
Figure 30. The State Value Updating Implementation for the Suggested 2-D Diamond WDF

To find the state values during the steady-state for the diamond filter, a similar approach as described for the 1-D filter is used. With the state variables defined in Figure 29, we

49

can calculate the state values $q_1(n)$, $q_2(n)$ and $q_3(n)$. We again use the adapter structure given in [4] and assume that coefficient is $|\gamma|$, then

$$E_3 q_1(m,n) = \gamma[x(m,n) - q_1(m,n)] - x(m,n).\tag{3.11}$$

$$E_4 q_2(m,n) = \gamma[x_1(m,n) - q_2(m,n)] - x_1(m,n).\tag{3.12}$$

where E_3 and E_4 are the delay operations on the $Z_1^{+1}Z_2^{-1}$ and $Z_1^{-1}Z_2^{-1}$ directions respectively. and $x(m,n)$ is the input at row m and column n.

Since there are two adapters for the diamond filter, we begin by considering the first adapter that operates in the $Z_1^{+1}Z_2^{-1}$ direction.

From (3.11):

$$q_1(m,n) = \gamma[x(m+1,n-1) - q_1(m+1,n-1)] - x(m+1,n-1)\tag{3.13}$$

For the steady-state condition, $x(m,n) = k$ for the diagonal direction $Z_1^{+1}Z_2^{-1}$ and equation (3.13) can be rewritten as:

$$q_1(m,n) = \gamma[k - q_1(m+1,n-1)] - k = k(\gamma-1) - \gamma q_1(m+1,n-1)\tag{3.14}$$

For the state values at $m+1,n-1$ and $m+2, n-2$:

$$q_1(m+1,n-1) = \gamma[k - q_1(m+2,n-2)] - k = k(\gamma-1) - \gamma q_1(m+2,n-2)\tag{3.15}$$

$$q_1(m+2,n-2) = \gamma[k - q_1(m+3,n-3)] - k = k(\gamma-1) - \gamma q_1(m+3,n-3)\tag{3.16}$$

and one may obtain the state values at any time delay in a similar fashion.

Substituting all the previous state values into (3.11) recursively, the state value at t=n becomes

$$q_1(m,n) = k(\gamma - 1) - \gamma\{k(\gamma - 1) - \gamma[k(\gamma - 1) - \gamma(k(\gamma - 1) + ... \tag{3.17}$$

$$= k(\gamma - 1) - \gamma k(\gamma - 1) + \gamma^2 k(\gamma - 1) - \gamma^3 k(\gamma - 1) + ... \tag{3.18}$$

$$= k(\gamma - 1)\sum_{i=0}^{\infty}(-1)^i\gamma^i \tag{3.19}$$

Since $0 \leq \gamma < 1$, the sum of the alternating sign exponential series in (3.19) converges and becomes:

$$q_1(m,n) = k\frac{\gamma - 1}{\gamma + 1}. \tag{3.20}$$

Finally, by dividing the output state value by the constant input k, the factor to determine the state values during steady state becomes

$$\Gamma = \frac{\gamma - 1}{\gamma + 1}. \tag{3.21}$$

The expression in (3.21) is the same as the one in (3.10). There is not surprising at all because although the expression have different number of delay elements, during steady state all values in the delay elements are identical.

For the adapter that operates at $z_1^{-1}z_2^{-1}$ direction, we start with Equation (3.12).

From (3.12):

$$q_2(m,n) = \gamma[x_1(m-1,n-1) - q_2(m-1,n-1)] - x_1(m-1,n-1) \tag{3.22}$$

For the steady-state situation, $x_1(m,n) = k$ for the diagonal direction $z_1^{-1}z_2^{-1}$ and Equation (3.22) can be rewritten as:

$$q_2(m,n) = \gamma[k - q_2(m-1,n-1)] - k = k(\gamma - 1) - \gamma q_2(m-1,n-1) \tag{3.23}$$

51

The state values q_2 at *m-1,n-1* and *m-2, n-2* are:

$$q_2(m-1,n-1) = \gamma[k - q_2(m-2,n-2)] - k = k(\gamma-1) - \gamma q_2(m-2,n-2) \quad (3.24)$$

$$q_2(m-2,n-2) = \gamma[k - q_2(m-3,n-3)] - k = k(\gamma-1) - \gamma q_2(m-3,n-3) \quad (3.25)$$

and one may obtain the state value at a further time delay in the same way.

Substituting all previous state values into (3.23) recursively, the state value at *t=n* becomes

$$q_2(m,n) = k(\gamma-1) - \gamma\{k(\gamma-1) - \gamma[k(\gamma-1) - \gamma(k(\gamma-1) + ... \quad (3.26)$$

$$= k(\gamma-1)\sum_{i=0}^{\infty}(-1)^i\gamma^i \quad (3.27)$$

Since $0 \leq |\gamma| < 1$, the sum of the alternating exponential series in (3.19) becomes:

$$q_2(m,n) = k\frac{\gamma-1}{\gamma+1}. \quad (3.28)$$

Again by dividing the output state value by the constant input k, the factor to determine state values during steady state becomes

$$\Gamma = \frac{\gamma-1}{\gamma+1}. \quad (3.29)$$

To find the register value q_2 during steady-state for an input dc value k, one may simply multiply the input value k with the coefficient Γ to obtain the steady-state $q_2(n)$.

The coefficient Γ is independent of the input value. This makes the computation of the steady-state state value extremely easy. Moreover, for image and video processing, the gray levels are usually within 256 levels of gray. One may use a lookup table with 256

entries to find the steady-state value for 256 levels of shades and totally eliminate the multiplication.

3.2.3 Comparison between Coefficient Adaptation and State Value Updating

Theoretically, the desired step response can be achieved by making the parameter γ varying. When a discontinuity is found, an adaptive algorithm will control the value of γ to produce the desired output. The output of the filter will be the same as the one using state value updating, but there are some differences between the overall structures due to the different approaches.

The 1-D filter will have state equations as shown in (3.1) and (3.2).

$$E\mathbf{q} = \mathbf{Aq} + \mathbf{B}x(n)$$

and

$$y = \mathbf{Cq} + \mathbf{D}x(n) .$$

From equation (3.1), (3.2), (3.3) and (3.4) The state vector $\mathbf{q}$ and system matrix $\mathbf{A}$ are:

$$\mathbf{q} = \begin{bmatrix} q_1 \\ q_2 \\ q_3 \end{bmatrix}, \quad \text{and} \quad \mathbf{A} = \begin{bmatrix} 0 & -\gamma & 0 \\ 1 & 0 & 0 \\ 0 & 0 & 0 \end{bmatrix}.$$

The input matrix $\mathbf{B}$, output vector $\mathbf{C}$ and the coupling vector $\mathbf{D}$ are:

$$\mathbf{B} = \begin{bmatrix} \gamma - 1 \\ 0 \\ 0 \end{bmatrix}, \quad \mathbf{C} = \begin{bmatrix} 0 \\ \dfrac{(\gamma - 1)}{2} \\ 0.5 \end{bmatrix}, \text{ and } \quad \mathbf{D} = \begin{bmatrix} -\dfrac{\gamma}{2} \end{bmatrix}.$$

The overall state equations are:

$$
E \begin{bmatrix} q_1 \\ q_2 \\ q_3 \end{bmatrix} = \begin{bmatrix} 0 & -\gamma & 0 \\ 1 & 0 & 0 \\ 0 & 0 & 0 \end{bmatrix} \begin{bmatrix} q_1 \\ q_2 \\ q_3 \end{bmatrix} + \begin{bmatrix} \gamma-1 \\ 0 \\ 0 \end{bmatrix} x(n) \tag{3.30}
$$

and
$$
y = \begin{bmatrix} 0 \\ \dfrac{(\gamma-1)}{2} \\ 0.5 \end{bmatrix} \begin{bmatrix} q_1 \\ q_2 \\ q_3 \end{bmatrix} + \begin{bmatrix} -\dfrac{\gamma}{2} \end{bmatrix} x(n) \tag{3.31}
$$

From (3.31) and (3.30), one may see that the output y is directly controllable by γ and so are q_1 and q_2. The relationships between γ, y, q_1 and q_2 imply that any change of γ will lead to a change in both y and the state values. Although the current output y can be adjusted to what we desire, the next output will be anything depending on the next input and next state values. To make sure the filter keeps producing the desired output in the subsequent operation, the control algorithm has to continuously track both the state values and the input. This nonlinear control mechanism will become an extra loop of the recursive filter. The overall nonlinear system's stability is thus not guaranteed [5]. One may see that the coefficient adaptive approach is quite different from the state value updating technique. In the later case, the control algorithm is simply a decision algorithm. After the algorithm has decided to change the state value, it just changes the state value and no further tracking or adaptation is needed. This prevents the algorithm from forming a closed loop and thus the system remains stable.

As well as using the output and state value tracking method described above, it still seems possible to have the parameter controlling algorithm work in the same way as state value updating does. From (3.30), because the coefficient γ can control the state value, whenever the control algorithm finds a discontinuity, it can find a proper coefficient γ to make Eq_1 to be the steady-state state value. No further tracking of the output and state values are necessary. However, because the current output y is also related to γ, any change accorded the value Eq_1 will also affect the current output. This will generate a single peak whenever the state value is changed.

We have seen two different approaches to using the varying coefficient γ. If the parameter is used to control the output directly, the whole system will become recursive and nonlinear. If on the other hand, the parameter is used to control the state value, the response will have an unwanted peak at the instant that the parameter changes. It is apparent that state value updating is an unique approach and is different from that using the adaptive coefficient method.

3.3 Frequency Spectra of the Output Produced by State Value Updating

State value updating is a nonlinear operation and it is decision-based. The nonlinear behavior makes its impulse response not representative. However, the non-linearity does not prevent us from examining different types of input-output frequency characteristics individually. By doing so, we can have a coarse picture of the nonlinear filter.

In this section, a list of common waveforms such as a step, an impulse, a ramp, and a pulse train are used to test the SVU WDF. Each waveform will be lowpass filtered by either the WDF or SVU WDF. Both the shapes and the frequency spectrum of the outputs will be compared. Moreover, each waveform will be downsampled and upsampled by a factor of eight using WDF or SVU WDF as the antialias and interpolation filters. By the conversion process, artifacts such as alias or phase distortion will be clearly visible. Furthermore, the decision algorithm used to control the filters will be presented in Chapter 4.

3.3.1 Test Results and Spectra

3.3.1.1 Step Response

As mentioned in the beginning of this chapter, the step function is important because it represents the boundary between objects. Using the suggested 1-D WDF, an input step shown in Figure 31, has an output shown in Figure 32 and the spectrum shown in Figure 33. Note that the ringing oscillates after the boundary in Figure 32. When the step is processed with the SVU technique, the output response is given in Figure 35 and it is clear that ringing is eliminated. The SVU processed spectrum is shown in Figure 36. One may see that the spectrum in Figure 36 and Figure 33 are very similar. Their frequency content above 0.25 radian/sec is mostly below -35 dB. Figure 34 and Figure 37 show the outputs after ½ downsampling and 2 times upsampling using the WDF and SVU respectively. The downsampling operation will overlap the spectrums so that aliasing will occur if the signal is not antialiased properly. From Figure 34 and Figure 36, after up/downsampling the SVU-filtered step retains its shape without any

noticeable aliasing. On the other hand, the WDF-filtered step has a large amount of ringing.

3.3.1.2 Impulse Response

Unlike the step input, an impulse contains uniform energy over the spectrum. When it is SVU-filtered, the residual spectrum above the halfband is still significant. The output and the output spectrum of an impulse response using the 1-D WDF are shown in Figure 38 and Figure 39 and the SVU-processed impulse response and the spectrum are in Figure 41 and Figure 42. Comparing Figure 38 and Figure 41, the ringing on Figure 41 is eliminated. However, when comparing the spectrums on the Figure 39 to Figure 42, it is evident that Figure 39 has more high frequency energy. The signal is then further downsampled and upsampled and followed by an interpolation. The impulse produced by the SVU remains the same (Figure 40). On the other hand, the WDF-filtered down/upsampled impulse (Figure 43) exhibits a serious ringing problem.

3.3.1.3 Pulse Train

Since the SVU detects discontinuity, it is useful to know if the SVU is capable of interpolating a downsampled DC signal. A pulse train representing downsampled DC is shown in Figure 44. It is known that the downsampled DC has a very strong peak at $f = 0.5$. The interpolated output using 1-D WDF is shown in Figure 45. The output is a constant DC level as expected. The SVU-processed output is shown in Figure 46. Again, it is a constant DC level.

3.3.1.4 Square Pulse

Repeating square pulses can model uniform high frequency texture. The input and output of the 1-D WDF are shown in Figure 47, Figure 48 and Figure 49 respectively. One may see from Figure 51 and Figure 52 that the SVU-processed output retains much of the shape of the original signal. The spectrum is also similar to the one produced by the WDF shown in Figure 49. However, after down/up sampling followed by an interpolation, the SVU-filtered result shows some aliasing in which the shape of the pulses are distorted (Figure 53) compared with the WDF-

reconstructed pulses in Figure 50. The rapid resetting of the state value due to the square pulses causes the aliasing.

3.3.1.5 Ramp Response

A common pattern is a continuous tone change which can be modeled by a ramp function. The input and output using the 1-D WDF are shown in Figure 54. The output and the spectrum produced by the 1-D WDF is shown in Figure 55 and Figure 56. The results produced by SVU shown in Figure 58 and Figure 59 have no significant differences from the one produced from the WDF alone.
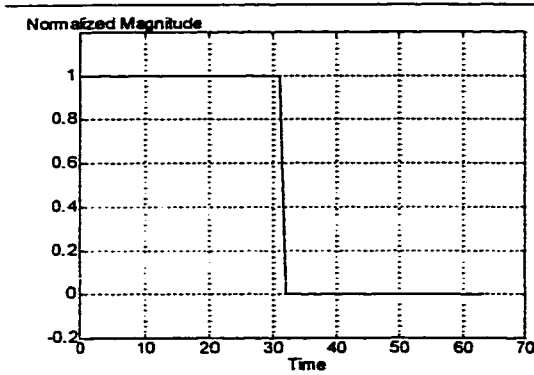
Figure 31. Input Step Function
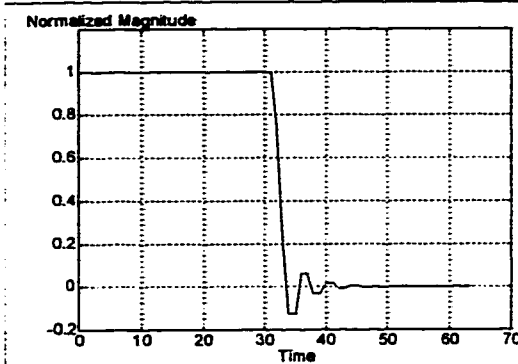
Figure 32. Step Response of the 1-D WDF with Coefficient = 0.5
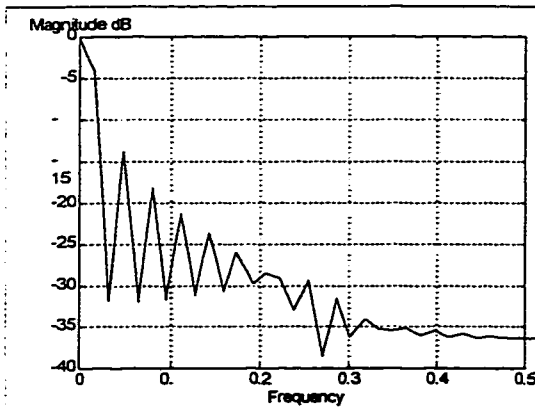
Figure 33. Spectrum of the Step Response using the WDF
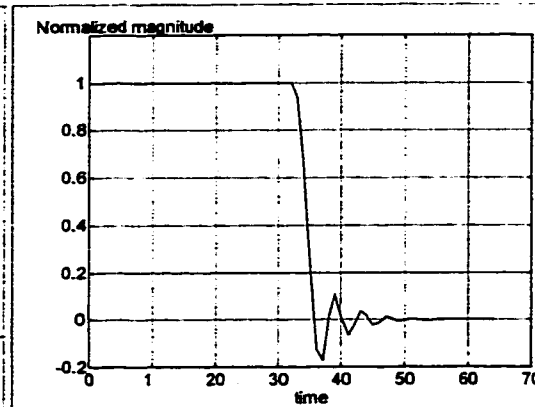
Figure 34. Down/Upsampled Step Response using the WDF
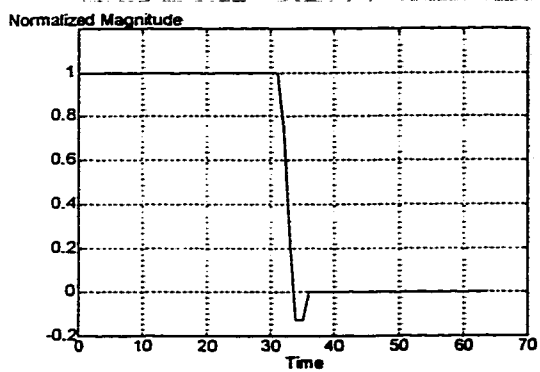
Figure 35. Step Response of the 1-D WDF using the SVU
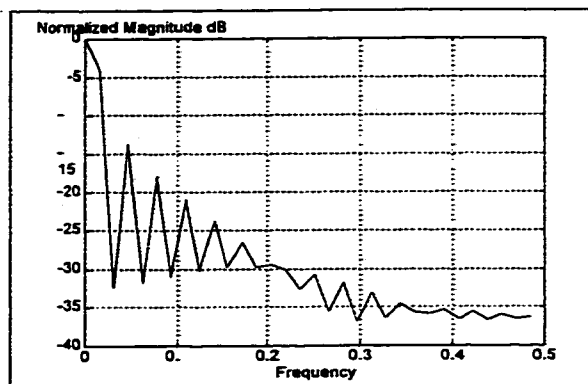
Figure 36. Frequency Spectrum of the Step Response using the SVU
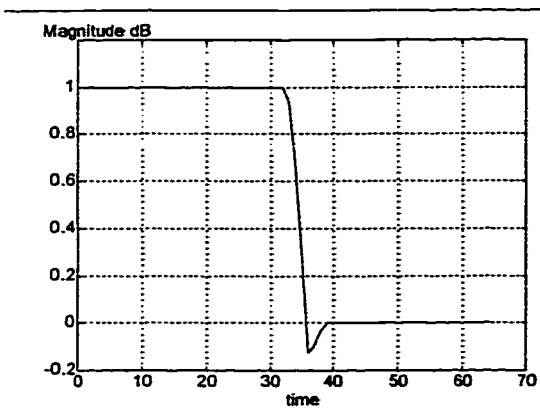
Figure 37. Down/Upsampled Step Response using the SVU
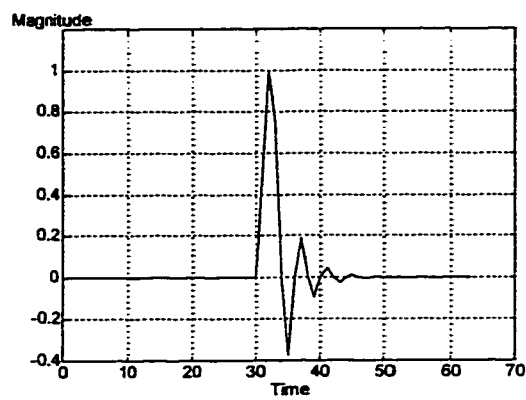
Figure 38. Impluse Response of the 1-D WDF
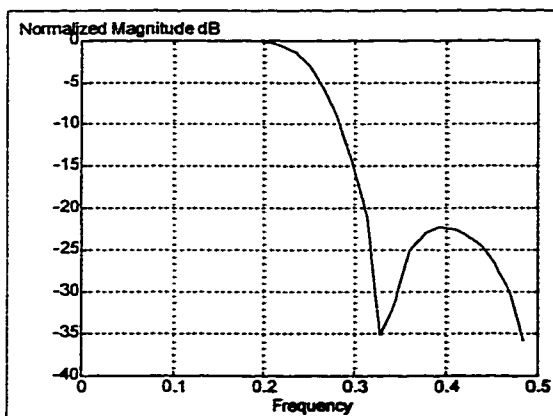
Figure 39. Frequency Spectrum of the Impluse Response
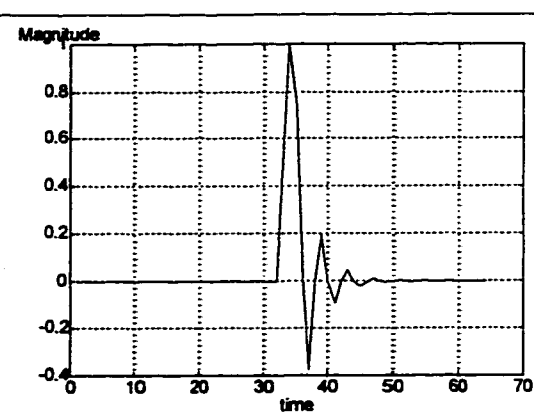
Figure 40. Down-Upsampled Impulse Response using the WDF

59
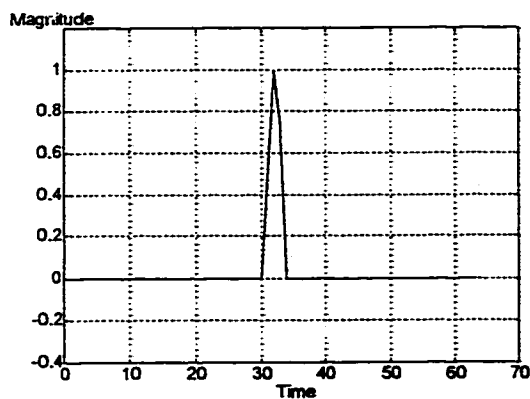
Figure 41. Impluse Response of the 1-D WDF using the SVU
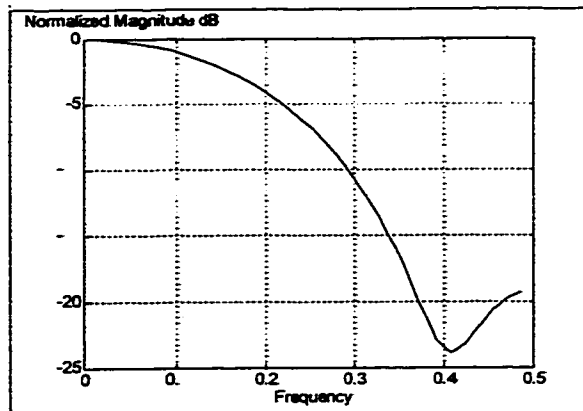
Figure 42. Frequency Spectrum of the Impluse Response using the SVU
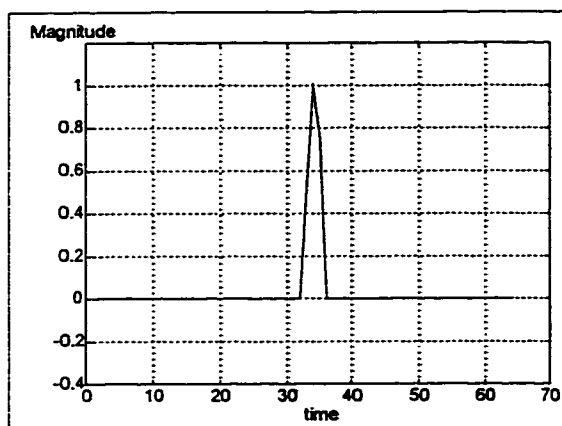
Figure 43. Down/Up-sampled Impulse Response using the SVU
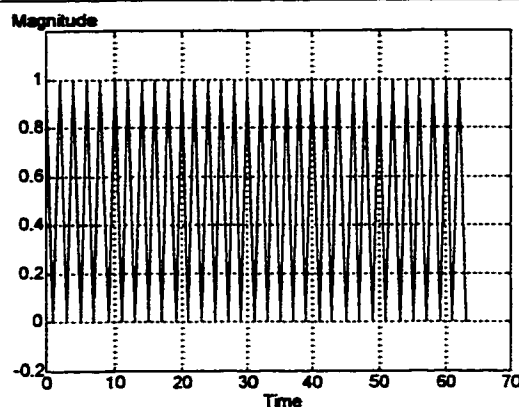
Figure 44. Input Pulse Train
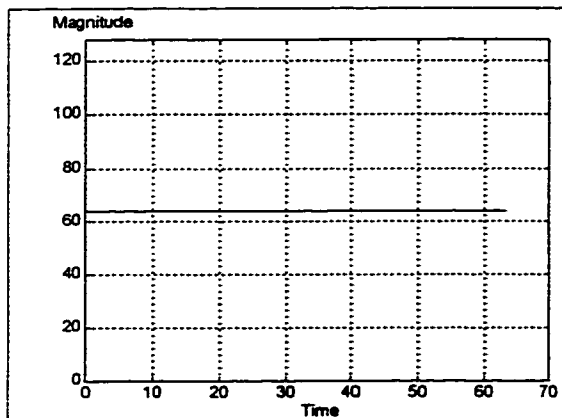
Figure 45. Pulse Train Response of the 1-D WDF
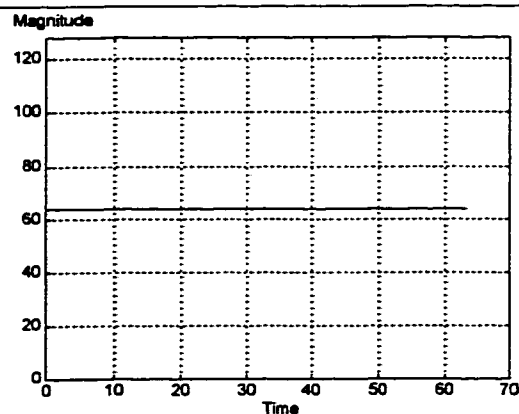
Figure 46. Pulse Train Response of the 1-D WDF using the SVU

60
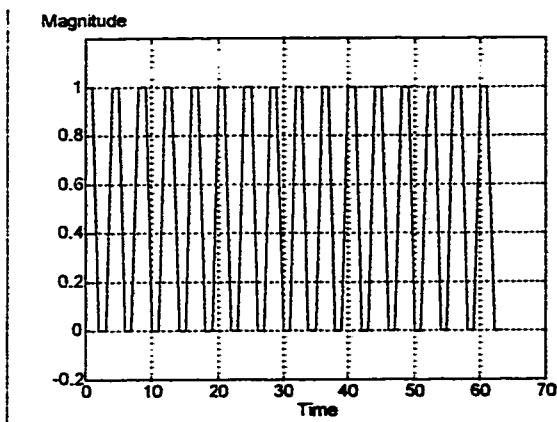
Figure 47. Input Square Pulses
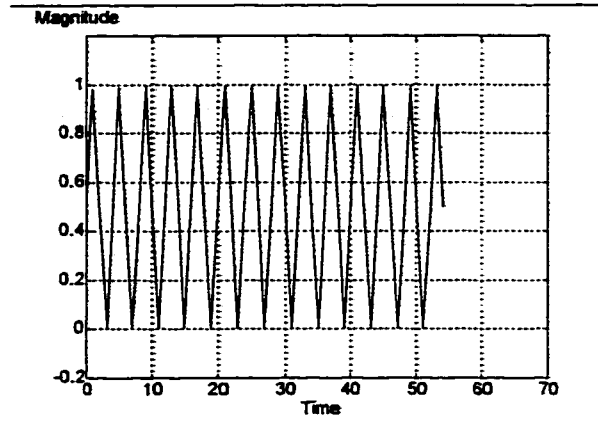
Figure 48. Square Pulses Response of the 1-D WDF
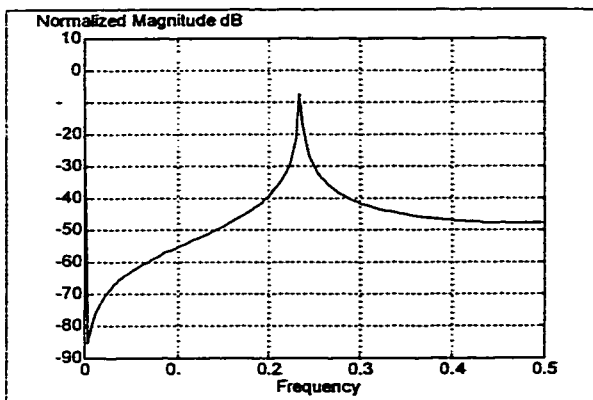
Figure 49. Frequency Spectrum of the Square Pulses 1-D WDF Response
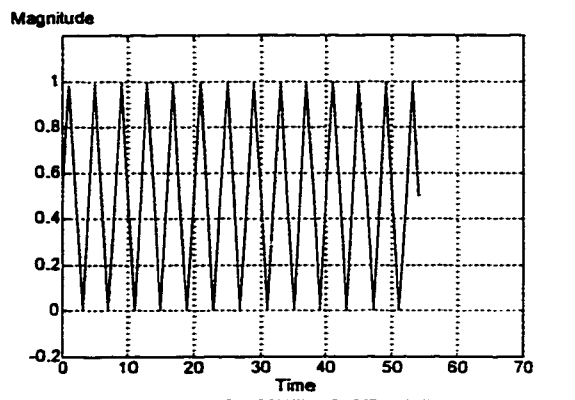
Figure 50. Down/Up-sampled Square Pulses Response using the WDF
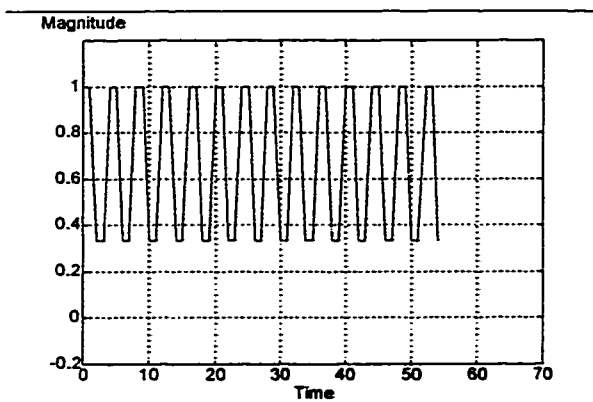
Figure 51. Square Pulses Response of the 1-D WDF using the SVU
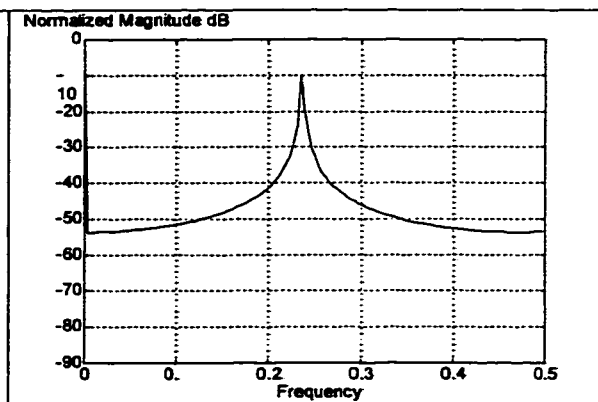
Figure 52. Frequency Spectrum of the Square Pulses Response using the SVU

61
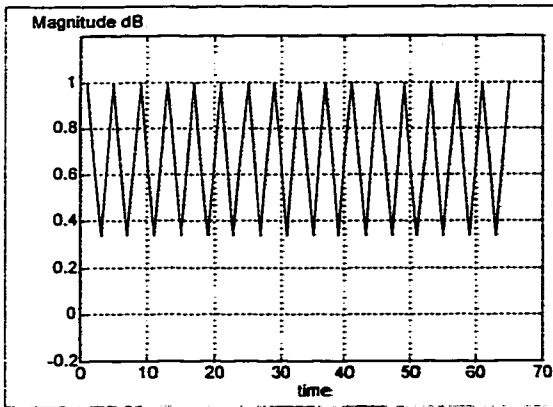
Figure 53. Down/Up-sampled Square Pulses Response using the SVU
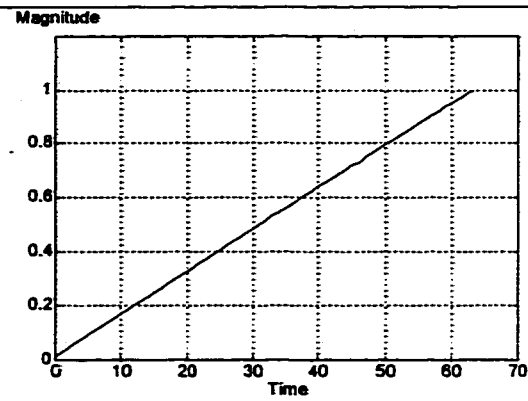
Figure 54. Input Ramp
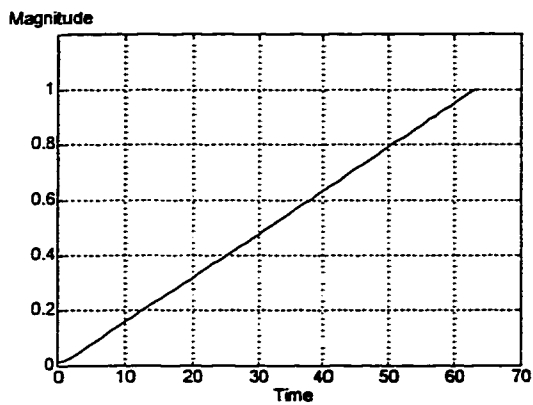
Figure 55. Ramp Response of the 1-D WDF
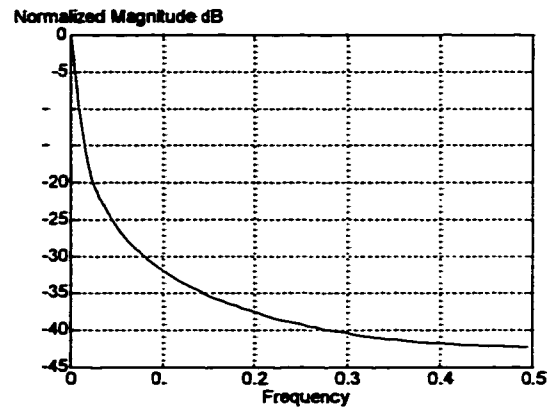
Figure 56. Frequency Spectrum of the Ramp Response Using the WDF
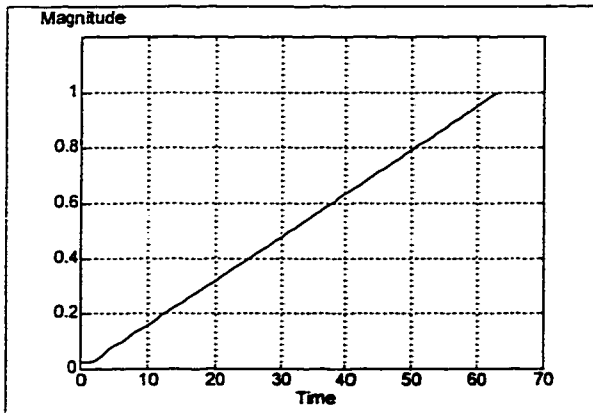
Figure 57. The Down/Up-sampled Ramp Response Using the WDF
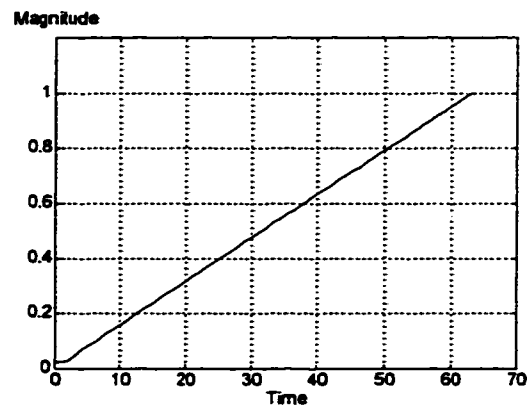
Figure 58. Ramp Response of the 1-D WDF Using the SVU
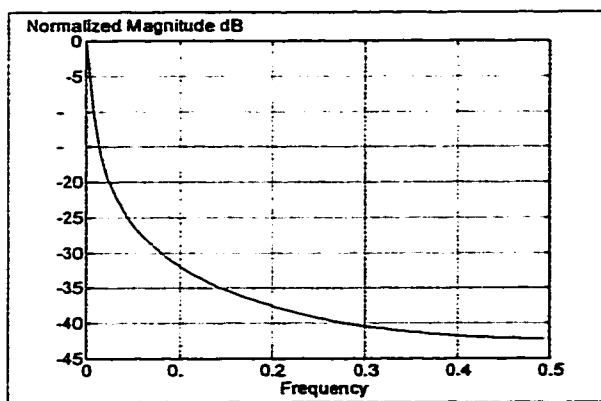
Figure 59. Frequency Spectrum of the Ramp Response Using the SVU
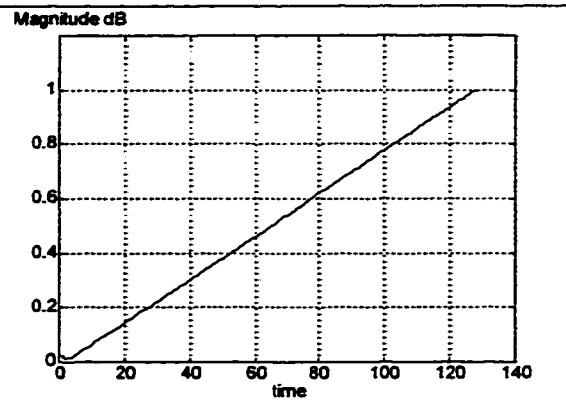
Figure 60. Down/Up-sampled Ramp Response Using the SVU

3.3.2 Diamond Filter

In previous section, we have seen the different responses of the 1-D WDF with an SVU. In this section, step and impulse will be tested on the 2-D diamond WDF using an SVU. Again, antialias filtering, down and upsampling followed by interpolation will be demonstrated.

3.3.2.1 Impulse Response

The 2-D impulse response of the diamond filter is shown in Figure 61 and the spectrum in Figure 62. In Figure 61, one will see that ringing appears after the main pulse. The ringing is not present in the SVU-processed impulse response shown in Figure 64. The corresponding spectrum in Figure 65 has lost all its sharp cutoff characteristic compared with Figure 62. The (1,1) square-quincunx (1,1) quincunx-square down/up sampled interpolated output are in Figure 63 and Figure 66 for the WDF and SVU consecutively. The WDF-filtered output in Figure 63 exhibits strong ringing while the SVU-filtered output has no ringing yet still keeps the shape of a lowpassed impulse.

3.3.2.2 Step Response

Another important shape is the step function. In Figure 67, a step function is introduced representing discontinuity in x, y and diagonal directions. The diamond-filtered response

63

is given in Figure 68 and the spectrum is shown in Figure 69. Similarly the SVU response is given in Figure 68 and the spectrum in Figure 72. One may notice the massive amount of ringing occurring in Figure 68 has been effectively eliminated in Figure 71. This represents an improvement of image. Moreover, the first overshoot remaining in Figure 71 enhances the contrast of the boundary. The spectrums in Figure 69 and Figure 72 have no significant difference except for a certain amount of diagonal frequency component remaining above ½ of the diagonal spatial frequency. The (1,1) square-quincunx (1,1) quincunx-square down/up sampled interpolated output are shown in Figure 70 and Figure 73 for the WDF-filtered and SVU-filtered waveform consecutively. The WDF-processed output (Figure 70) has very serious ringing after the discontinuity. The SVU result (Figure 73) has retained the shape without ringing.
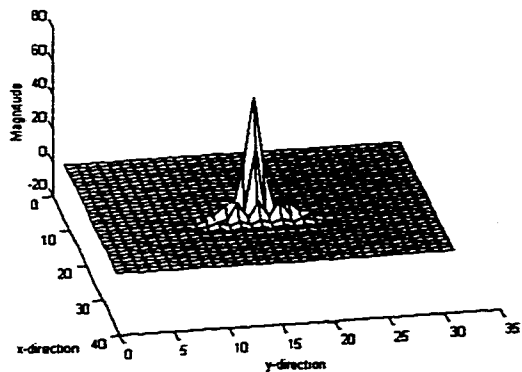
Figure 61. Impulse Response of the Diamond Filter
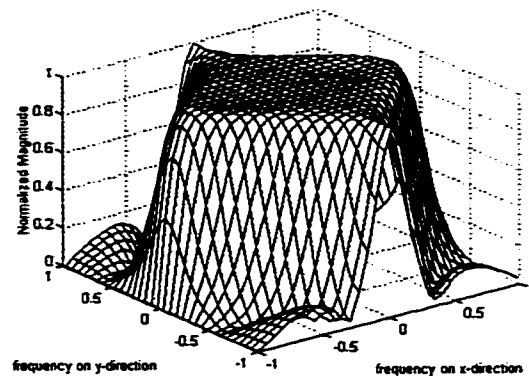
Figure 62. Spectrum of the Impulse Response Using the Diamond filter
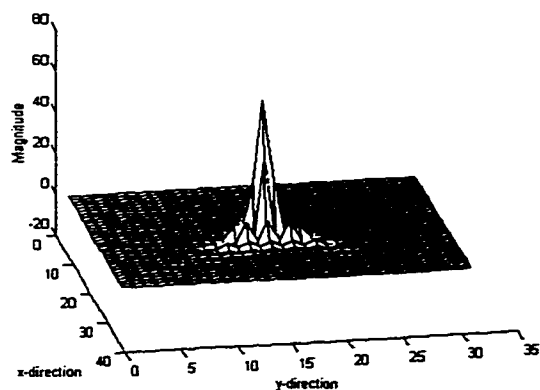
Figure 63. Down/Up-Sampled Impulse Response Using the WDF
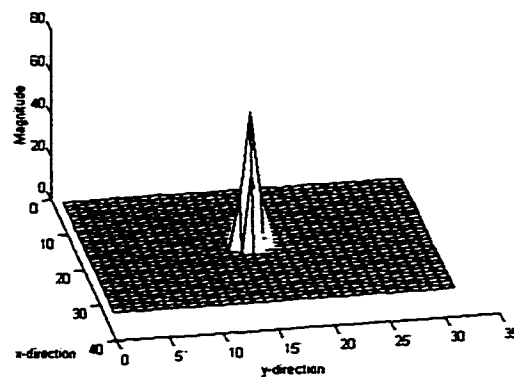
Figure 64. Impulse Response of the Diamond Filter Using the SVU
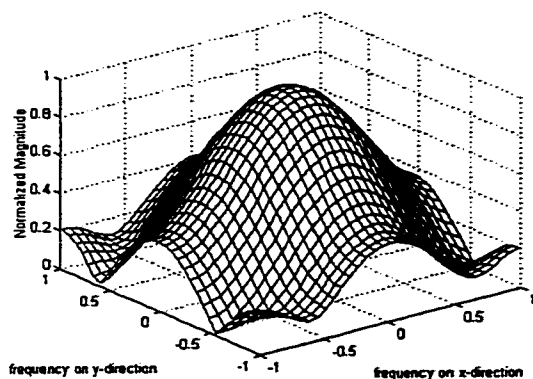
Figure 65. Spectrum of the Impulse Response Using the SVU
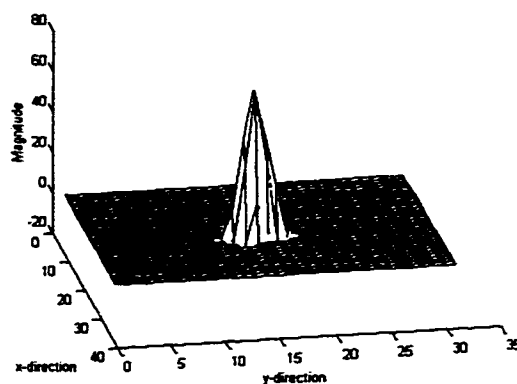
Figure 66. Down/Up-Sampled Impulse Response Using the SVU

65
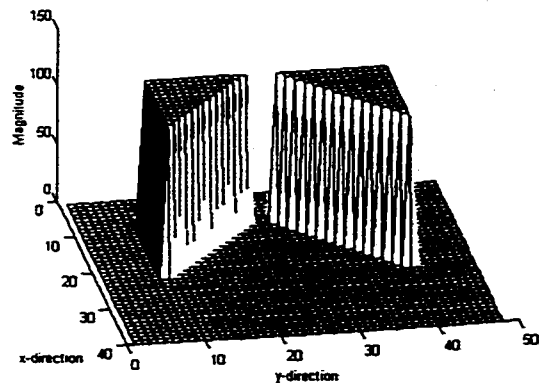
Figure 67. Step function in Diagonal and x-y Direction
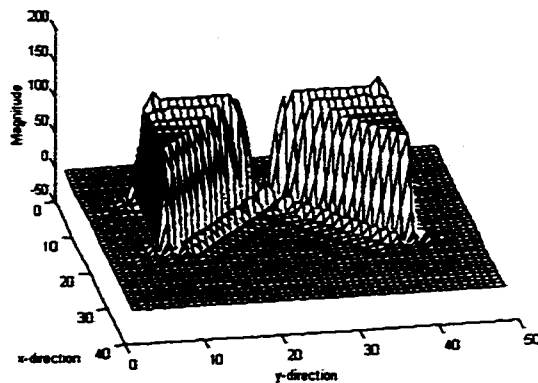
Figure 68. Step Response of the Diamond WDF
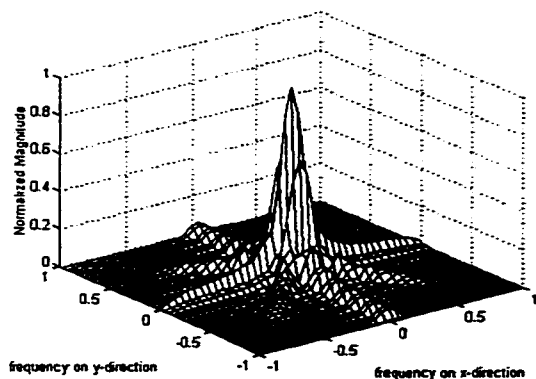
Figure 69. Spectrum of the Step Response Using the WDF
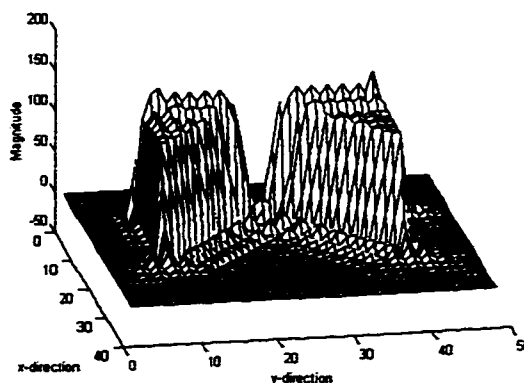
Figure 70. Down/Up-Sampled Step Response Using the WDF
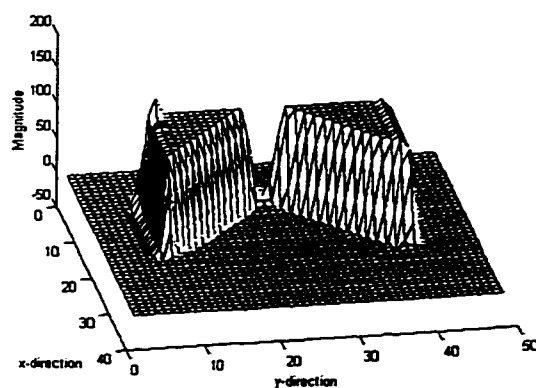
Figure 71. Step Response of the Diamond Filter Using the SVU
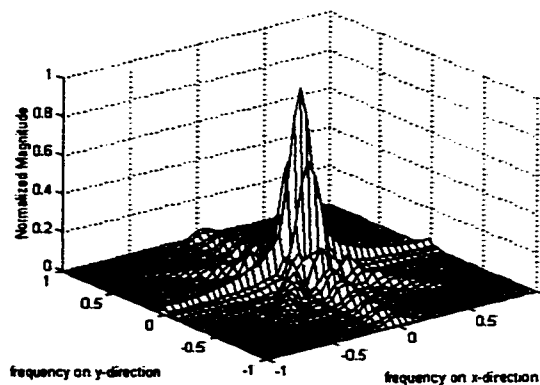
Figure 72. Spectrum of the Step Response Using the SVU

66
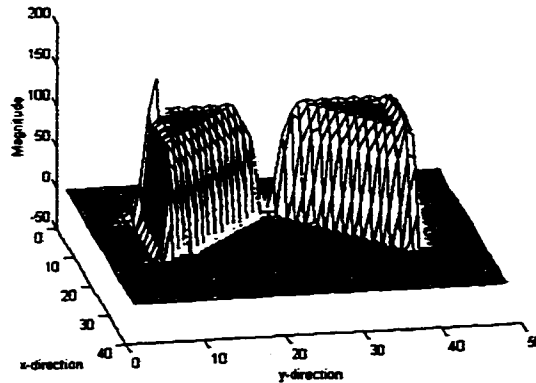
Figure 73. Down/Up-Sampled Step Response Using the SVU

3.4 Summary

In this chapter, we have examined the development of the state value updating technique. With the state value assignments presented in this chapter, one may use the steady-state factor to calculate the steady-state state value for the filters. If the state value is updated at the proper moment, the ringing can be eliminated by explicitly making the filter "forget" the previous discontinuity. The coefficient adaptive method has also been discussed. Because of the nature of the suggested WDFs, the coefficient is closely related to the output and the state values, and hence a closed loop from the output to the adaptive algorithm is needed. This nonlinear feedback system is not guaranteed to be stable and is quite different from the structure of the SVU filter. If the algorithm is used to control the coefficient so that the state-value changes as an SVU filter, the output will exhibit spurious peaks.

At the end of this chapter, different waveforms were used to test and compare the response of the SVU with WDF. We have seen that SVU can eliminate ringing in most cases while keeping a certain amount lowpass filtering adequate for sampling structure conversion. In later chapters, more simulation using images and video sequences will be

67

presented. The decision algorithms that have been omitted from this chapter will be presented in the later chapters.

References

[1]   R. H. Fletcher and D. W. Burlage, "An initialization technique for improved MTI performance in phase array radars, " Proc. IEEE, vol. 60. pp. 1551-1552, 1972

[2]   W. S. Chornoboy, "Initialization for improved IIR filter performance," IEEE Trans. Signal Processing, VOL., (30, NO. 3, pp.543-550, March, 1992

[3]   R. J. Mayhan, *Discrete-Time and Continuous-Time Linear System*, Addison-Wesley, Reading, Mass. 1983

[4]   L. Gazsi, "Explicit Formulas for Lattice Wave Digital Filters, " *IEEE Transaction on Circuit and Systems*, VOL. CAS-32, NO.1, January 1985.

[5]   K. S. Narenda, A. M. Annaswamy, *Stable Adaptive Systems*, Prentice Hall, Englewood Cliffs, N. J. 1989.

4 (*L,K*)Quincunx and Rectangular Sampling Structure Conversions Using the State Value Updating Technique

4.1 Introduction

A digital image is a discrete 2-D signal, which is obtained by 2-D sampling. Unlike a 1-D sampling process, sampling a 2-D signal requires specification of both of the sampling frequency and the sampling structure. The sampling structure describes the geometry of the sampling process and it has its own frequency characteristic. The frequency characteristic is an important factor for determining how efficient a particular sampling geometry is. For instance, the commonly used rectangular structure [1] is not the most efficient structure in terms of frequency density [2]. Therefore, from time to time, alternative sampling structures are used for certain applications to take full advantage of different structures. Thus, a sampling structure conversion process is needed to convert digital images into different sampling structures. In this chapter, we will examine rectangular-quincunx sampling structure conversions using 2-D lowpass filtering. The 2-D conversions can be used spatially for HDTV systems and spatiotemporally for digital television deinterlacing [3] as described in Chapter 6.

4.2 (*L,K*) Rectangular and Quincunx Sampling Structure Conversions

Consider a 2Dimensional image $x(t_1, t_2)$ in a continuous spatial domain. The spatial Fourier transform is given as $X(\omega_1, \omega_2)$. Assuming the signal to be band-limited in a rectangular region such that

$$X(\omega_1, \omega_2) = \begin{cases} X^*(\omega_1, \omega_2) & \text{if } |\omega_1 T_1| < \pi, \ |\omega_1 T_1| < \pi, \\ 0 & \text{otherwise.} \end{cases} \tag{4.1}$$

where T_1 and T_2 are positive constants. The signal $x(t_1, t_2)$ can be sampled into a discrete signal $x(mT_1, nT_2)$ without any loss of information [4]. Since this is a two-dimensional sampling process, the *structure* (sampling rate and the geometry) of the sampling process is needed. For the sampled signal $x(mT_1, nT_2)$, it has a rectangular sampling matrix [5] which is called a basic sampling matrix **R** [6] such that:

$$\mathbf{R} = \begin{bmatrix} 1 & 0 \\ 0 & 1 \end{bmatrix}, \tag{4.2}$$

and the sampling process can be described by using the sampling matrices **R** so that

$$t' = \begin{bmatrix} t_1 \\ t_2 \end{bmatrix} = \mathbf{R} \begin{bmatrix} mT_1 \\ nT_2 \end{bmatrix}. \tag{4.3}$$

A subset of the basic sampling matrix **R** is a parameterized rectangular $\mathbf{R}_{L,K}$ structure and a parameterized quincunx sampling structure $\mathbf{Q}_{L,K}$ [5]. Their sampling matrix are given in (4.4) and (4.5) as

$$\mathbf{R}_{L,K} = \begin{bmatrix} L & 0 \\ 0 & K \end{bmatrix}, \tag{4.4}$$

$$\mathbf{Q}_{L,K} = \begin{bmatrix} L & L \\ K & -K \end{bmatrix}. \tag{4.5}$$

where L and K are positive integers. The sampling matrix $Q_{L,K}$ represents the sampling structure the spectrum shown in Figure 74[3].
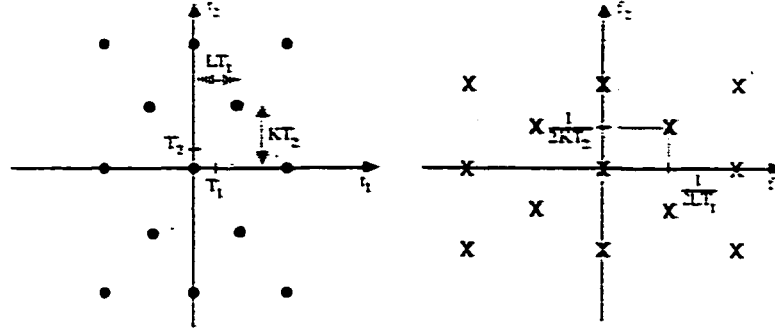
Figure 74. $Q_{L,K}$ **Sampling Structure and the Spectrum**

To convert a basic rectangular structure to an (L,K) quincunx structure, an (L,K) diamond filter is used to band-limit the signal spectrum. The band-limited signal is then decimated using an (L,K) quincunx matrix. For conversion from an (L,K) quincunx to a basic rectangular structure, the signal is upsampled and interpolated by a 2D (L,K) rectangular lowpass filter. A block diagram for the sampling structure conversion process between a quincunx and a basic rectangular structure is shown in Figure 75.
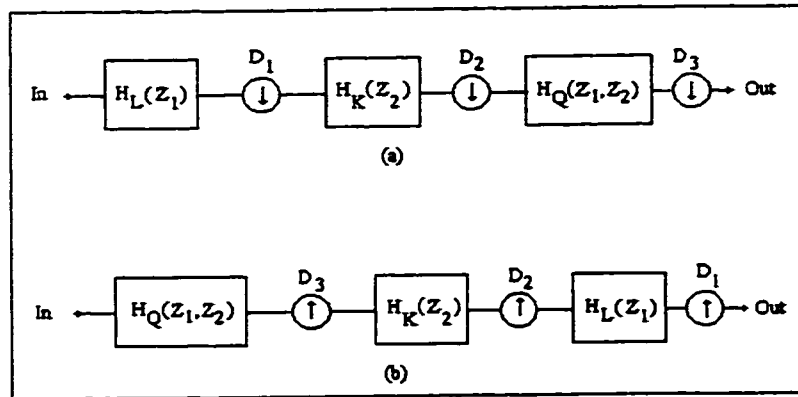
Figure 75. Conversions between a basic rectangular structure and a quincunx structure

(a) Conversion from a basic rectangular to a (Q, K) quincunx, (b) Conversion from a (Q,K) quincunx to a basic rectangular.

72

4.3 Sampling Structure Conversion Using WDFs

The 2-D diamond WDFs and the 1-D WDF suggested in Chapter 2 are used in this chapter. To achieve a sampling rate reduction by a factor of 8, a (2,2) diamond filter is needed (see Figure 76). The diamond filter mentioned in Chapter 2 is actually a (1,1) diamond filter. In order to obtain a (2,2) filter, the suggested 1-D lowpass filters are cascaded with the (1,1) diamond filter.
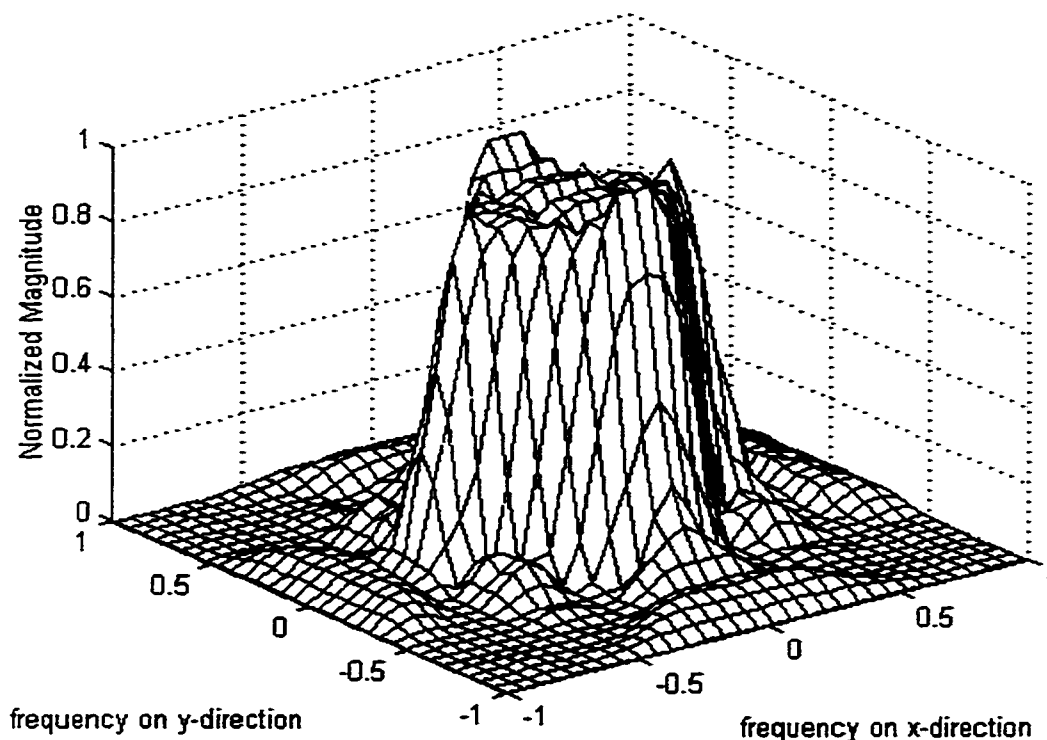
Figure 76. The Spectrum of the (2,2) Diamond Filter

One may use the cascaded configuration shown in Figure 75 to obtain the (2,2) frequency characteristic. The rectangular image is first lowpassed by the suggested 1-D WDF in both the x and y directions. It is then decimated into a quarter of its original size followed by a (1,1) diamond filter and a (1,1) quincunx decimation. One may reverse the sampling structure from a (2,2) quincunx structure to the original rectangular structure using the WDFs. The (2,2) quincunx structure is first upsampled to a (1,1) quincunx structure. The

73

(1,1) diamond WDF then interpolates it. The resulting (1,1) quincunx image is then again upsampled in both the x and y directions and is interpolated by the 1-D WDFs.

Although the WDFs are nearly linear, phase distortion will still exists even with a small coefficient value. A multiple IIR filtering process such as the cascaded method shown in Figure 75 will causes the phase to accumulate. To reduce the phase error, one may use anticausal filtering [6].

4.4 Conversion Using State Value Updated WDFs

To effectively reduce ringing caused by phase distortion, an SVU technique is used with the WDFs. As demonstrated in Chapter 3, the frequency content of the signal filtered by a (2,2) diamond filter using SVU will not be the same as the one filtered by the WDFs alone. In other words, some unwanted high frequency components may remain or even be generated during the nonlinear operations. This implies that after a sampling structure conversion process using SVU, aliasing is unavoidable and perfect reconstruction is unlikely. Fortunately, most images can be modeled by a first-order Markov process [7], which contain mostly low frequency components. The weak high frequency components contained in these images do not cause significant aliasing even without much attenuation. Therefore, SVU filters are adequate for these kinds of images and processes.

4.4.1 Decision Algorithm for Sampling Structure Conversion

The objective of the decision algorithms used in both 1-D and 2-D SVU filters are to detect any discontinuity that may introduce noticeable ringing. In the case of 1-D filtering, the algorithm is relatively simple, and the sole responsibility is to detect a single discontinuity.

The decision algorithm is presented as the follows:

```
factor = (coeff - 1)/(coeff +1)
if abs(x(i) - x(i-2)) > threshold(x(i))
{
        State1 = x(i) * factor
}
```

The value *coeff* used in the algorithm is the adapter coefficient. The value *factor* is the factor Γ shown in Chapter 3 used to calculate the state value during the steady state. The value *State1* is the state value q_1 defined in Figure 27. The value *threshold* is a pre-defined vector corresponding to the Just Noticeable Difference (JND) and is a function of the luminance $x(i)$. The algorithm should be located inside the loop of the WDF. Within the loop, the algorithm should check for the difference between the current pixel $x(i)$ and

75

the previous pixel $x(i-2)$. If the discontinuity exceeds the threshold, the state value will be set to its steady-state value using $x(i)$ after the first overshoot.

In the case of diamond filtering, our interest is to stop ringing only in the diagonal directions. The decision algorithm should detect diagonal discontinuity that contributes to ringing during diamond filtering. To ensure that the algorithm only activates on diagonal discontinuities, additional decisions have to be made for finding the discontinuities in the x and y directions. If only vertical or horizontal edges exist, the algorithm will not activate the SVU mechanism and this part of the image will be filtered in a normal linear manner.

When a discontinuity occurs, various frequency components of the discontinuity propagate diagonally at various speeds. In a 1-D filtering process, the directions of propagation are obvious, since it only has one dimension. For the 2-D situation, the ringing is spread over several directions as shown in Figure 77 for a (1,1) diamond filter.
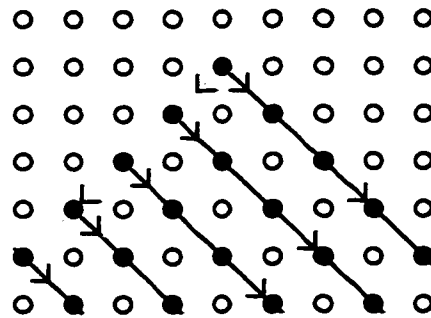
Figure 77. Routes of propagation for a (1,1) Diamond WDF filtered impulse

One may notice that by stopping the ringing in the dotted-line direction, the ringing can still propagate in the solid-line directions. In order to restrict the impulse response to a limited area, the following algorithm is suggested:

The algorithm has two parts. The first one resides right after processing the $Z_1^{+1}Z_2^{-1}$ direction and is shown below:

```
d1=(int)abs(x(i+1, j-1)-x(i+2, j-2));
if (d1 > threshold(x(i,j)))
{
        d4=abs(x(i+2, j-2)-x(i+3, j+1));
        d5=abs(x(i+2, j-2)-x(i+3, j-1));
        d6=abs(x(i+2, j)-x(i+3, j+1));
        d7=abs(x(i+2, j)-x(i+3, j-1));
        if (NOT ((d4>thrsh) AND (d5>thrsh) AND
                (d6>thrsh) AND d7>thrsh)))
        {
                tc1(i) = x(i, j)*factor;
                Stop_Flag(i, 2) = 1;
        }
        else
        {
                Step = 1;
        }
}
```

The second part follows processing in the $Z_1^{+1} Z_2^{-1}$ direction and is shown in the following:

```
d8=abs(x(i-1, j-1)-x(i-2, j-2));
if (d1 > thshd_vect(x(i, j)))
{
        dump=x(i, j)*factor;
        td1(i, 1)=c1*(s3Dump)-s3;
};
/*CHECK FOR STOP FLAGS */
if ((Stop_Flag(i-1, 1) == 1) OR (Stop_Flag(i-3, 1) == 1))
{
        d2=abs( x(i, j)-x(i-1, j-1));
        d3=abs(x(i, j)-x(i+1, j-1));
        if (NOT ((d2 >thrsh)
                OR (d3>thrsh)
                OR (Stop_Flag(i, 1))
                OR (Step == 1))
        {
                dump=x(i, j)*factor;
                td1(i, 1)=c1*(s3Dump)-s3;
        };
};
```

The 2-D algorithm will first perform ordinary WDF filtering in the $Z_1^{+1} Z_2^{-1}$ direction followed by discontinuity detection between $x(i+1, i-1)$ and $x(i+2, i-2)$. If a discontinuity in the diagonal direction exists, the algorithm will use the difference $d4$, $d5$, $d6$ and $d7$ to determine if a line discontinuity in the x direction is also present. If so, the algorithm proceeds as a WDF with no intervention. If there is no step on the x direction, the state value will be updated using the steady-state state value and the *Stop_Flag(i)* will be set to

1 to prevent the ringing from propagating in the $Z_1^{-1}Z_2^{-1}$ direction. If there is indeed a step in the x direction, the *Step* flag is set to 1 and no adaptation will be done.

After processing in the $Z_1^{+1}Z_2^{-1}$ direction, the process in the $Z_1^{-1}Z_2^{-1}$ direction will continue. The second half of the WDF filtering proceeds and is followed by another discontinuity detection scheme. The detection scheme uses *d8* to determine if there is a discontinuity in $x(i-1, j-1)$ and $x(i-2, j-2)$. If so, the algorithm will proceed and test for the presence of the *Stop_Flag* inherit from the previous calculation. Furthermore, the algorithm has to make sure that there is no discontinuity immediately adjacent to either the discontinuity or any vertical step so that excessive updating of the state value is less likely to occur.

Although the 2-D algorithm may have a complex appearance, most of the decisions and detection can be done concurrently. Therefore, the extra time for decision and detection is not significant. The only drawback may be the additional lines of buffers required for holding the input data and the Stop_Flags.

4.5 Simulations

In the simulations to follow, two images are used for testing. Each image will be converted from a (1,1) rectangular to a (2,2) quincunx structure. The (2,2) structure is then converted back to a (1,1) rectangular conversion as described in Figure 75. The process simulates a coding and decoding process with a compression ratio of 8. The chosen images are Lenna (Figure 78), and Harbor (Figure 84). The FIR filter suggested in [3], WDFs [6], and WDFs with an SVU technique will process each image. Both the WDF and SVU WDF simulations have causal filtering and anti-causal filtering. Both the 1-D and 2-D WDF filters use 0.5 as the adaptive coefficients. Although there is no reliable objective picture quality assessment available [7] [8], the mean square error (MSE) and signal to noise ratio (SNR) are presented with the results nevertheless. The calculation of MSE is based on Equation (4.5).

$$\text{MSE} = \left[\frac{1}{nm} \sum_{j=1}^{m} \sum_{i=1}^{n} (x_{i,j} - y_{i,j})^2 \right]^{\frac{1}{2}}. \tag{4.5}$$

The value $x_{i,j}$ is the pixel from the original picture and $y_{i,j}$ is the pixel from the processed picture. The calculation of SNR is given as:

$$\text{SNR} = 10 \log_{10} \left[\frac{\sum_{j=1}^{m} \sum_{i=1}^{n} x_{i,j}^2}{\sum_{j=1}^{m} \sum_{i=1}^{n} (x_{i,j} - y_{i,j})^2} \right] \tag{4.6}$$

For the FIR filter, the impulse response has a 9x9 region of support and is given as[3]:

$$FIR = \frac{1}{32}\begin{bmatrix}
-1 & -3 & -2 & 0 & 0 & 0 & -2 & -3 & -1 \\
-3 & -2 & -1 & 2 & 4 & 2 & -1 & -2 & -3 \\
-2 & -1 & 4 & 8 & 12 & 8 & 4 & -1 & -2 \\
0 & 2 & 8 & 14 & 20 & 14 & 8 & 2 & 0 \\
0 & 4 & 12 & 20 & 20 & 20 & 12 & 4 & 0 \\
0 & 2 & 8 & 14 & 20 & 14 & 8 & 2 & 0 \\
-2 & -1 & 4 & 8 & 12 & 8 & 4 & -1 & -2 \\
-3 & -2 & -1 & 2 & 4 & 2 & -1 & -2 & -3 \\
-1 & -3 & 2 & 0 & 0 & 0 & -2 & -3 & -1
\end{bmatrix}$$

The sampling structure conversion results for the image Lenna are shown in Figure 79 (FIR filter only), Figure 80 (WDFs only), Figure 81 (SVU WDFs only), Figure 82 (causal WDFs with anticausal WDFs), and Figure 83 (WDFs with anticausal SVU WDFs). By comparing the FIR-filtered Lenna in Figure 79, WDF-filtered Lenna in Figure 80 and SVU-filtered Lenna in Figure 81, it is seen that the FIR-filtered picture is blurred but free of ringing. This result is expected, because FIR filters have linear phase. The result produced by WDFs remains sharp because of the sharp cutoff and boundary overshoots. On the other hand, the ringing is serious. For the SVU-filtered picture in Figure 81, the result has no noticeable ringing and the sharpness is comparable to the picture filtered by WDF.

With anticausal filtering, the anticausal WDF result in Figure 82 is sharper than the result produced by casual WDFs. Because phase distortion is partially compensated, some ringing is gone, but some is still visible around the rim of the hat. For the anticausal SVU shown in Figure 83, the result is also sharper than the causal SVU-filtered result due to phase compensation. Because SVU was used during the interpolation, the ringing is further eliminated. It has less ringing than the anticausal WDF-filtered result. Table 2 shows the MSE and SNR measurements.

Table 2 MSE and SNR For Test Image Lenna

Methods	FIR	IIR-IIR	SVU-SVU	IIR-IIR*	IIR-SVU*
MSE	7.9	11.74	11.25	14.28	13.85
SNR	24.54	21.1	21.47	19.4	19.67

* indicates an anticausal filtering process.

The results using the testing image Harbor is shown in Figure 85, Figure 86, Figure 87, Figure 88 and Figure 89. The filters used are the FIR filter, WDF, SVU WDF, causal WDF with anticausal WDF, and WDF with anticausal SVU WDF filters. The results are similar to the previous test with Lenna in which the FIR result lost much of the high frequency component. In this case, since Harbor has more high frequency component than the picture Lenna, the loss of sharpness is pronounced. The WDF result has a serious ringing problem and SVU result has no visible ringing.

For the anticausal filtering results, the anticausal WDF-filtered image Figure 88 has no visible ringing. A major distortion shown on the boat is caused by imperfect cutoff of the WDF on the y direction. Table 3 shows the MSE and SNR.

Table 3 MSE and SNR for the Test Image The Harbor

Methods	FIR	IIR-IIR	SVU-SVU	IIR-IIR*	IIR-SVU*
MSE	30.11	31.77	31.23	33.08	32.58
SNR	11.90	11.44	11.57	11.09	11.22

* indicates an anticausal filtering action.

4.6 Summary

Sampling structure conversion is a process used to convert between different sampling structures. To covert between structures, processes such as antialias filtering and interpolation filtering are needed. The 2-D filtering process demands efficient filters so that complexity can be reduced. WDFs are an answer for efficient filtering. However, unless anticausal filtering can be used, the accumulation of nonlinear phase due to multiple filtering can seriously damage the quality of the result.

In this chapter, the SVU technique was applied to the sampling structure conversion process. The simulations have shown that SVU WDF filtering is an efficient way to perform antialias and interpolation without the need for anticausal filtering. Moreover, the quality of the results are good even when compared with the FIR filter results. If anticausal filtering is possible, using a combination of WDFs and anticausal SVU WDFs can further improve sharpness. It is shown that the improvement

References

[1]   R. M. Mersereau and T. C. Speake, "The processing of periodically sampled multidimensional signals, " *IEEE Trans.ASSP.,* vol. ASSP-31, NO. 1, February 1983.

[2]   R. M. Mersereau, "The processing of hexagonally sampled two-dimensional signals, " *Proc. IEEE,* vol. 67, pp. 930-949, May 1979.

[3]   P. Siohan, "2D FIR filter design for sampling structure conversion," *Trans. CAS. for Video Tech.,* Vol. 1, NO. 4, pp. 337-350, Dec., 1991.

[4]   D. P. Petersen and D. Middleton, "Sampling and reconstruction of wave-number-limited functions in N-dimensional Euclidean space", *Information and Control.,* vol. 5, pp. 279-323.

[5]   E. Dubois, "The sampling and reconstruction of time-varying imagery with application in video systems", *Proc. IEEE,* VOL. 73, NO.4, pp 502-522, April 1985.

[6]   Q. S. Gu, L. C. K. Lee, M. N. S. Swamy, "2D IIR digital filters for sampling structure conversion for video signals," submitted to *IEEE CAS.*

[7]   R. J. Clarke, *Transform Coding of Images,* Academic Press LTD., London, 1985.

[8]   H. Maarmolin, "Subjective MSE measures," IEEE Trans. on Systems, Man, and Cybernetics, Vol. SMC-16, No. 3, pp. 486-489, May/June, 1986.
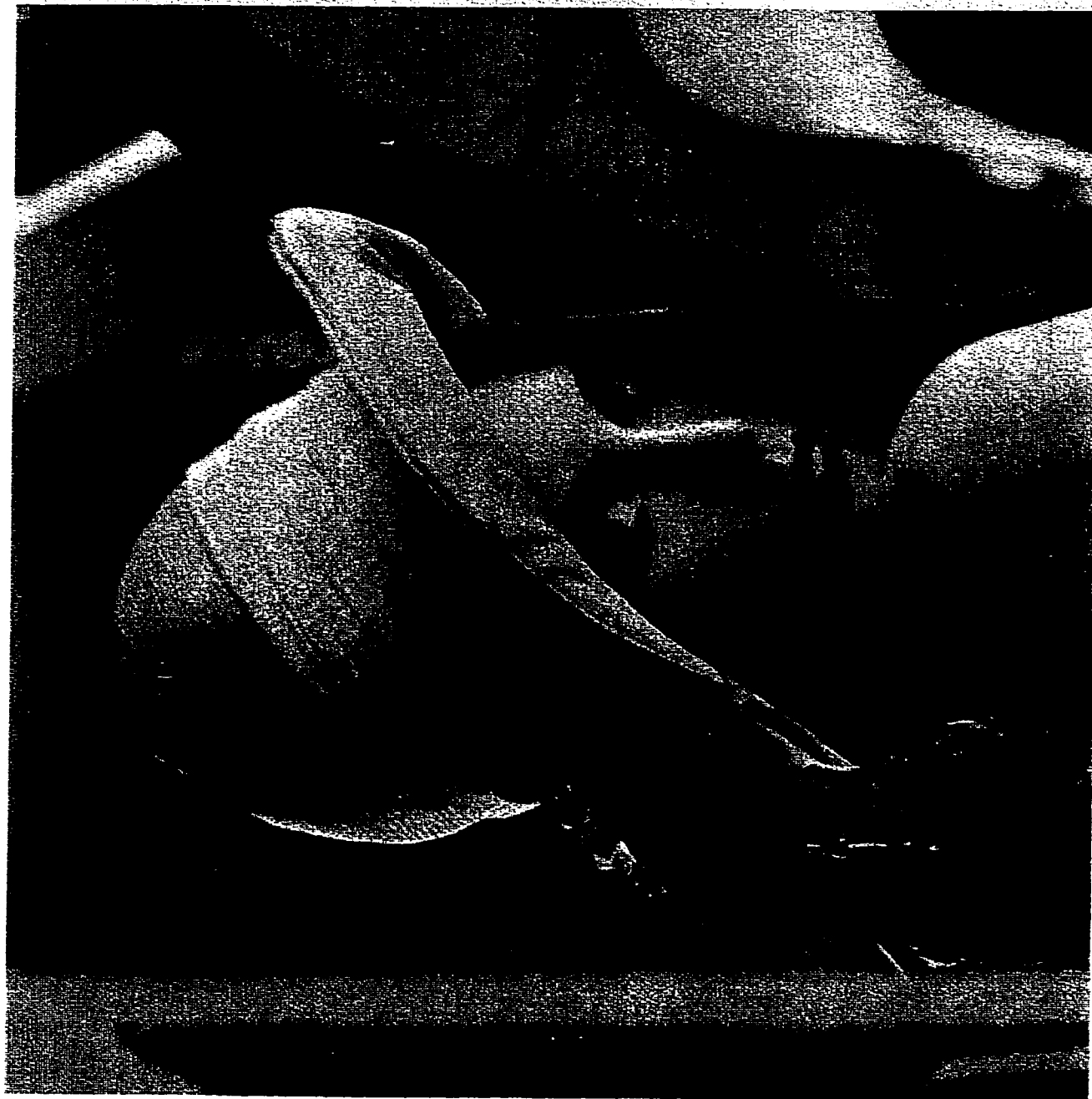
Figure 78. Original Test Image: Lenna

84
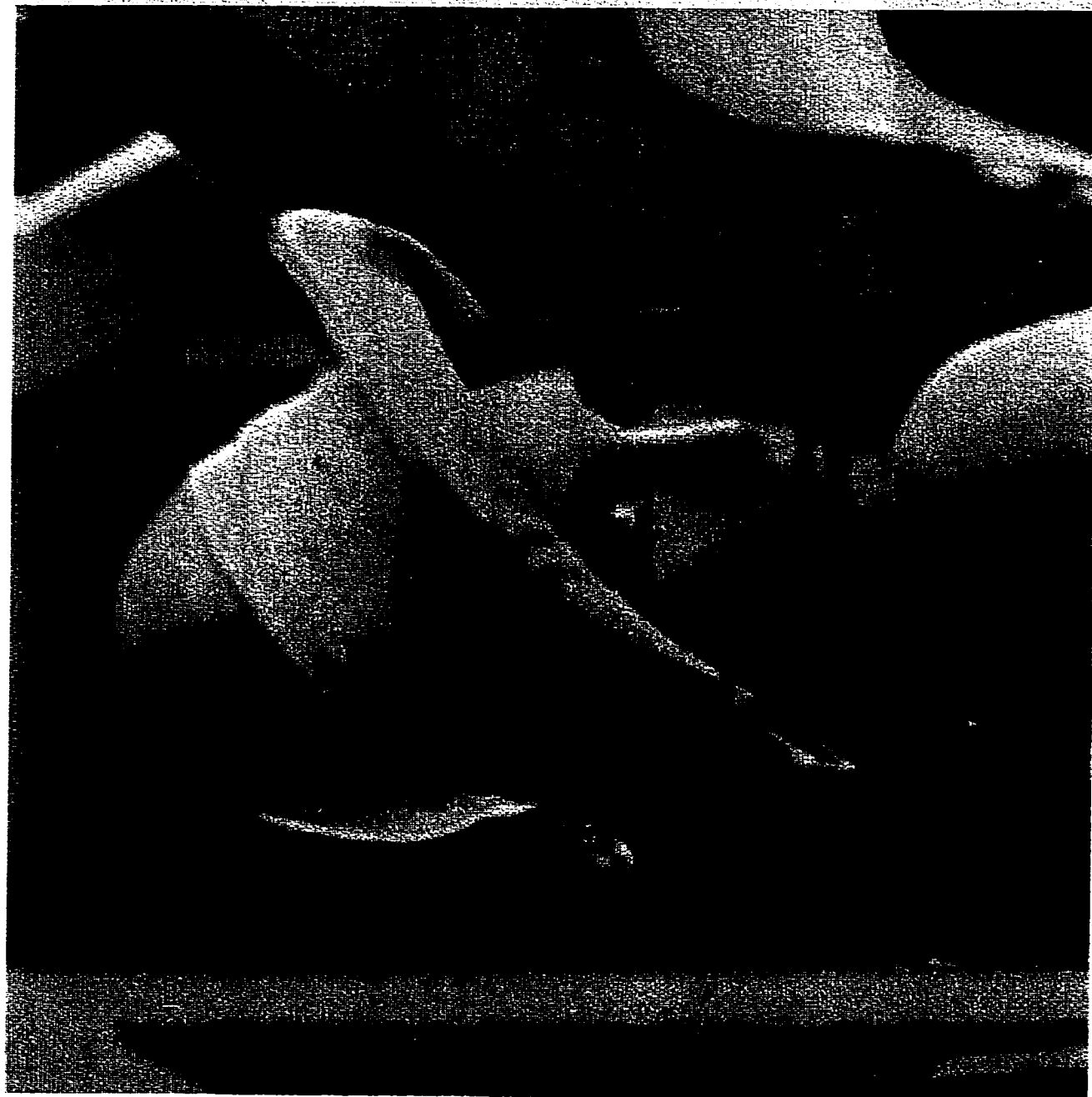
Figure 79. FIR Filtered Image: Lenna
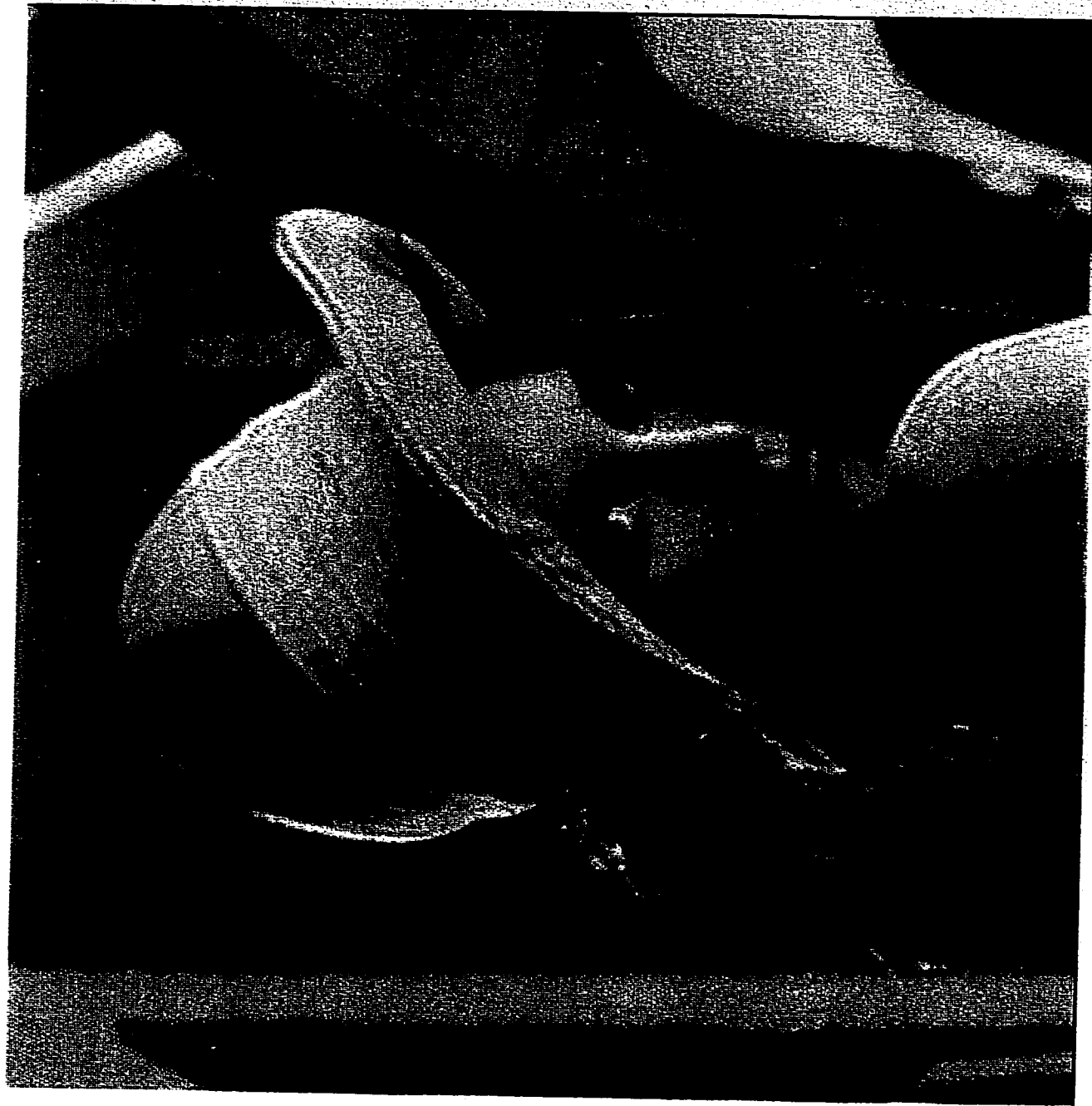
Figure 80. WDF Filtered Image: Lenna
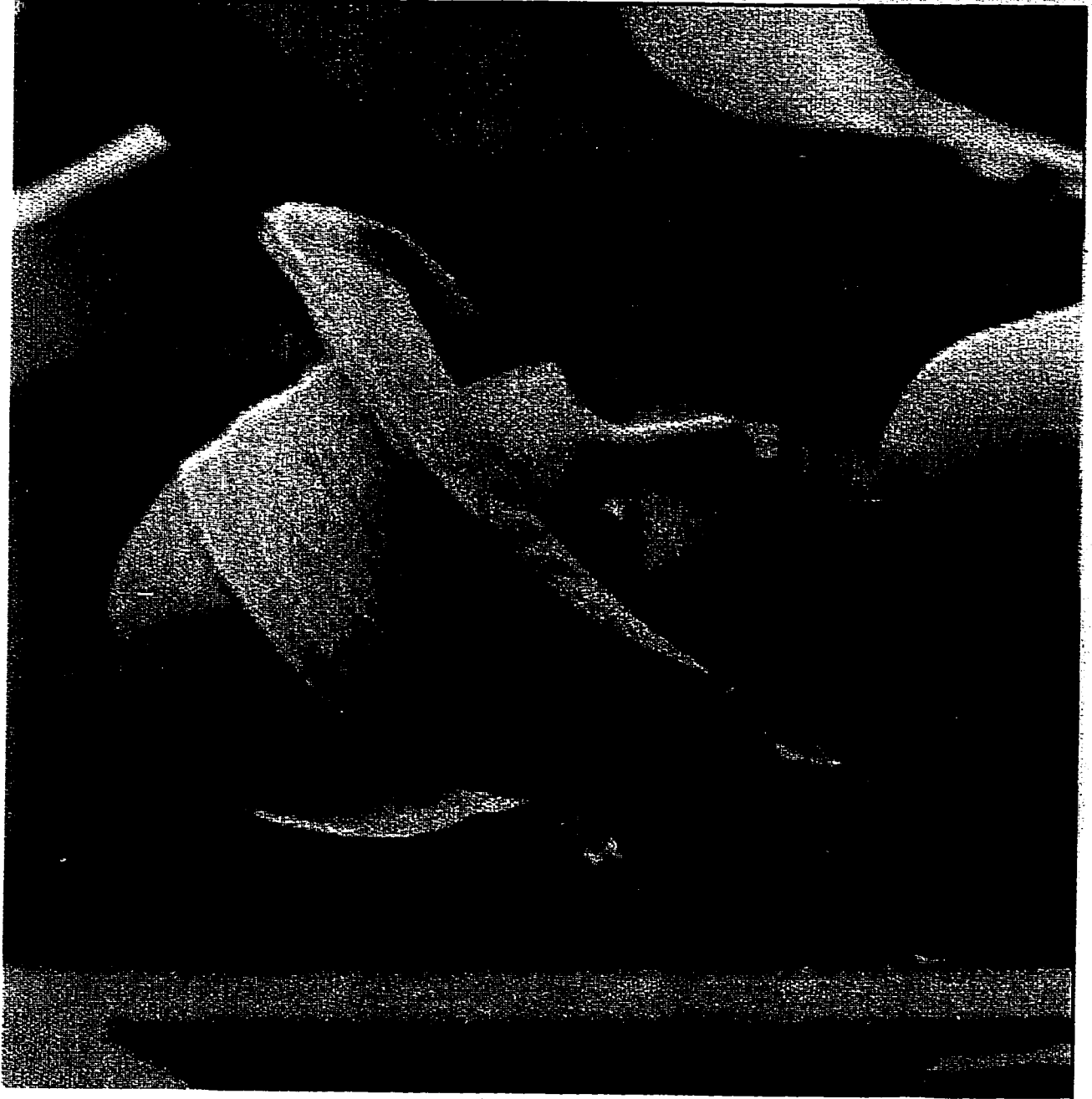
Figure 81. SVU Filtered Image: Lenna
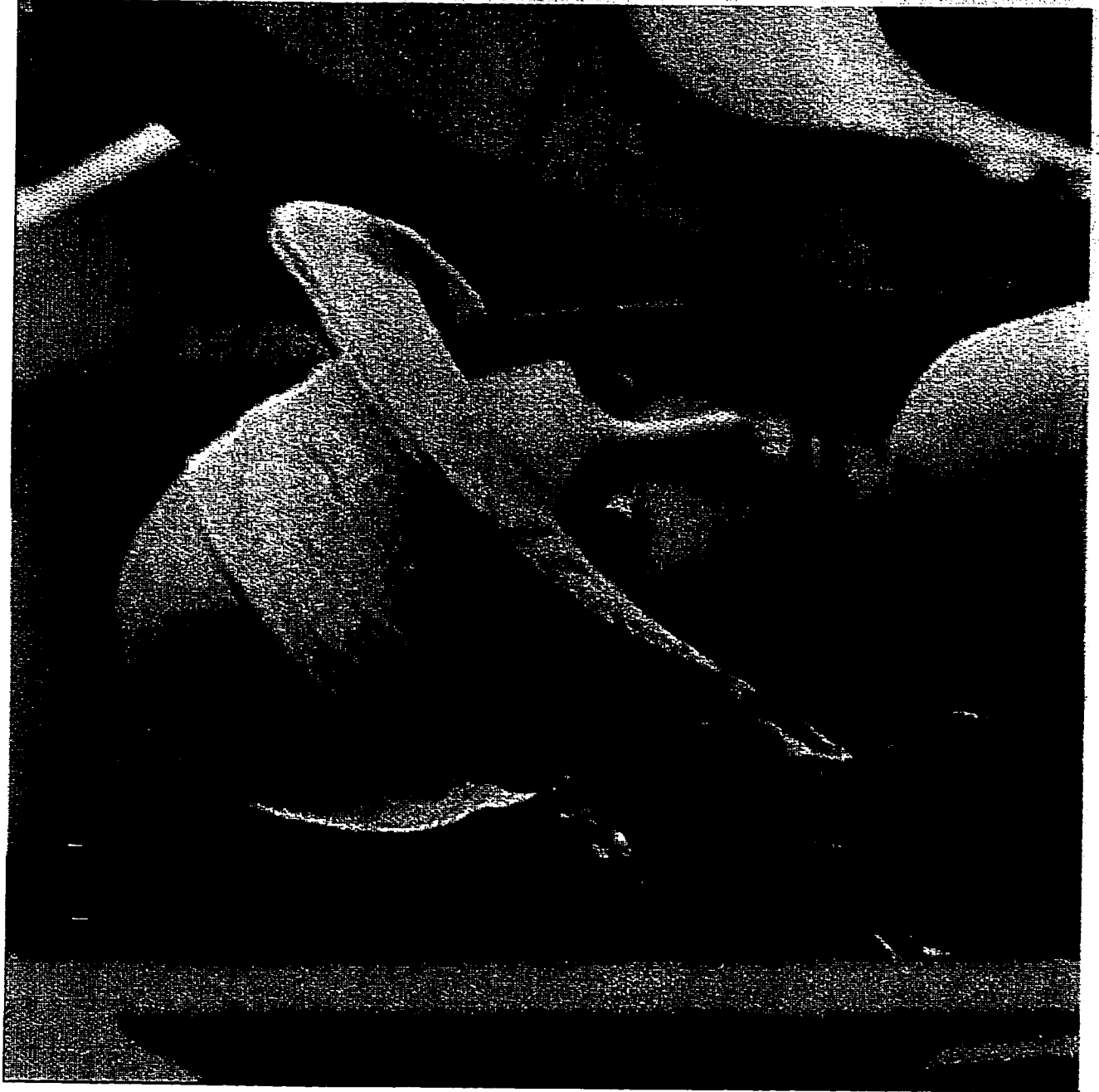
Figure 82. WDF and Anticausal WDF Filtered Image: Lenna
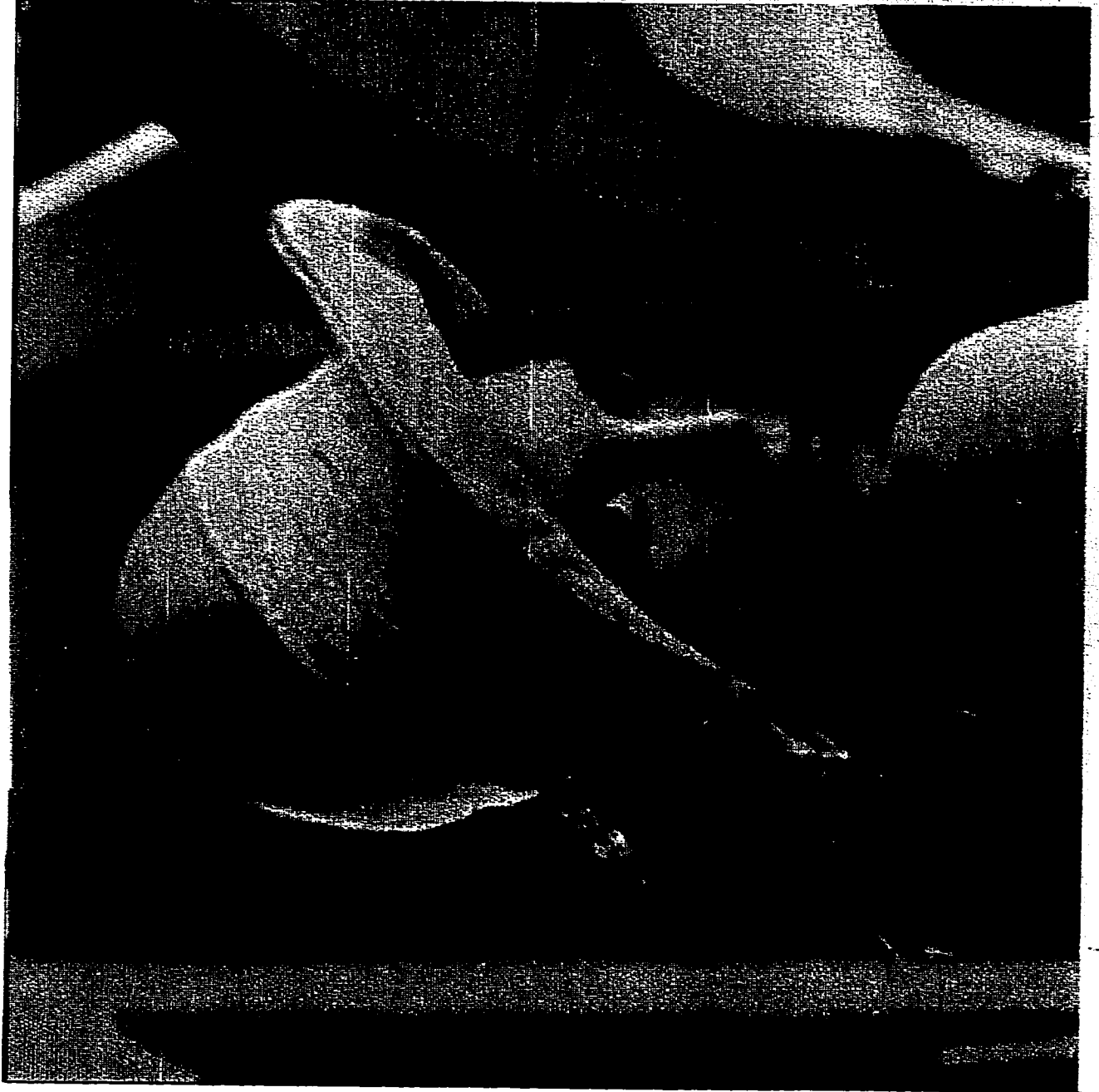
Figure 83. WDF and Anticausal SVU Filtered Image: Lenna
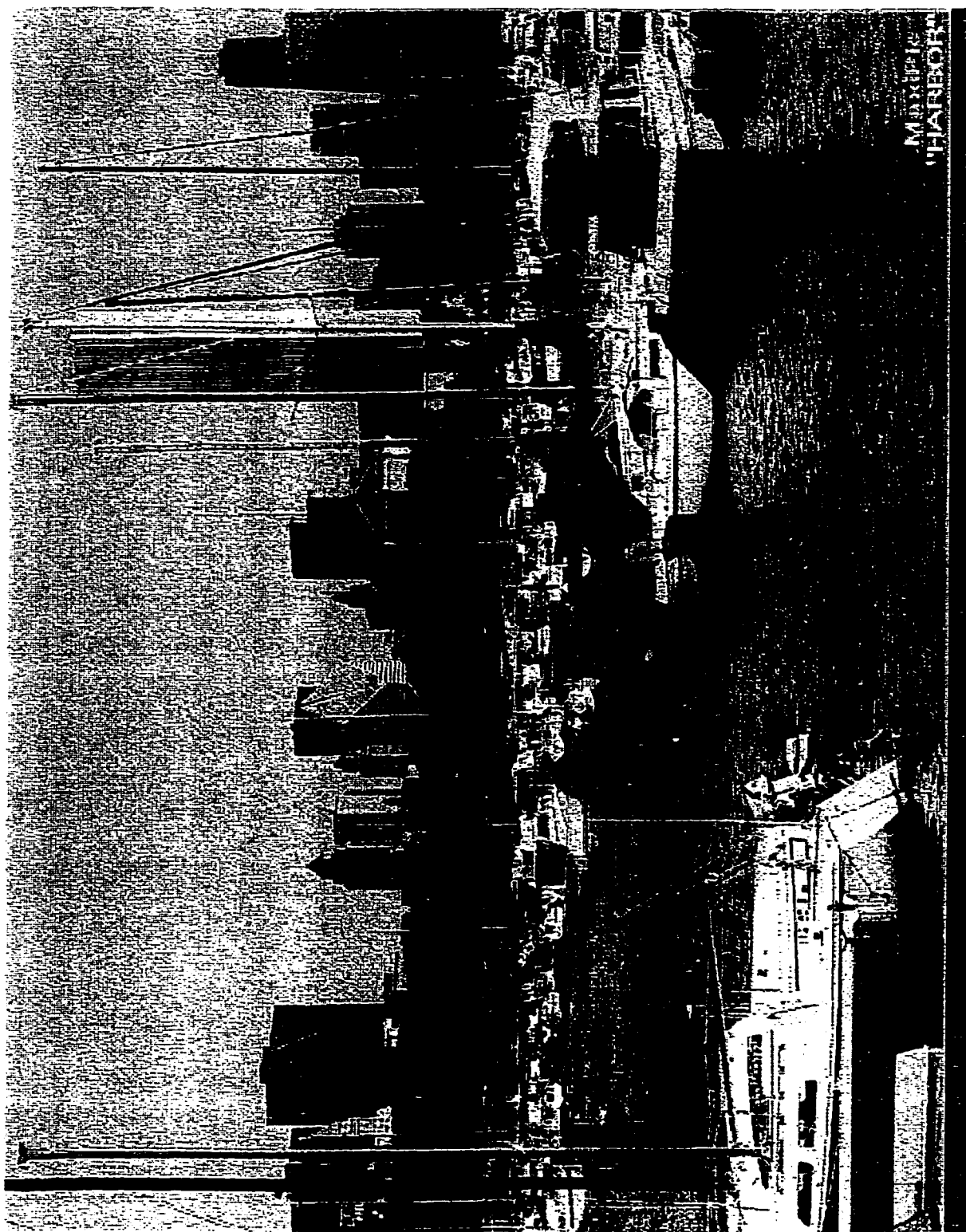
Figure 84. Original Test Image: Harbor
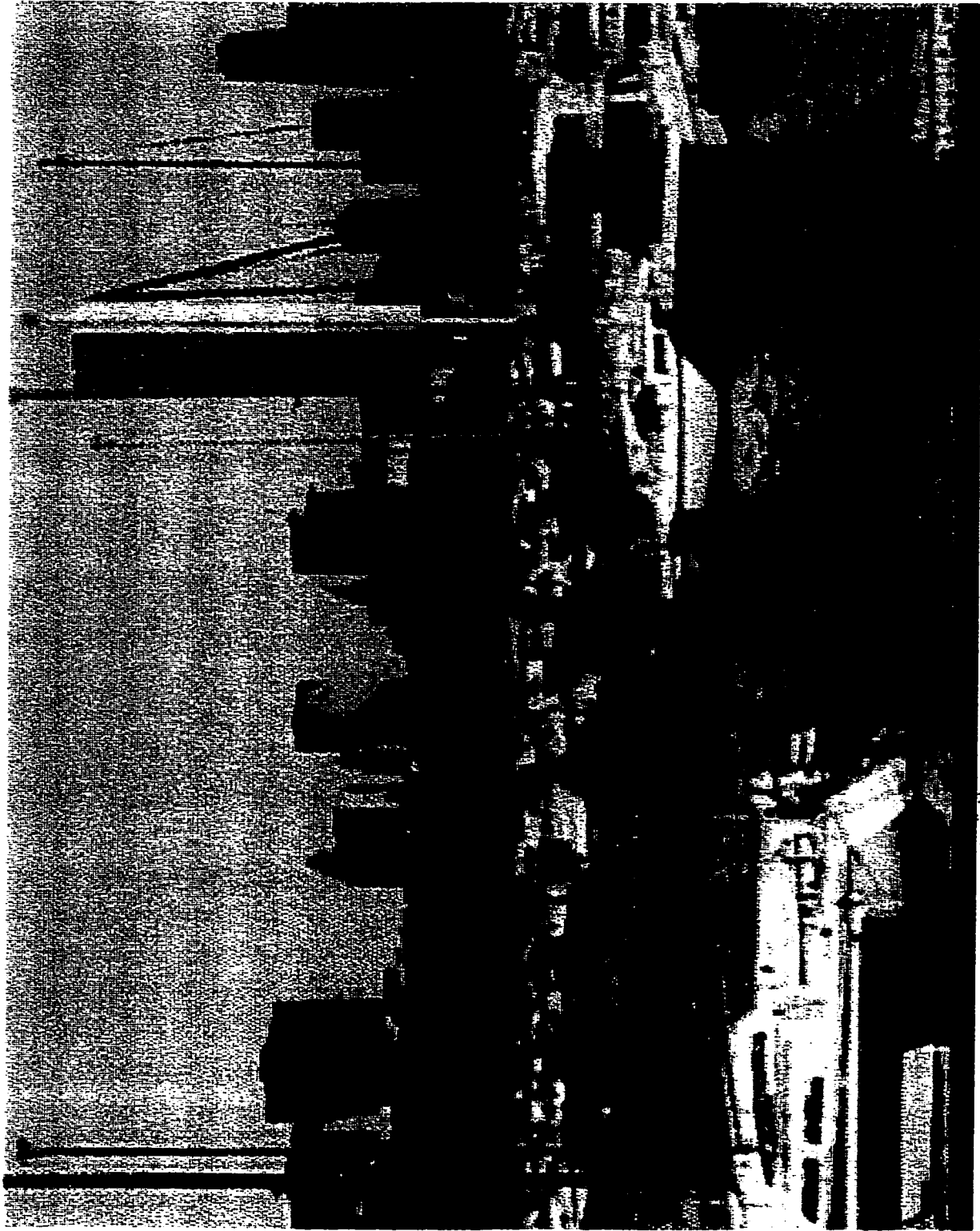
Figure 85. FIR Filtered Image: Harbor
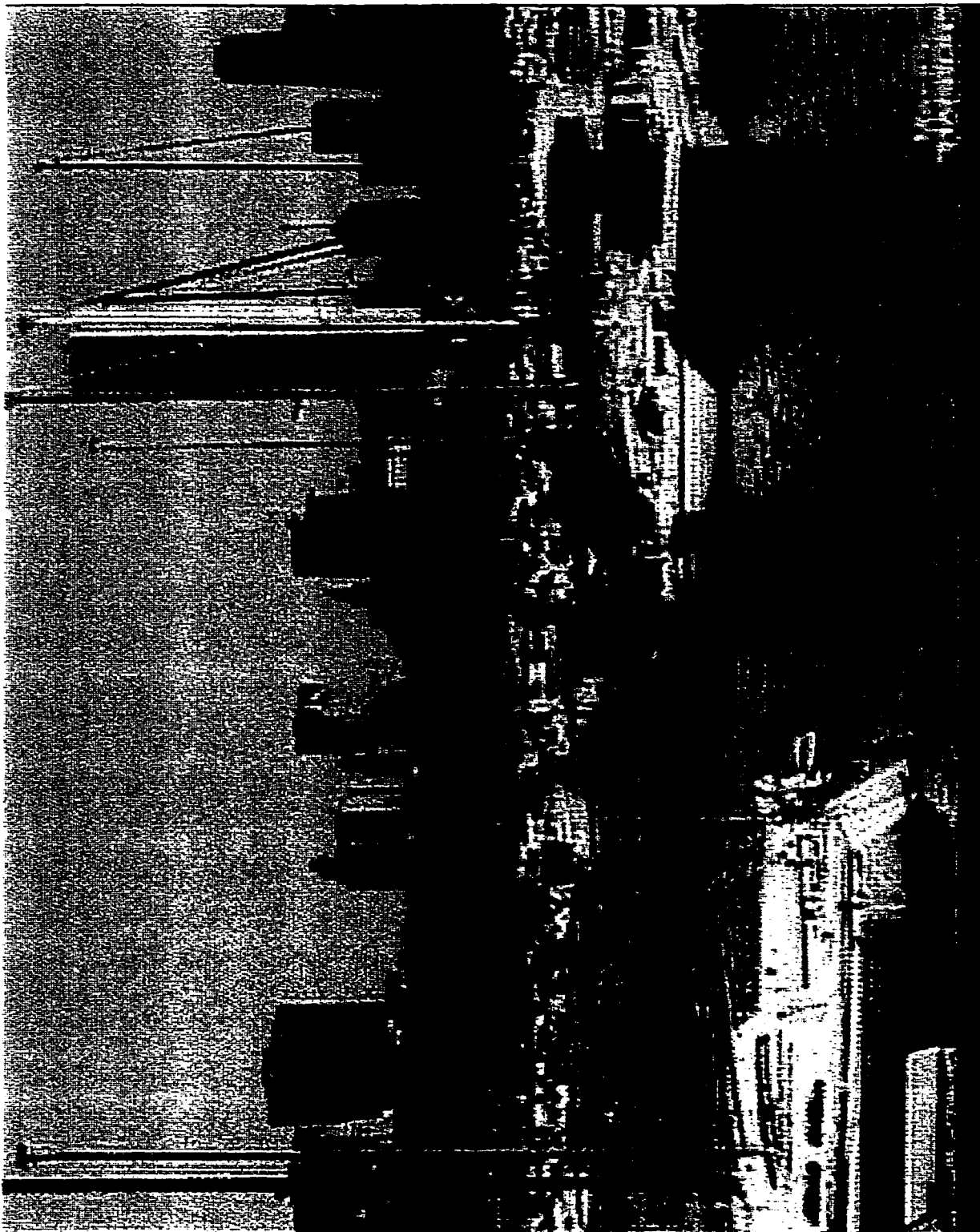
Figure 86. WDF Filtered Image: Harbor
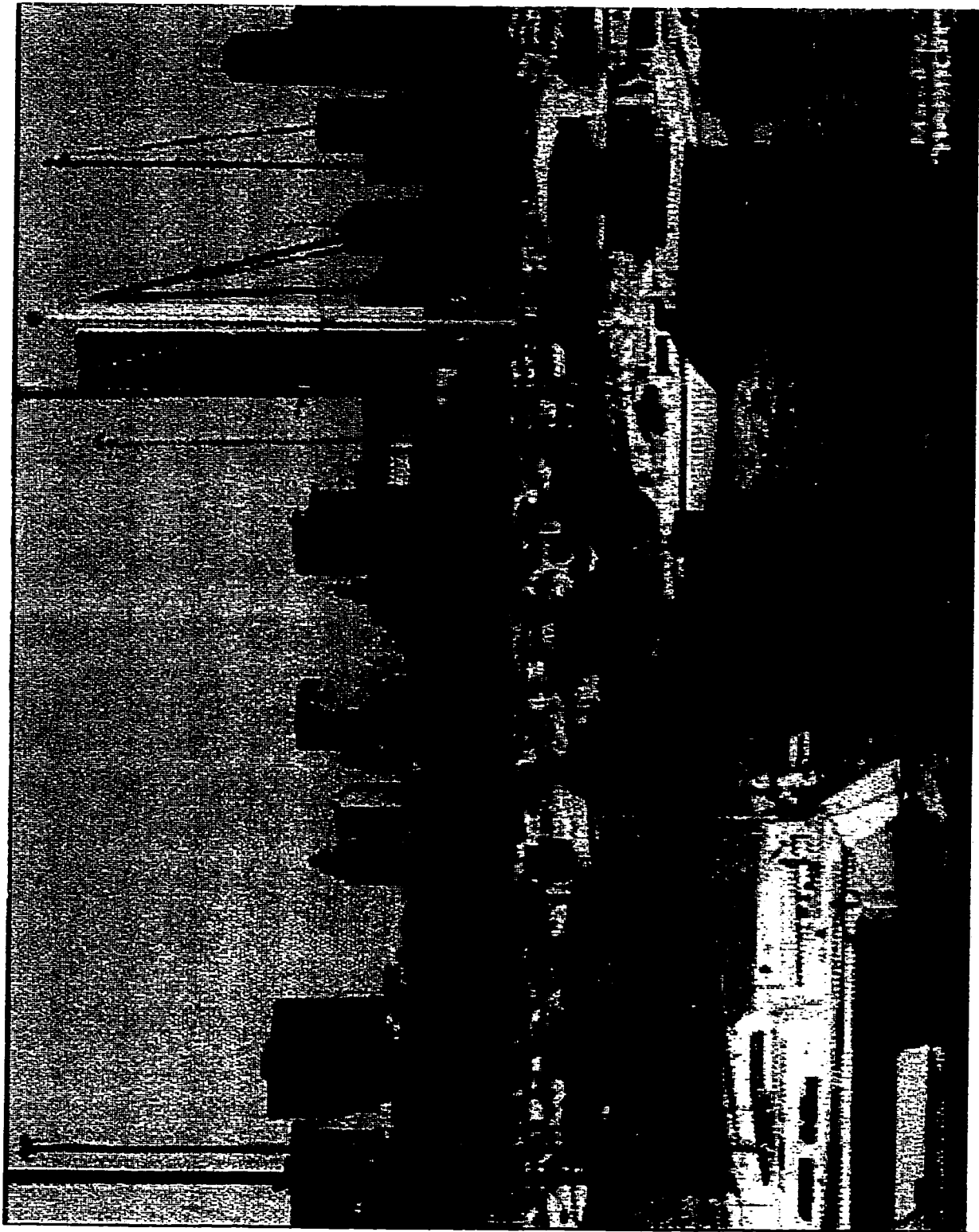
Figure 89. WDF and Anticausal SVU Filtered Image: Harbor
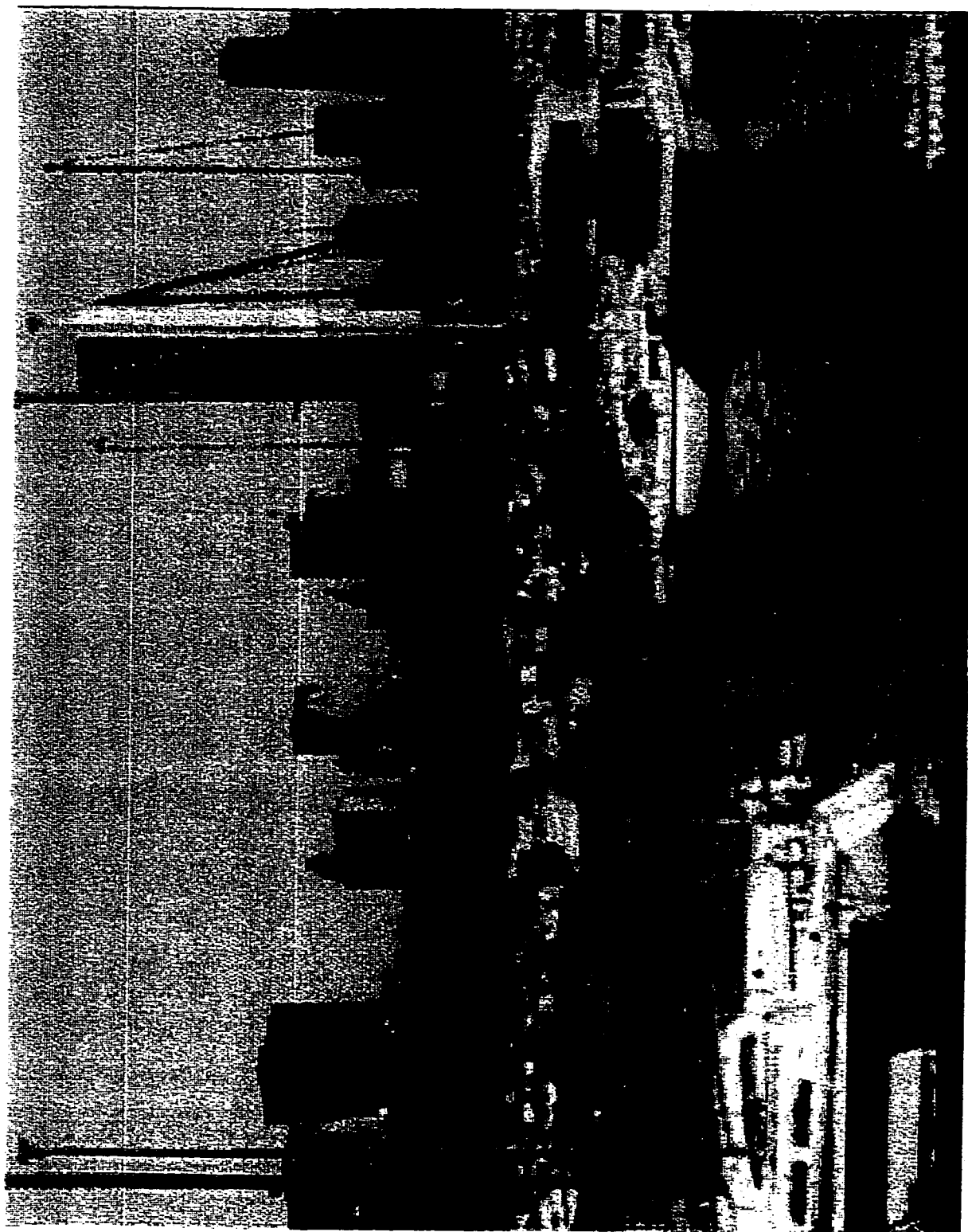
Figure 87. SVU Filtered Image: Harbor
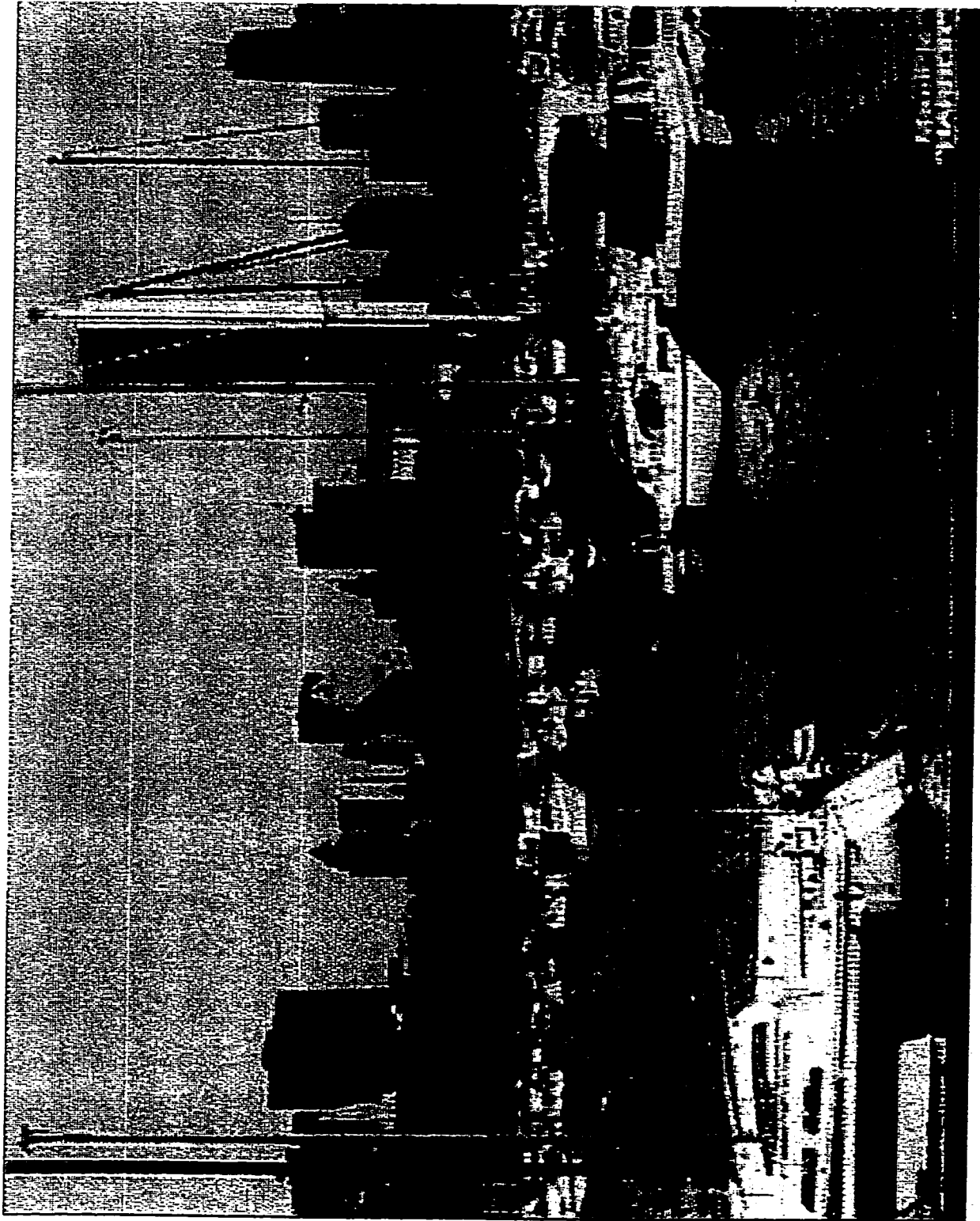
Figure 88. WDF and Anticausal WDF Filtered Image: Harbor

5 Video Deinterlacing using State Value Updating Technique

5.1 Introduction

Virtually all televisions today use interlace scanning. By interlacing a video signal, the bandwidth of the video signal can be reduced by one-half. On the other hand, undesired effects such as flickering are also introduced. To avoid the problems associated with interlaced displays, progressive scanning (pro-scan) displays are used in some of the proposed advanced TV standards [1] [2]. To display an interlaced signal on a pro-scan screen, a deinterlacing system is necessary to recovery the missing interlaced scan lines.

There are many deinterlacing methods available to provide the missing scan lines but they either produce low quality results or are very complex. An attempt to restore the missing scan lines was done by interpolation using WDFs [3]. The problem of deinterlacing can be viewed as an interpolation process in the spatial-temporal domain. With WDFs, good deinterlaced sequences can be produced without the need for complicated motion detection algorithms. Moreover, the whole system is simple because only a single (1,1) diamond filter is needed to perform the interpolation process. Unfortunately, because of the nonlinear phase response of WDFs, ringing is still noticeable in certain situations. In this chapter, the SVU technique will be analyzed for useability in reducing the non-linear phase ringing by WDFs during deinterlacing

5.2 Interlaced Scanning

A continuous video signal can be considered as a 3-D signal $f(x, y, t)$ with variables in x, y and time t. A truly continuous 3-D signal is not common, most of the 3-D signals are discrete in one or more dimensions. A 35 mm movie film storing a sequence of pictures or *frames* can be considered a quantization in the t domain and can be expressed as:

$$f(x, y, n) = f_c(x, y, nT).$$

(5.1)

where T represents the sampling period and n is the digital time.

Most common video signals raster scanning methods. Raster scan lines sweep through a frame from left to right and from top to bottom. The scanning process is equivalent to the sampling process in the y domain while x stays continuous. If the frame elements are scanned in a progressive order along a line and progressively line by line, the scanning method is known as *progressive scanning*. If the scanning process skips lines periodically, it is *interlaced scanning*. There are many varieties of interlaced scanning methods. For interlace scanning on the y-t plane, the interlaced signal can be expressed as:

$$f(x, y, n) = f_c(x, jY, nT)$$

(5.2)

where j is the index for the y position and Y is the sampling matrix (see Chapter 4) for y and t plane. For a TV standard such as NTSC, the interlaced pattern is a quincunx structure on the y-t plane (Figure 90) and is called 2:1 line interlacing.
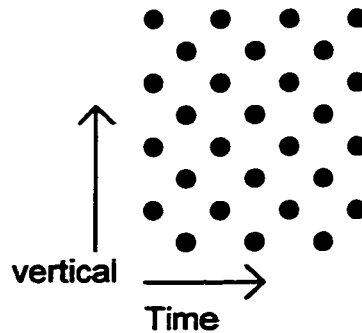
Figure 90. 2:1 Line Interlace Sampling

For 2:1 interlace scanning, each sampled *x-y* plane contains one-half the original pixels and is known as a *field*. It is called a *frame* when the two interlaced fields are added together.

There are two major causes for interlace artifacts. First, if both the temporal frequency and spatial frequency of the video signal are high, interlaced scanning will introduce aliasing [4]. This is because of the lack of antialias filtering. Second, because relatively large screens are used in high-ended, advanced TV systems, more screen is presented to the human viewer's peripheral vision, which is known to have high flicking-sensitivity. As a result, the apparent flicker increases with the size of the screen. Several common artifacts [5] caused by interlacing known are[5]: interline flicker, large area flicker, visibility of scan lines, unstable still picture and flickering slow motion. To solve the flickering problems, deinterlacing of the video signal at the receiver end is the only known solution if we want to retain the conventional TV transmission system.

5.3 Some Approaches for Deinterlacing [5]

5.3.1 Line Repetition

A simple approach for replacing a missing scan line from an interlaced signal is to repeat each line of the interlaced signal, thereby overwriting the missing lines (see Figure 91).
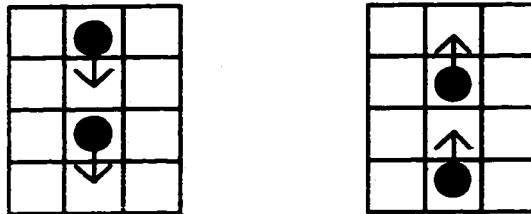
Figure 91. Deinterlacing using Line Repetition

This method has nothing to do with the time domain and is simple to use. Since moving area in the y-direction are generally low in resolution, This method is efficient when dealing with moving areas. However, for static areas, the loss of resolution in the y-direction is inevitable.

5.3.2 Field Insertion

Unlike line repetition, field insertion uses only the temporal information. To replace the missing lines, the previous field is added to the current field to form a complete frame (see Figure 92).
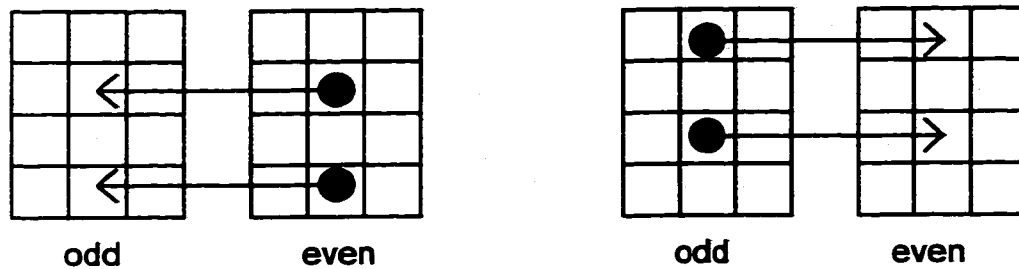
Figure 92. Deinterlacing using Field Insertion

In static areas, the information stored in both fields is combined and all the information can be retrieved. For time-varying areas, the same moving object may appear in different locations of the two consecutive fields. By inserting the previous field in the current field, two mismatched objects will form unmatched lines (see Figure 93).
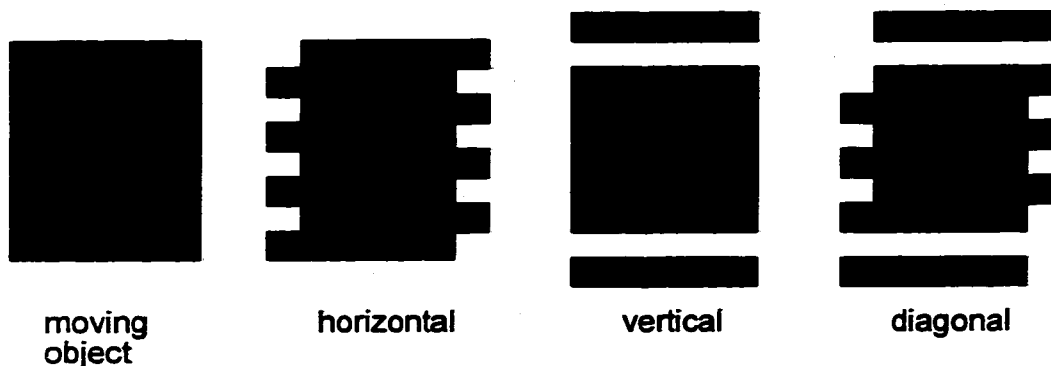
Figure 93. Artifacts in Moving Objects using Field Insertion

5.3.3 Median and Adaptive Median Filter Interpolation[5]

Median filters are known to have good edge-preserving qualities[6]. Since the median filter's output is chosen from a collection of pixels, ideally it is possible to choose the neighboring pixel of the missing pixel when the pixel cluster is in motion, and uses the pixel from the previous field when the pixel cluster is static. A multiple median filter[5] method is given in Figure 94.

100

odd field	even field	odd field

where the grid shows: odd field with a, b, c; even field with d, e, f / y / g, h, i; odd field with j, k, l.

state	filter
stationary	$y = \text{med}[\, b, k, e, h, X_t\,]$
motion 1	$y = \text{med}[\, b, k, d, e, f, g, h, i, \overline{X_t}\,]$
motion 2	$y = \text{med}[\, b, k, d, e, f, g, h, i, \overline{X_s}\,]$
motion 3	$y = \text{med}[\, d, e, f, g, h, i, \overline{X_s}, \overline{X_s}, \overline{X_s}\,]$

where $\overline{X_t} = (b + k) / 2$ (temporal average)

and $\overline{X_s} = (e + h) / 2$ (spatial average)

Figure 94. Multiple Median Filter Method

The multiple median filter consists a variety of median filters to deal with different *motion states*. The motion states are: stationary, slow motion (motion 1), intermediate motion (motion 2) and fast motion (motion 3). By controlling the region of the median filter and repeating certain pixels, four different median filters are used to deinterlace video signal according to different modes of motion. To make the median filters aware of different motion situations, an adaptive algorithm using eleven point differences over three fields [5] is shown in Figure 95.
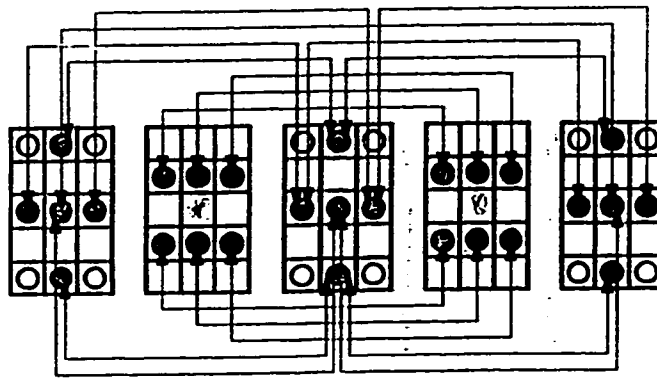
Figure 95. Eleven Points Motion Detection Algorithm

The simulations produced by the eleven points adaptive multiple median filter will be used to compare to that produced by SVU.

101

5.3.4 Diamond WDF Interpolation

From the previous section, we have seen that the interlaced video signal has a diamond sampling structure on the y-t plane (see Figure 90). The situation is in fact a (1,1) quincunx-rectangle sampling structure conversion problem. However, there are some differences between the two. First, there is little or no antialias filtering before downsampling on the y-t plane[4]. Thus, perfect reconstruction is not possible if both the temporal frequency and spatial frequency exceed the (1,1) diamond spectrum. Second, the signal is now time-dependent. The anticausal filtering technique used in the previous chapter would be difficult to use here.

If a video signal is bandlimited in the (1,1) frequency spectrum, a (1,1) diamond filter is a suitable choice for the deinterlacing problem. Video signals with a high-spatial/low-temporal spectrum or a low-spatial/high-temporal spectrum can be interpolated without any motion adaptive process. The elimination of the motion adaptive process simplifies the implementation of the filter substantially. There are still problems associated with the diamond deinterlacing method. First, the imperfect cutoff on the t axis will have minor aliasing during reconstruction for high-temporal frequency signals. Fortunately, the aliasing only appears on high-temporal frequency patterns, to which human eyes are insensitive.

The second problem is the ringing effect due to motion. Unlike the ringing on still images, ringing on the y-t plane appears as a form of *ghost* (see Chapter 3). The ghosts have alternating intensity and follow moving objects. Because interlaced signals have little or no antialias filtering, a moving object occupies different locations at each field. Consequently, each moving object is indeed a patch of impulses or steps in the t direction. After a nonlinear phase filtering process, the delayed high frequency components of the impulses or steps will appear as ghost images with alternating intensity. To solve the ringing problem, the SVU technique will be considered in the following sections.

5.4 Deinterlacing Using State Value Updating

Because of the non-uniform delay due to nonlinear phase, part of the frequency components of a step or impulse (on the time axis) continue to exist. To stop the ringing, SVU can be used to remove the delayed components. When the SVU method is used with a WDF, the WDF will perform the linear filtering part. If there is a large discontinuity, a decision mechanism will set the state value to adapt to the input. A decision algorithm is suggested in this section. The algorithm will detect the discontinuity and adapt the state value when necessary. The first half of the algorithm is shown in the following:

```
d1 = abs(x(i ,j) - buff(i, j))
if (d1 > threshold)
{
        Delay1(i, j) = factor * x(i, j)
        Stop_Flag = True
}
```

As in the sampling structure conversion problem, the steady-state conversion factor is the value *factor*. The array *buff(i, j)* is the buffer storing the previous field. *Delay1(i, j)* is the state variable Eq_1 defined in Figure 4.4. The value *d1* is the pixel difference between fields. They are compared with *threshold* to determine if steady-state adaptation is necessary. If so, the adaptation will take place in the delay element and *Stop_Flag* will be set to TRUE. The *Stop_Flag* has the same function as the one in Chapter 5. The calculated value is then used in the second half of the filter, responsible for filtering in the $Z_1^{-1}Z_2^{-1}$ direction.

The second half of the decision algorithm is shown in the following.

```
d2 = abs(s1 - buff(i, j))
if (d2 > threshold)
{
        Delay2(i, j) = fct * s1;
}
else if (Stop_Flag)
{
        Stop_Flag = 0;
        Delay2(i, j) = factor * x(i, j)
};
```

The value *Delay2(i, j)* is the state variable Eq_2 defined in Figure 4.4. The pixel difference in the $Z_1^{-1}Z_2^{-1}$ direction is calculated into *d2*, and compared with the threshold. If there is

103

a discontinuity, the state value will adapt to the value sI calculated by the first half of the filter in the $Z_1^{+1}Z_2^{-1}$ direction. If no discontinuity at $Z_1^{-1}Z_2^{-1}$ is found in the $Z_1^{+1}Z_2^{-1}$ direction, the state value will be adapted to the current input pixel value to prevent ringing.

Since the aliasing due to state value updating only happens for moving parts, there is a larger tolerance for aliasing. This results in a simpler algorithm than the one used for sampling structure conversion. The drawback of this algorithm is that false decisions are made on the boundaries of static objects. Since there are always two different values on each side of the boundary, the algorithm will mistake the static boundary as a moving object and cause unwanted state value updating. A solution is to add an additional buffer to store an additional field, but this may complicate the hardware and may not justify the slight improvement.

5.5 Simulation Results

In this section, the three deinterlacing methods that were described in this chapter will be tested, the eleven-point motion adaptive multiple median filter, the WDF deinterlacing method and the SVU deinterlacing method. The diamond WDFs use 0.5 as the adapter coefficient. The simulations will use three video sequences for testing. A single field from each of the original sequences is shown in Figure 96, and Figure 100.

The first sequence used for testing is Ping-Pong (Figure 96). Both the hand and the ball in the picture are moving objects and the rest are static. A single frame of the adaptive median deinterlaced sequence, IIR deinterlaced sequence and SVU deinterlaced sequence is shown in Figure 97, Figure 98 and Figure 99 respectively. The median deinterlaced frame shows good reconstruction on both moving and static areas although there is a minor loss of resolution in static areas. Figure 98, the WDF deinterlaced frame has an imperfect reconstruction appearing as lines on both of the balls. Both of the hands and the balls have a surrounding ring caused by ringing in the t direction. Nevertheless, the reconstruction on the static area is very good and the resolution is higher than median filtering. In Figure 99, the SVU deinterlaced frame has little or no ringing on the moving object, but there is a minor resolution loss on the edge of the table.

The second sequence used for testing is The House (Figure 100). This sequence has the house moving slowly and the foreground moving fast. A single frame of the adaptive median deinterlaced sequence, IIR deinterlaced sequence and SVU deinterlaced sequences are shown in Figure 101, Figure 102 and Figure 103. The median deinterlaced frame in Figure 101 shows very good reconstruction on both static and moving parts. However, some small and highly contrary moving objects have false color. The false color is shown on the street light at the far left side and on the edges of some flowers. The false color may be caused by different logical decisions of the filter operating on each of the R, G and B signals. A frame of the WDF deinterlaced sequence is shown in Figure 102. For this sequence, the ringing is serious, especially on the branches. In Figure 103 a

frame of the SVU-deinterlaced sequence is shown. The SVU sequence has neither visible ringing nor ghosts, but some degree of imperfect reconstruction is found in some moving objects.

The final sequence used is The Train shown in Figure 104. This sequence has the train staying relatively static and the rest are slowly moving objects. The median deinterlaced frame is shown in Figure 105. Again, some false color appears on the edges of several moving objects. The WDF-deinterlaced frame shown in Figure 106 has very good interpolation on both the moving and static parts, but a small amount of ringing is still noticeable. Finally, the SVU-deinterlaced frame shown in Figure 107 has no visible ringing but does have a minor imperfect reconstruction on the edge of the moving objects.

The simulations show that each of the method have certain of weaknesses. The median method produce mismatched decisions for each RGB signal, resulting in false colors on the edges of some moving objects. The WDF deinterlaced sequences are not appropriate for high contrast patterns, since the ringing caused by the recursive y-t filtering is noticeable. This effect is especially serious in the sequence The House (Figure 5.12). Finally, the SVU deinterlacing method has shown a good reconstruction on the static object and it has only minor artifacts on some fast moving objects. Although the SVU is a recursive filter, there is no visible ringing. When the sequence is viewed continuously, the imperfect reconstruction of the SVU should have minimum effect. It is because human eyes do not easily recognize high spatial detail of moving objects.

5.6 Conclusion

The problems of deinterlacing were discussed in this chapter. Presented were several deinterlacing methods along with a deinterlacing method using the SVU technique. A decision algorithm was also suggested for the SVU technique for use by deinterlacing. In some aspects, SVU deinterlacing is not as good as the eleven-point motion adaptive multiple median filter. Nevertheless, the motivation for using both the WDF and SVU is to achieve a simple structure like an IIR filter that can produce results comparable to more complicated systems. Although the SVU uses a decision algorithm, its complexity is much lower than the eleven-point motion detector. Moreover, imperfect reconstruction appearing as lines at the fast-moving edges are not a serious problem during continuous viewing because the human eye is not good at discerning high-resolution fast-moving objects. The simulations have shown that the relatively simple SVU deinterlacing method can produce acceptable results.

References

[1]   D. Pele, B. Choquet, and P. Siohan, "Field rate conversion by motion estimation/compensation," *Proc. 2nd Int. Workshop on Signal Processing of HDTV*, Torino, Italy, vol. 1, August 1989.

[2]   H. Kurashita, M. Ishizuka, and N. Yamaguchi, "A decoder for a letter-box-type wide-aspect EDTV system," *Jour. SMPT*, pp. 790 - 796, Nov. 92.

[3]   Q. Gu, C. K. L. Lee, M. N. S. Swamy, "2D digital filters for deinterlacing of video signals," CCECE, Vancouver, Canada, Sept., 1993.

[4]   D. E. Pearson, *Transmission and Display of Pictorial Information*, Pentech Press, London, 1975.

[5]   Y. Neuvo, "Scan rate up-conversion in television receivers", *UCSB/CIPR* Santa Barbara, CA. 1992.

[6]   I. Pitas, A. N. Venetsanopoulos, *Nonlinear Digital Filters*, Kluwer Academic Publishers, Massachusetts, 1990.
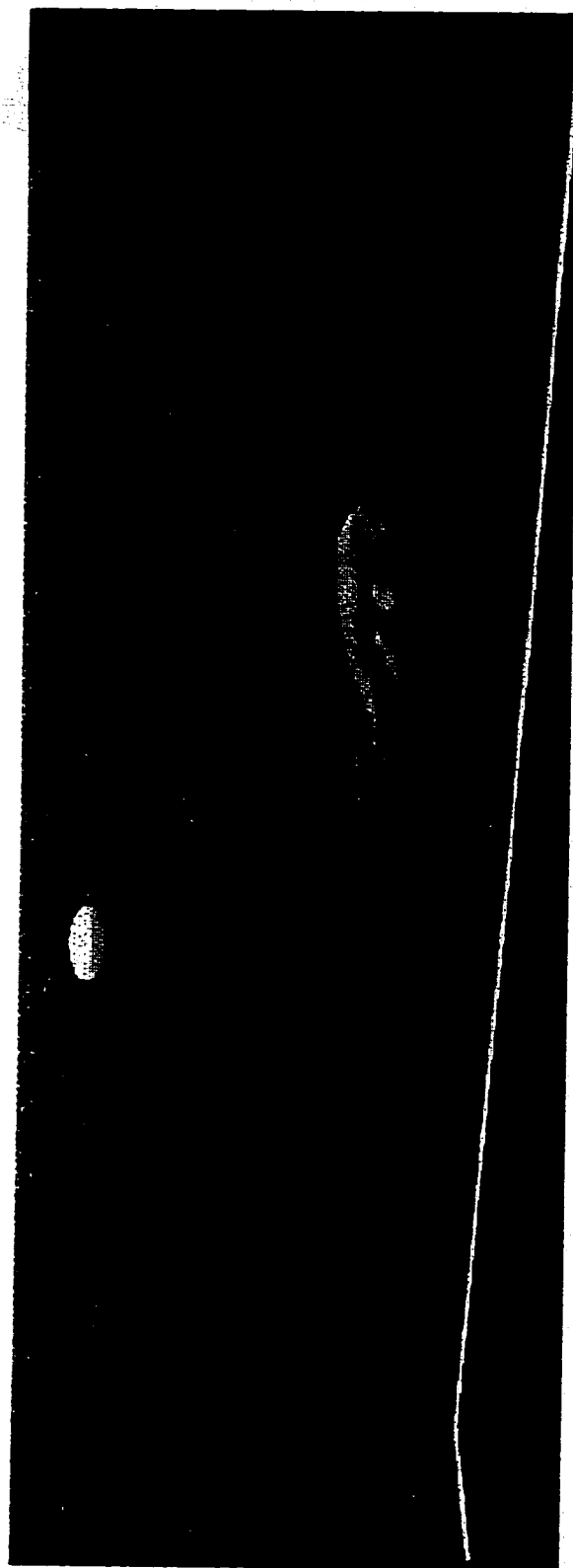
Figure 96 Original Ping-Pong Sequence
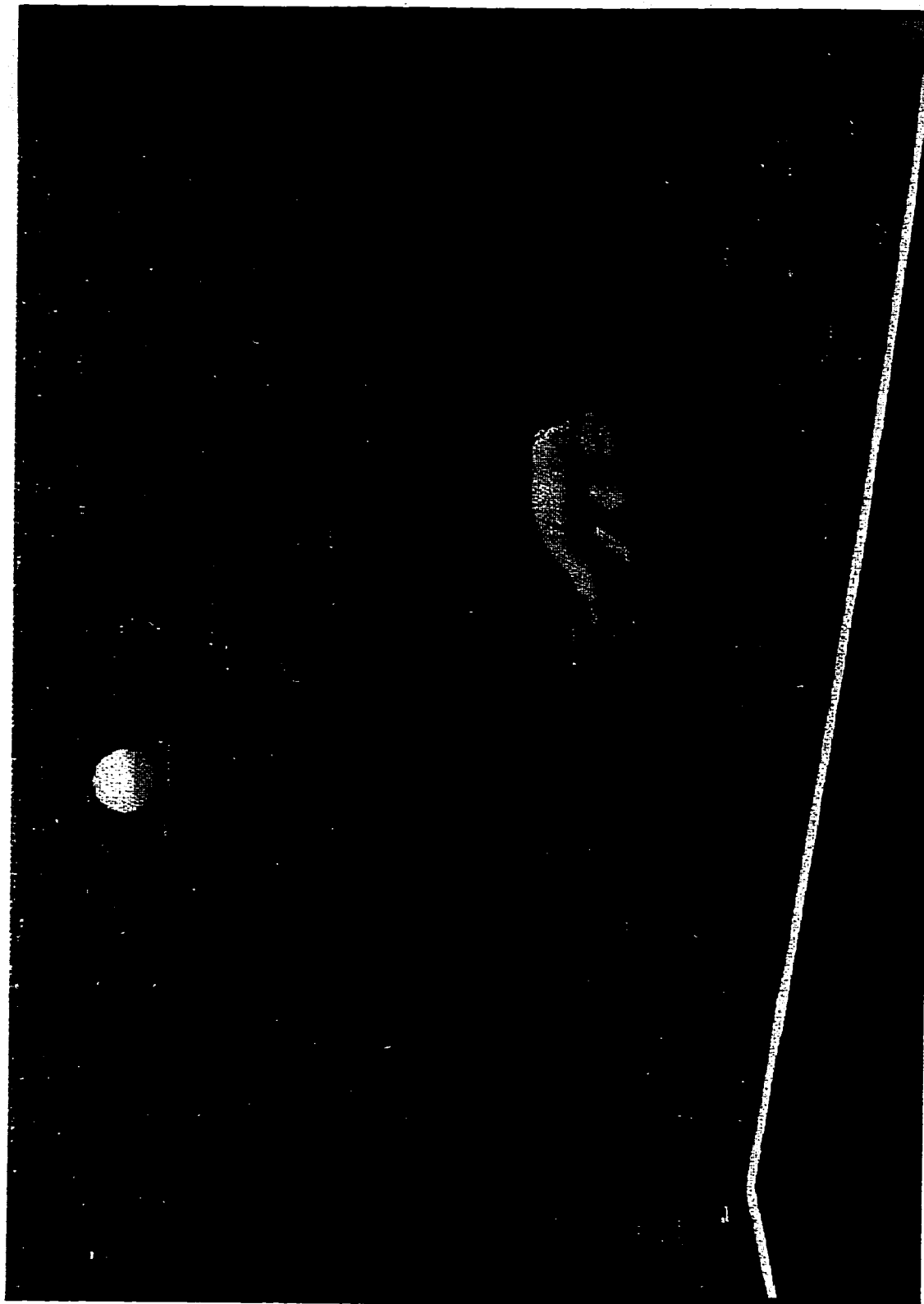
Figure 97 Adaptive Multiple Median Deinterlaced Frame of Ping-Pong
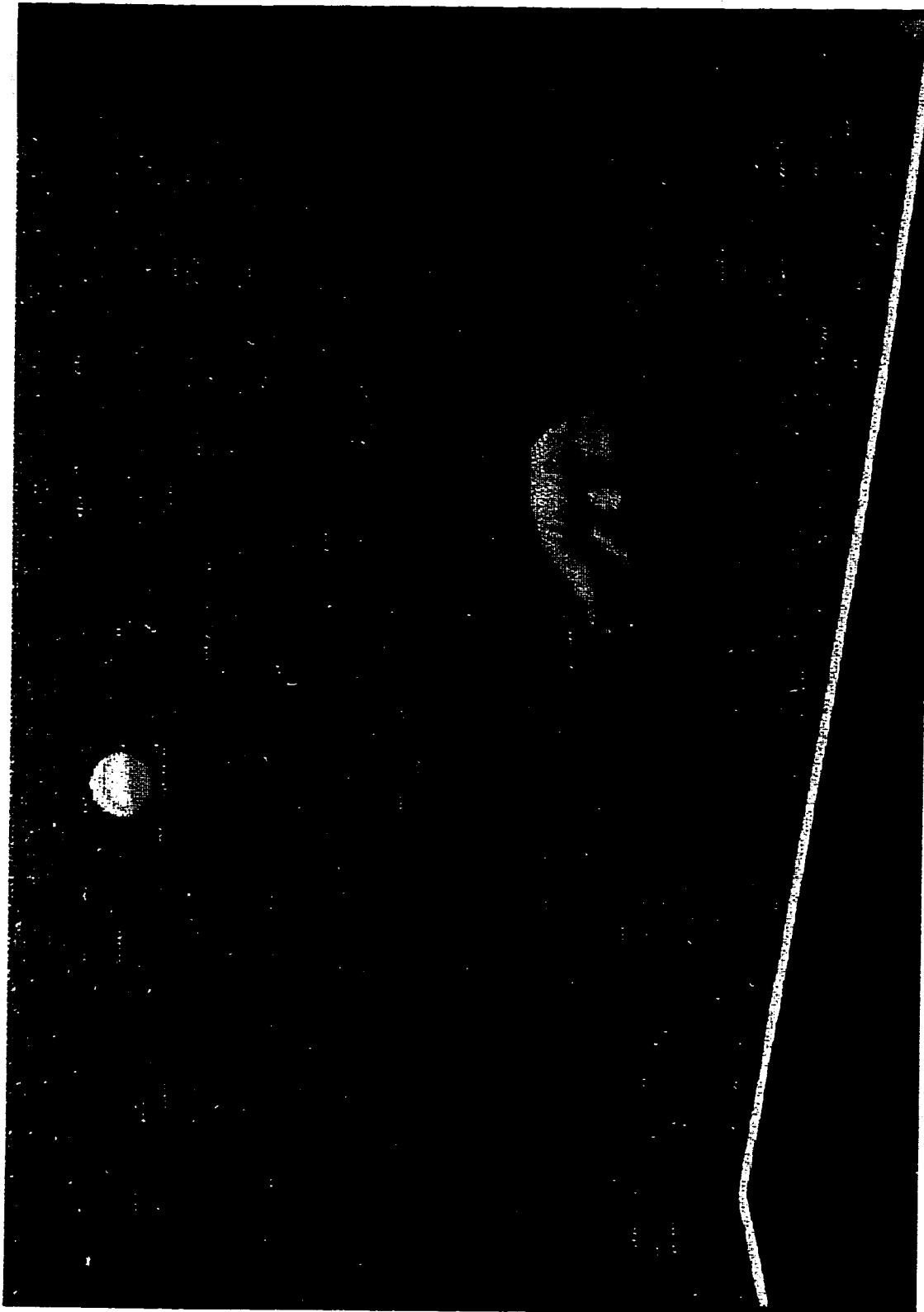
Figure 98 WDF Deinterlaced Frame of Ping-Pong

111
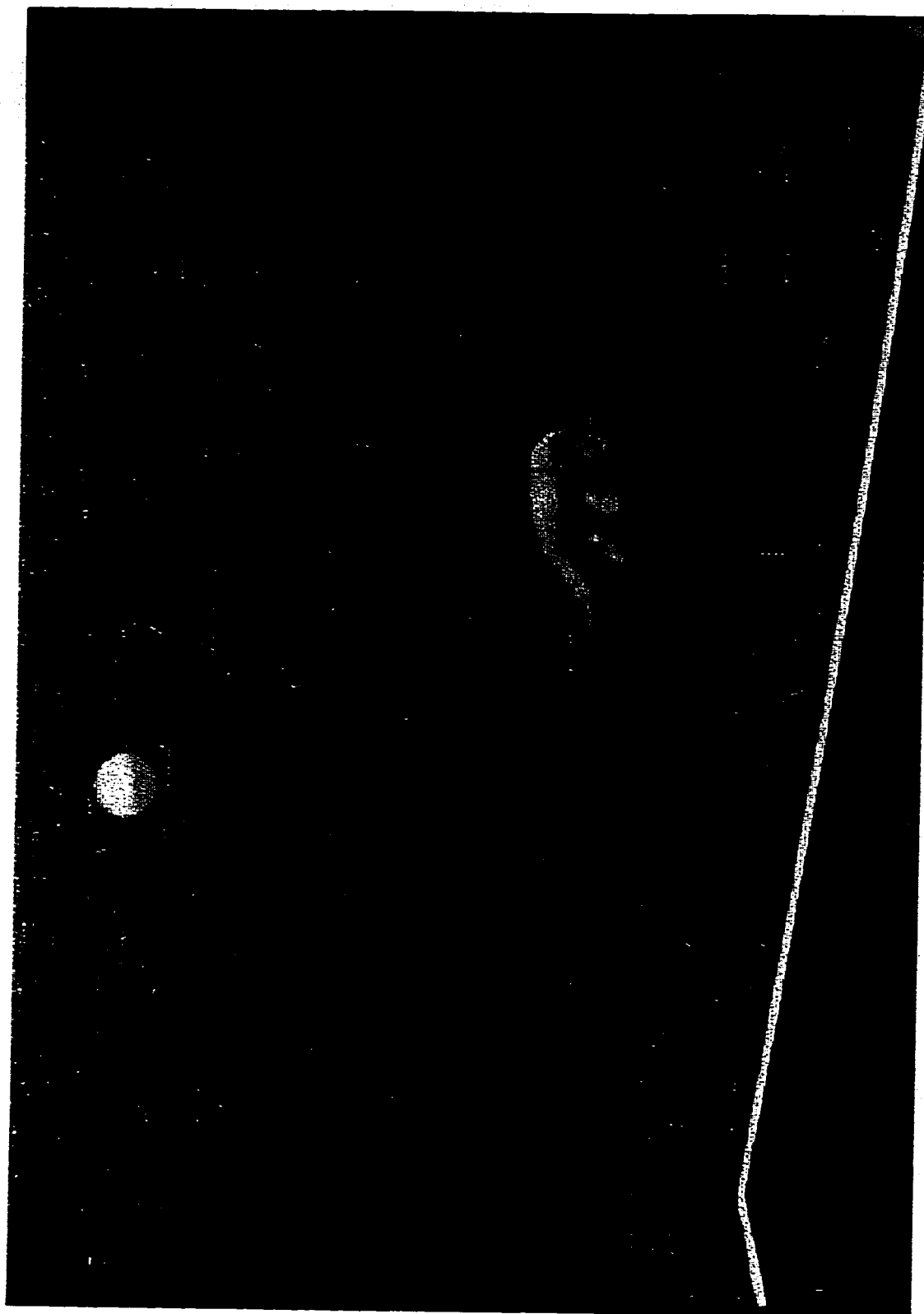
Figure 99 SVU Deinterlaced Frame of Ping-Pong

Figure 100 Original House Sequence

113

Figure 101 Adaptive Multiple Median Deinterlaced Frame of the House

Figure 102 WDF Deinterlaced Frame of the House

Figure 103 SVU Deinterlaced Frame of the House
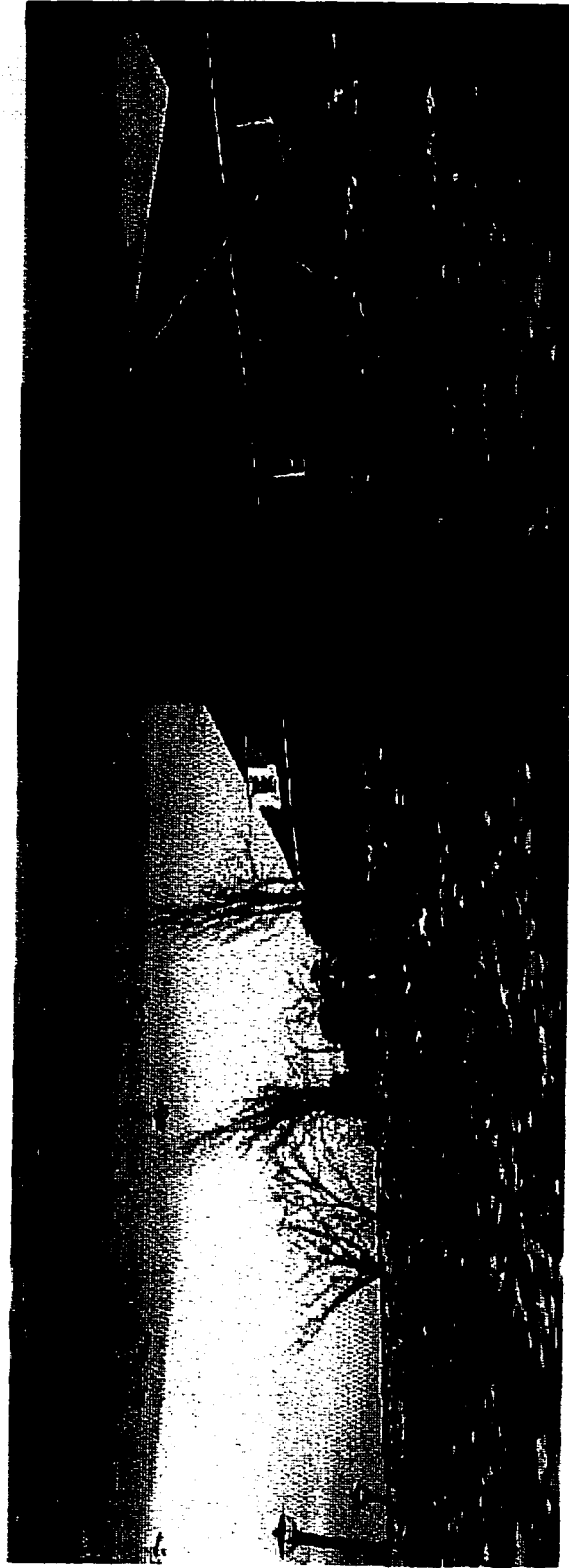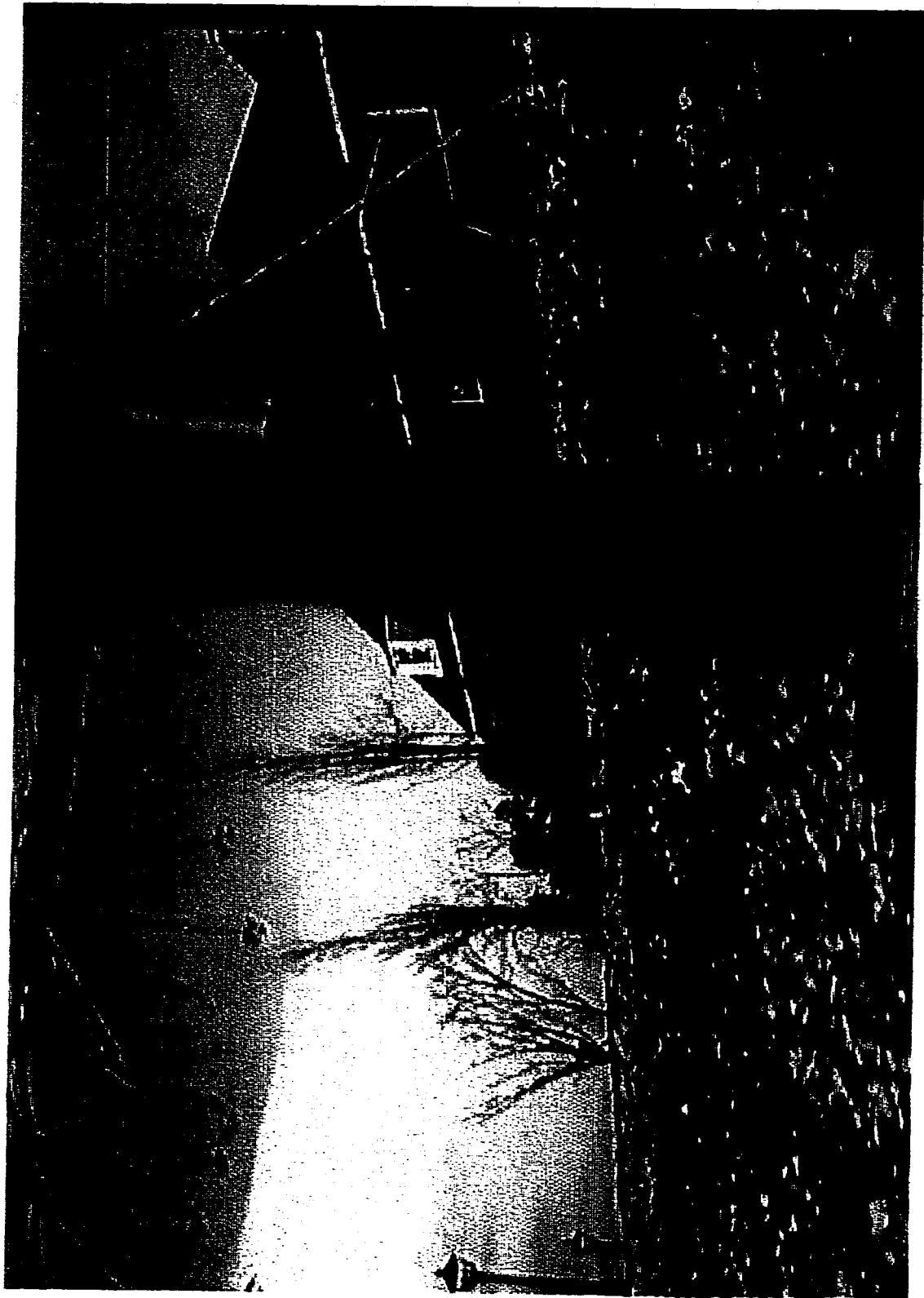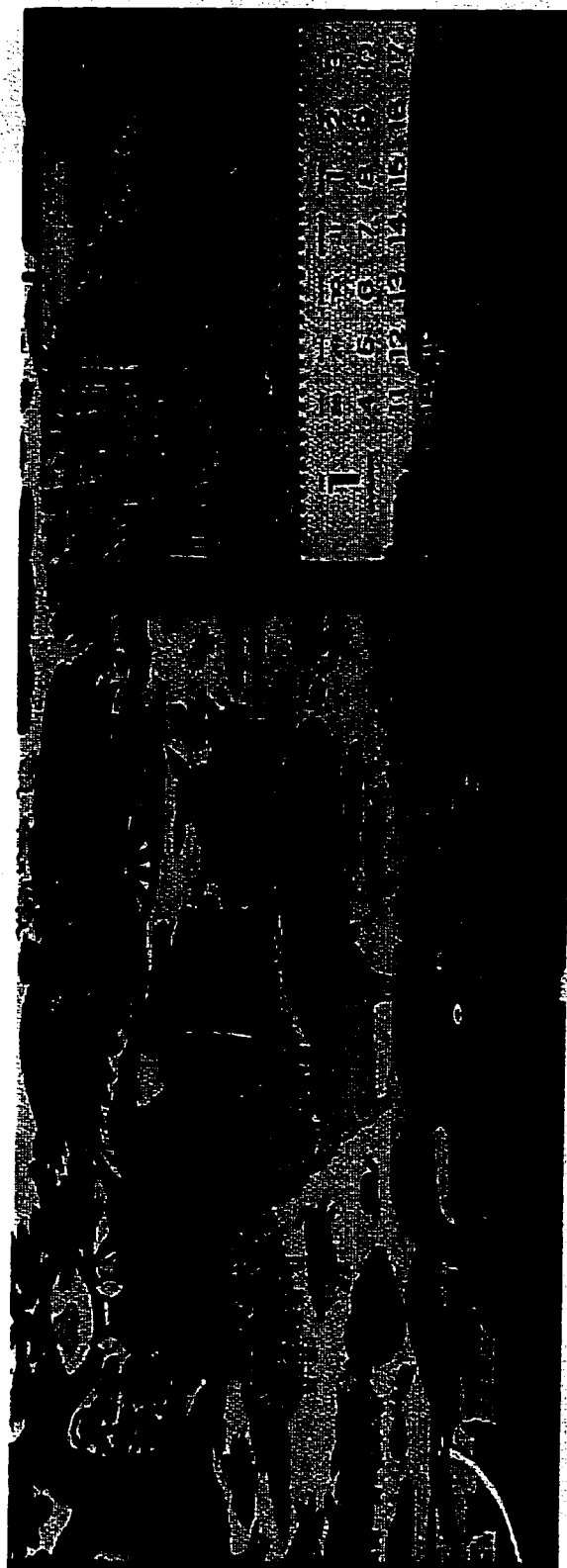
Figure 104 Original Train Sequence
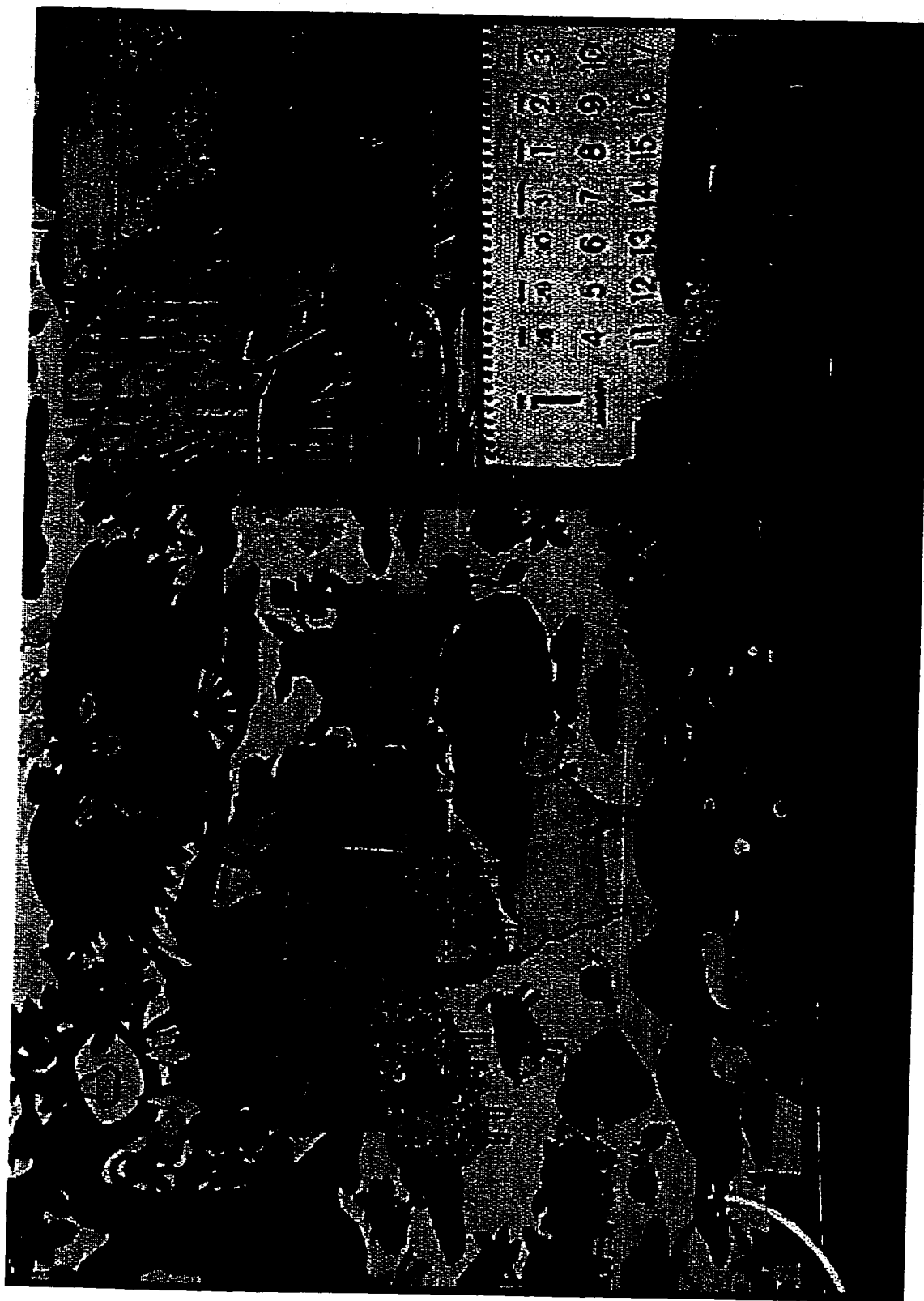
Figure 105 Adaptive Multiple Median Deinterlaced Frame of the Train
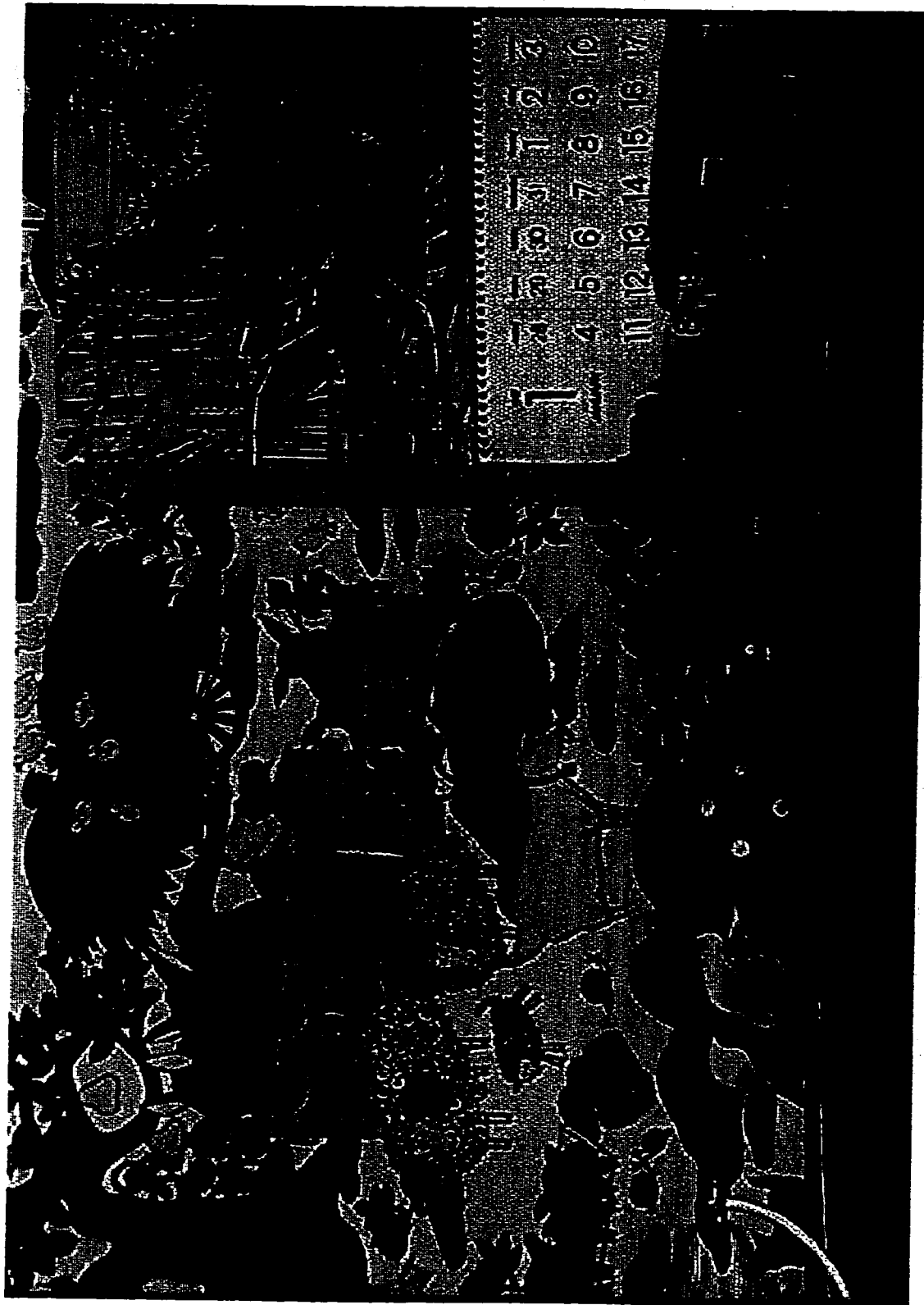
Figure 106 WDF Deinterlaced Frame of the Train
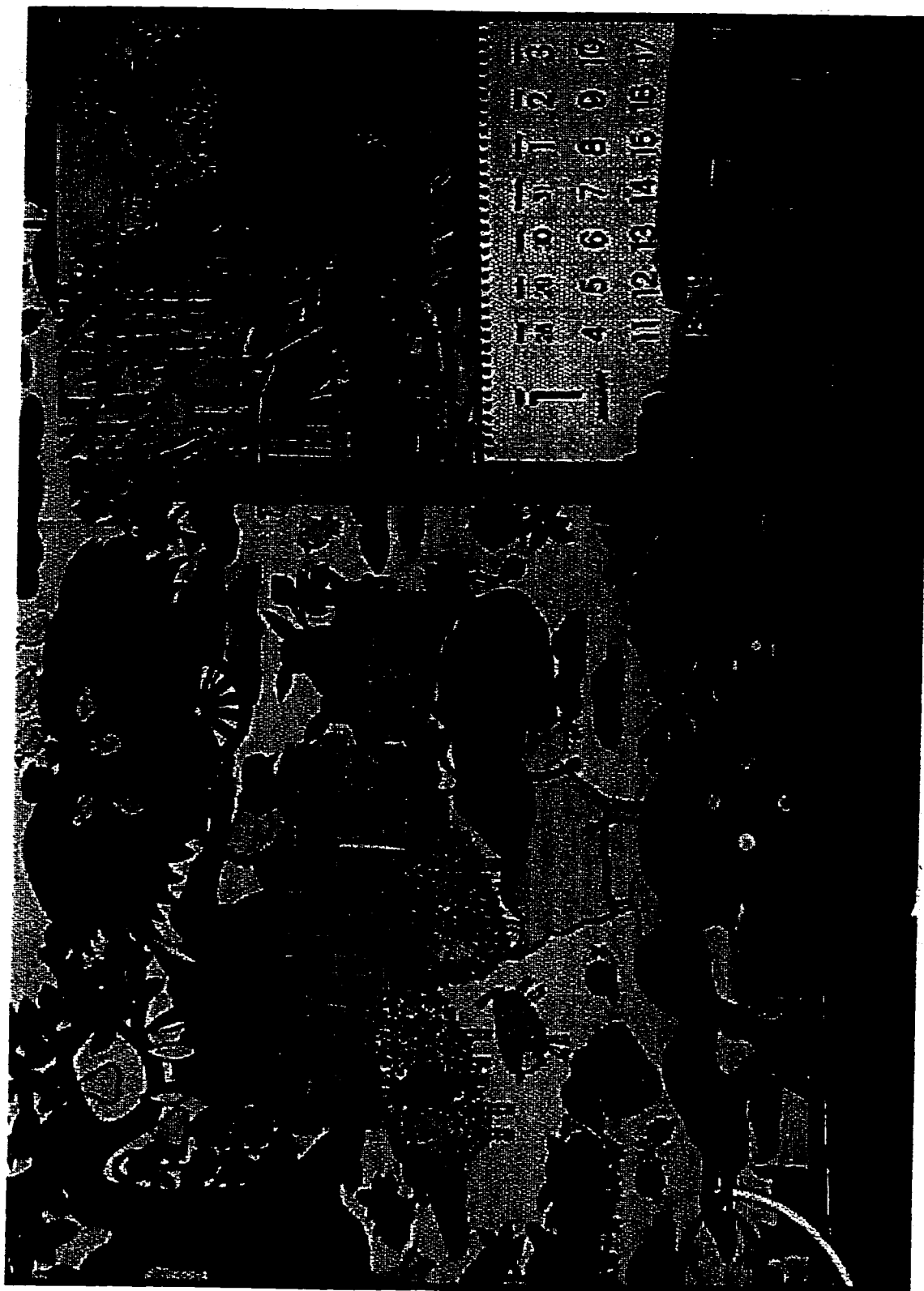
Figure 107 SVU DeInterlaced Frame of the Train

6 Three Dimensional Y/C Precombing and Separation using State Value Updating

6.1 Introduction

Video standards such as NTSC were originally designed without regard to color. Later, when color was added, quality was reduced in exchange for the compatibility of the existing bandwidth and receivers. Recent studies [1 - 4] of video signals allow us to reclaim the lost quality while keeping current system compatibility. The key is to process the TV signals in a 3-D space instead of the traditional 1-D space.

A color NTSC signal consists of two major parts: The luminance and the chrominance. The chrominance can be further broken down into a sum of two quadrature components: the in-phase component and the quadrature component. The components are quadraturely modulated by the color subcarrier at the frequency f_{sc}. The baseband of an NTSC signal $y(t)$ can be written in the following form:

$$\begin{aligned} y(t) &= L(t) + C(t) \\ &= L(t) + I(t)\cos(2\pi f_{sc}t + \phi) + Q(t)\sin(2\pi f_{sc}t + \phi) \end{aligned} \tag{6.1}$$

where $L(t)$ is a luminance signal, $C(t)$ is a chrominance signal, $I(t)$ is the in-phase part of the chrominance, and $Q(t)$ is the quadrature part of the chrominance. The subcarrier frequency f_{SC} is specified as 3.58 MHz. The video signal $y(t)$ is also known as a *composite* signal. The composite signal is subsequntly properly bandlimited and modulated by a carrier f_s to form the NTSC signal.

Traditionally, the video signal is processed in a 1-D domain. The spectrum of $y(t)$ was perceived to be as shown in Figure 108.
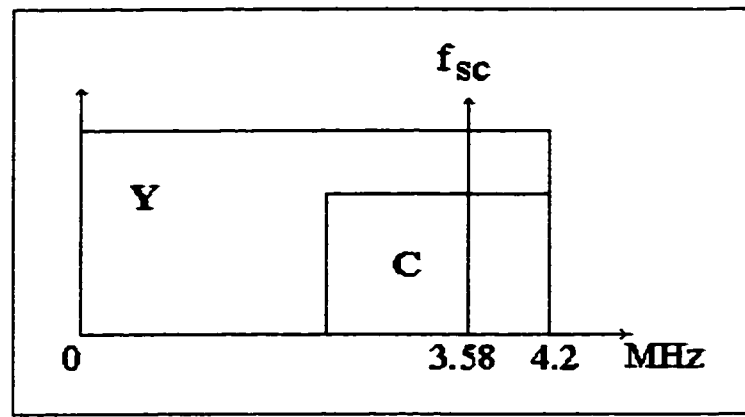
Figure 108. Frequency spectrum of a 1-D NTSC composite signal

In the traditional view, the spectral components of luminance and chrominance occupy and interleave the same band. Crosstalk of the luminance and chrominance is unavoidable if either or both of the components are wide and strong. The crosstalk effect appears as a form of false color if the luminance has strong high frequency components. On the other hand, if the chrominance has strong high frequency components, the picture will have false spatial texture. To eliminate the crosstalk effect, bandlimiting is needed. However, for the case of 1-D processing, bandlimiting the luminance reduces the resolution in the x direction. Therefore, the crosstalk effect causes a tradeoff between acceptable resolution and compatibility.

If one looks at the NTSC signal in a 3D perspective, one may see that the interlaced scanning is indeed a (1,1) quincunx structure on the *y-t* plane. The spectrum of the interlacing scan will have the form shown in Figure 109 [4].
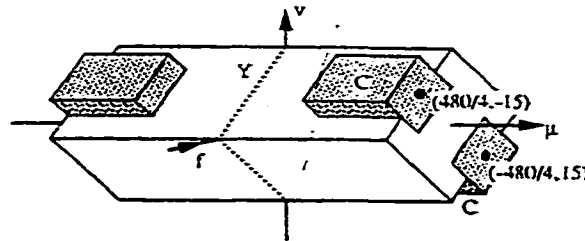
Figure 109. Original 3D Frequency Spectrum of an Interlaced Scan [4]

For the chrominance, the specification of the color subcarrier f_{sc} is an odd multiple of $f_l/2$ and $f_{fr.}/2$. The term f_l is the line frequency and $f_{fr.}$ is the frame frequency. The NTSC standard requires that the phase of the subcarrier to be shifted by 180° from line to line and from frame to frame. The phase of the subcarrier is shown in Figure 110 [3].
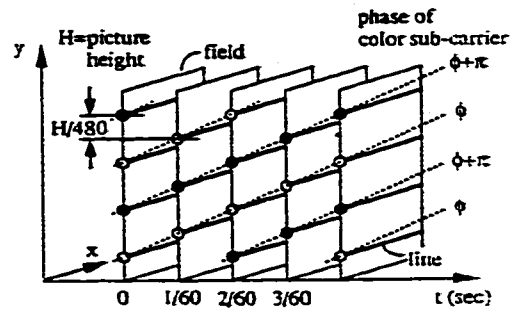
Figure 110. Interlace Scan and the Phase of the Color Subcarrier [3]

The phase shifts of the subcarrier contribute to the 3D modulation of the chrominance and the 3D spectrum is shown in Figure 111 [4].
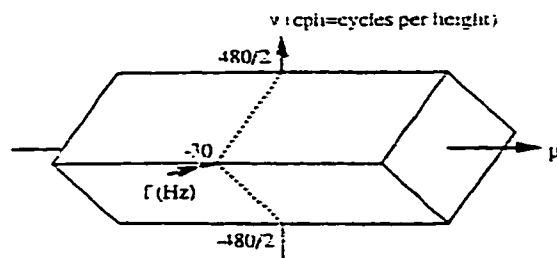
Figure 111. 3D Frequency Spectrum of an NTSC Signal [4]

From the 3D spectrum, one may see that the luminance can be bandlimited to prevent crosstalk with no decrease of resolution in the x-direction. To separate the luminance and

124

chrominance signal in a 3-D domain, we need filters to operate in a 3-D domain. In a later section, both FIR and WDF filtering will be discussed, and finally, the WDF using the SVU technique will be presented.

6.2 3D Y/C Precombing and Separation using Field-Combs
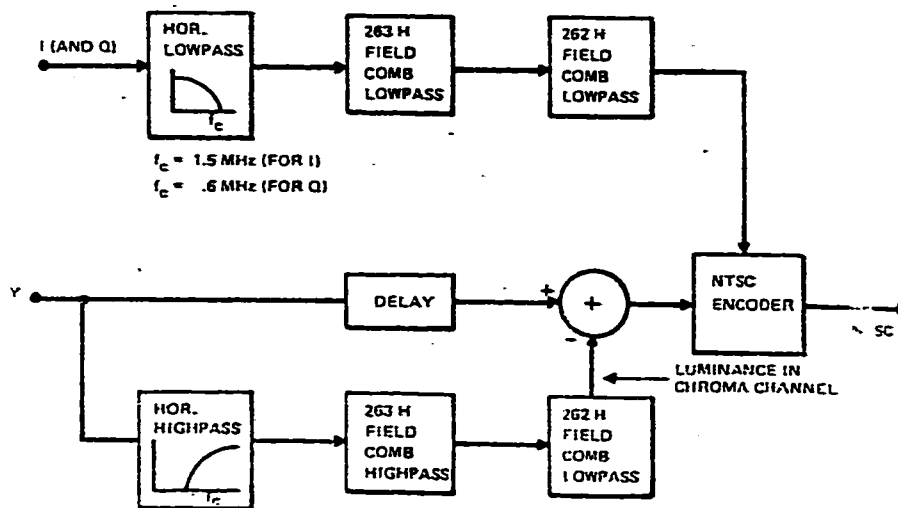
Figure 112. Y/C Precombing Structure

In the precombing system shown in Figure 112, chrominance signals I and Q will be bandlimited to the cutoff at 1.5 MHz and 0.6 MHz using horizontal lowpass filtering. The cutoffs are specified by the NTSC standard. Since the chrominance is an interlaced signal, diamond filtering will be performed after horizontal filtering. The chrominance diamond filter is composed of two field-combs (see Figure 113). The cutoffs of the diagonal spatial frequencies are $\sqrt{2}/2$. The resulting bandlimited chrominance is ready to be modulated into the precombed luminance.

For the luminance, space has to be made to allow the modulated chrominance to fit in. The luminance is first divided into two routes to make space. On one of the routes in Figure 112, all spectral components are removed except for those occupying the chrominance space. The filtered luminance is then subtracted from the original luminance signal to produce holes to fit in the chrominance. Then, both luminance and chrominance are combined and sent to a standard NTSC modulator.

To separate the luminance and chrominance on the receiver side, a block diagram showing the process is given in Figure 113 [2].

Figure 113. Receiver's 3D Y/C Separation

The field-combs used in Figure 113 and Figure 114 are of primary importance in this chapter. There are three types of field-combs we will use: FIR field-combs, WDF field-combs and SVU WDF field-combs.
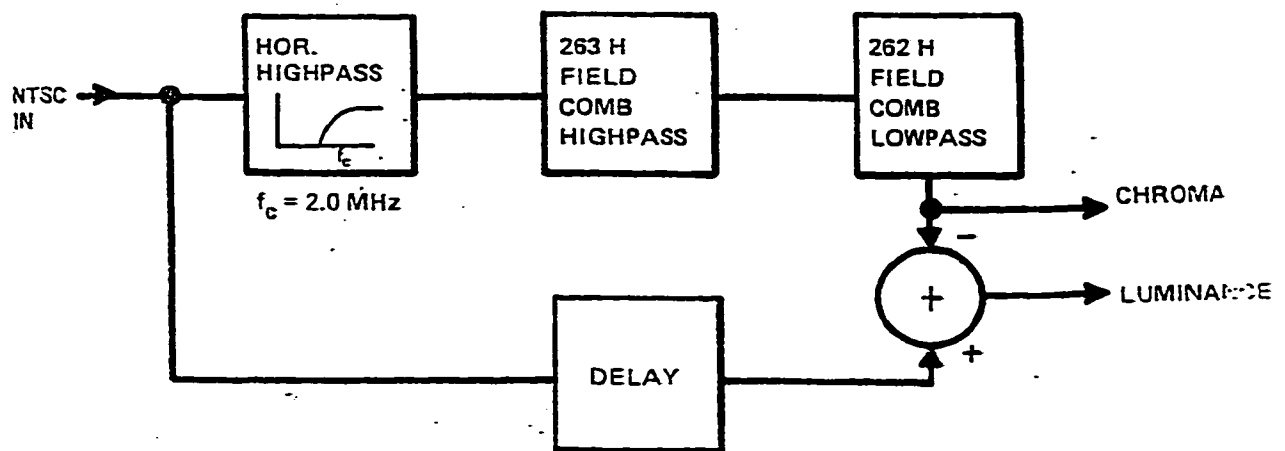
6.2.1 FIR Field-Combs [2]

The FIR field-combs are weighted-sum averaged along the diagonal direction on the y-t plane. The FIR field-comb will have perfectly linear phase, but the frequency response is limited by the ability of FIR filtering. The field-comb suggested by Strolle [2] is shown in Figure 114.

262 H FIELD COMB

263 H FIELD COMB

a

b

TIME

TIME

OUT = .5 x IN (Y, T)
± .3 x [IN (Y-1, T-1) + IN (Y + 1, T + 1)]
∓ .05 x [IN (Y-3, T-3) + IN (Y + 3, T + 3)]

OUT = .5 x IN (Y, T)
± .3 x [IN (Y + 1, T-1) + IN (Y-1, T + 1)]
∓ .05 x [IN (Y + 3, T-3) + IN (Y-3, T + 3)]
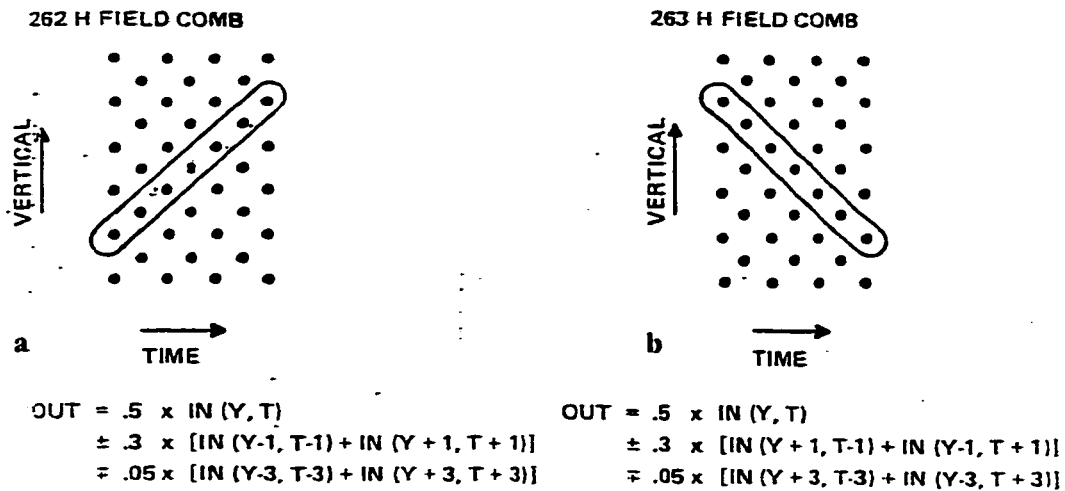
Figure 114. FIR Field Comb Implementation
(a) 262 FIR field comb and (b) 263 FIR field comb.

6.2.2 WDF Field-Combs

The WDF field-comb filters are halfband lowpass WDFs operating along the diagonal axes of the y-t plane (see Figure 115). The combined operations result in a diamond frequency characteristic. The cutoffs of the diagonal spatial frequencies are $\sqrt{2}/2$. The resulting bandlimited chrominance is ready to be modulated into the precombed luminance.
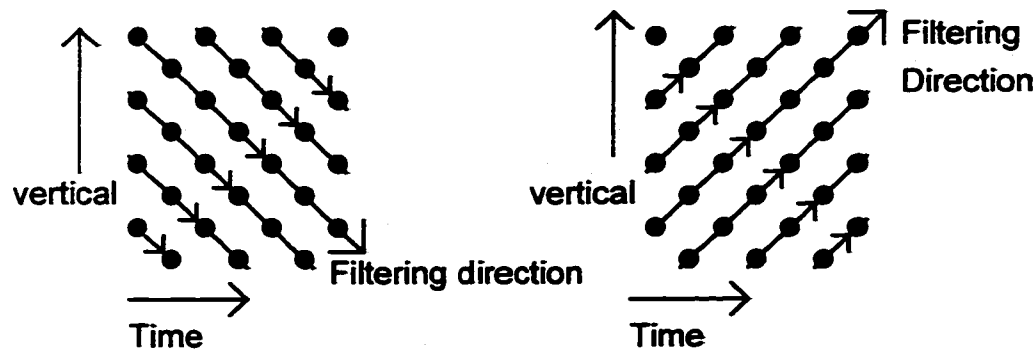
Figure 115. WDF Field-Combs

6.2.3 Field-Comb Using WDFs and the SVU Technique

With the WDF field-combs as shown in Figure 114, the SVU technique is also used to reduce ringing due to diagonal luminance filtering in Y/C precombing and separation. If the decision algorithm detects a discontinuity, the decision algorithm will set the state values to simulate a steady-state condition. The algorithm is similar to the 1-D SVU algorithm used in chapter 6 and is shown as following:

```
factor = (Coeff - 1)/(Coeff + 1)
dl = bas(x(i, j) - Buffer(i, k))
if (dl > threshold)
{
        Delay[i][j][2] = factor*x(i, j)
};
```

The value *factor* is the factor to calculate the steady-state state values. The delay plane Delay(*i*, *j*, 2) corresponds to the state value E*q*1 in Figure 27 of Chapter 3. The array *buffer(i, j)* is the storage of the previous field. The above statements can be inserted anywhere after the linear filtering process.

6.3 Simulation Results

In this section, the cooperative process shown in Figure 112 and Figure 113 uses FIR filters, WDFs and SVU WDFs to produce different Y/C precombed and separated pictures. For all methods, the horizontal lowpass filtering is the same. The I component is lowpassed to 1.5MHz cutoff using a fifth order WDF with the coefficients 0.5, 0.5, 0.5, 0.5 and 1. The Q component uses a second order WDF cascaded with a third order then another second order lowpass WDF to achieve 0.6 MHz cutoff. The second order filter has 0.5 and 1 as the coefficients and the third order filter has 0.35, 0.35 and 1 as the coefficients. The highpassed luminance signals for all cases are obtained by subtracting the lowpassed signal from the original signal. The lowpassed filters are second order WDF with coefficients 0.35 and 1.

For the FIR field-comb, the specifications are given in Figure 6.6. The WDF and SVU field-combs are the diamond WDF using 0.5 and 1 as the coefficients.

The test sequences are the same as those in Chapter 5. Each of the sequences has a field shown in Figure 96 (Ping-Pong), Figure 100 (The House) and Figure 104 (The Train). All sequences are precombed, encoded and separated using the procedures shown in Figure 112 and Figure 113. Combining the effects of FIR precombing and WDF separation, and FIR precombing and SVU separation, are also studied. Finally, because it is possible to use 3-D separation and deinterlacing together to improve picture quality, the WDF-separated sequences will be deinterlaced using WDF and compared with the SVU-separated and SVU-deinterlaced sequences. As in Chapter 5, the mean square error (MSE) and signal to noise ratios (SNR) are given for comparison. The MSE and SNR are calculated using Equation (3.5) and Equation (3.6) consecutively. Because the pictures are in color, the MSE and SNR will be calculated for each of the R, G and B value is. The average values will be presented in the tables. Because there are no original deinterlaced sequences, the deinterlaced results cannot be calculated

For the first testing sequence Ping-Pong, a field of each of the FIR-FIR (Figure 116), WDF-WDF (Figure 117), SVU-SVU (Figure 118), FIR-WDF (Figure 119) and FIR-SVU (Figure 120) precomb-separation sequences are shown.

The field of FIR-FIR precombed and separated sequence for Ping-Pong shows no visible artifacts. The WDF-WDF processed field in Figure 117 shows visible banding on the upper side of the hand. In Figure 118, the SVU-SVU processed field shows no artifacts although the SVU uses a WDF for linear filtering. For the FIR and WDF hybrid process, both of the FIR-WDF (Figure 119) and FIR-SVU (Figure 120) pairs are good. The FIR-WDF hybrid using WDF deinterlacing shown in Figure 119 has ringing effects around the ping pong but the FIR-SVU in Figure 120 hybrid has none. The MSE and SNR are shown in Table 4.

Table 4. MSE and SNR for the Sequence Ping-Pong

Method	FIR-FIR	IIR-IIR	SVU-SVU	FIR-IIR	FIR-SVU
MSE	55.96	68.11	62.11	64.14	59.59
SNR (dB)	25.43	22.43	23.88	23.72	24.62

For the test image The House, the original video field is shown in Figure 100. The FIR-FIR processed field shown in Figure 123 has no visible artifacts while the IIR-IIR processed field shown in Figure 124 exhibits ringing near several moving objects. The SVU-SVU processed field in Figure 125 has some ringing but less than the ringing in the case of IIR-IIR processing. For the FIR-IIR hybrid process, Figure 126 improved over the IIR-IIR case, but some ringing around the branches and street light on the left corner are still noticeable. For deinterlaced hybrid processing, the FIR-IIR combination using IIR deinterlacing (Figure 128) has a phase and ringing problem accumulated which seriously damages the picture. The FIR-SVU hybrid using SVU deinterlacing (Figure 129) has minor ringing on the branches but the overall quality is acceptable. The calculated MSE and SNR are shown in Table 5.

Table 5. MSE for the Sequence The House

Method	FIR-FIR	IIR-IIR	SVU-SVU	FIR-IIR	FIR-SVU
MSE	48.33	51.13	50.39	49.79	49.92
SNR (dB)	21.21	20.35	20.70	20.76	20.77

For the last test sequence: Train, one of the original fields is shown in Figure 104. The FIR-FIR processed field has some false color appearing in the central-left top area. The false color may due to the moving diagonal pattern, resulting in the FIR field comb being unable to band-limit the luminance spectrum. Note that the numbers on the calendar also have some minor false color. An FIR-FIR field is shown in Figure 130. For the IIR-IIR processed field (Figure 131), ringing occurs around moving patterns as expected. For the SVU-SVU (Figure 132), most of the ringing effects are suppressed, but there is still some residual ringing next to several very high contrast patterns. For the FIR-IIR hybrid process, the result is greatly improved (Figure 133) but some ringing still remains if observed closely. The ringing appears on the fence and on red pattern next to the ball. For the FIR-SVU hybrid (Figure 134), the ringing appearing on the fence and the red pattern next to the ball has been removed or reduced. The WDF-deinterlaced FIR-WDF hybrid (Figure 135) shows serious ringing but the SVU-deinterlaced FIR-SVU hybrid Figure 136) has drastically reduced ringing. The table of MSE and SNR is shown in Table 6.

Table 6. MSE and SNR for the Sequence The Train

Method	FIR-FIR	IIR-IIR	SVU-SVU	FIR-IIR	FIR-SVU
MSE	52.51	55.22	54.43	53.96	54.07
SNR (dB)	18.39	17.49	17.82	18.06	18.03

The simulations have shown that FIR-FIR Y/C precombing and separation have very clean pictures since there are no ringing problems, but occasional false color appearing around sharp edges is not pleasant to look at. The SVU-SVU Y/C processed picture has some ringing but is still better than the WDF-WDF Y/C processed pictures. Both the FIR-WDF and FIR-SVU Y/C processed pictures have good quality, but the FIR-WDF pictures still has a ringing problem. For the deinterlaced sequence, the accumulation of phase error due to Y/C processing and deinterlacing will increase the ringing effect. Therefore, the WDF-deinterlaced FIR-WDF Y/C-processed pictures have more ringing problems than the SVU-deinterlaced FIR-SVU Y/C-processed pictures. In the latter case, most of the ringing was gone unless there are some very high contrary patterns. Finally, for the MSE and SNR, FIR-FIR pictures have the lowest MSE and the highest SNR. This result may suggest that FIR-FIR pictures have the least ringing problem, which is expected. For the WDF and SVU comparisons, both the WDF-WDF and FIR-WDF combinations have a larger MSE and a lower SNR than the SVU-SVU and FIR-SVU pair.

6.4 Summary

Composite television signals are encoded into luminance and chrominance signals. Crosstalk is unavoidable if signals are encoded and separated using traditional 1-D methods. A better way to encode and separate composite signals is by using 3-D processing. It has been shown that signals have to be repetitively lowpass-filtered in 3-D Y/C processing. If the lowpass filters are FIR filters, then the whole system will be expensive. If the filters are recursive, such as WDFs, then phase distortion will be the main problem. To find a better way to balance between quality and complexity, the SVU technique was evaluated for this application.

In this chapter, we have studied the cooperative Y/C processing method [2] using three kinds of filters: FIR filters, WDFs and WDF SVU. The SVU WDF is more effective than the WDF alone. The ringing caused by WDFs has been reduced to a very low degree using SVU. It is especially true when the Y/C-separated sequences are further deinterlaced. If there are no SVU processes to reduce phase distortion, the nonlinear phase effect will be accumulated throughout the entire process, resulting in a serious ringing problem.

In the simulations, hybrid systems used FIR filters for encoding. The separation was performed using WDFs or SVU WDFs. The hybrid systems are particularly useful because broadcasting stations usually do the encoding. The stations are less price-sensitive than consumers and can afford more complex FIR filters to perform perfect 3-D precombing for encoding. In this case, the simulations show that SVU WDFs have separation results comparable to, or even better than, the results obtained using FIR filters for separation. Although in some cases SVU results still have a minor ringing problem, the great computational advantage of SVU will offset the problem.

The simulations conclude that WDFs with the SVU technique provides a low-hardware-requirement solution in performing Y/C precombing and separation over FIR filters,

while producing an acceptable result. By combining the SVU deinterlacing technique in Chapter 6, a complete IDTV system can be implemented using SVU technique on the receiver end. This can substantially reduce the complexity and cost of the receivers.

References

[1]   E. Dubois, M. N. S. Sabri and J. Y. Ouellet, "Three-dimensional spectrum and processing of digital NTSC signals," *SMPTE Jour.*, pp. 372 - 378, April 1982.

[2]   C. H. Strolle, "Cooperative processing for improved NTSC chrominance/luminance separation," *SMPTE Jour.* pp. 782 - 787, August 1986.

[3]   E. Dubois and W. Schreiber, "Improvements to NTSC by multidimensional filtering," *SMPTE Jour.*, Vol. 97, pp. 446 - 463, June 1988.

[4]   T. Fukinuki and N. Suzuki, "Multidimensional signal processing for NTSC," *IEICE Trans. Fundamentals*, VOL. E75-A, NO. 7, July 1992.
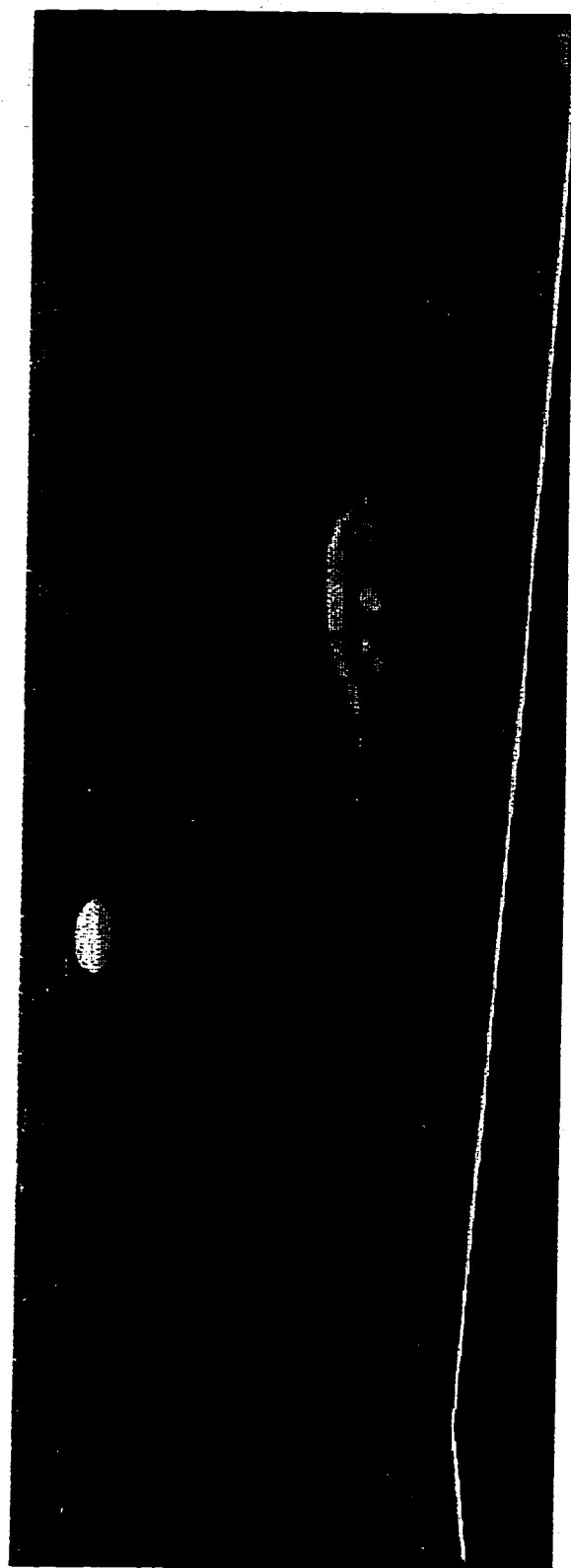
Figure 116. FIR - FIR Precombed and Separated Ping-Pong
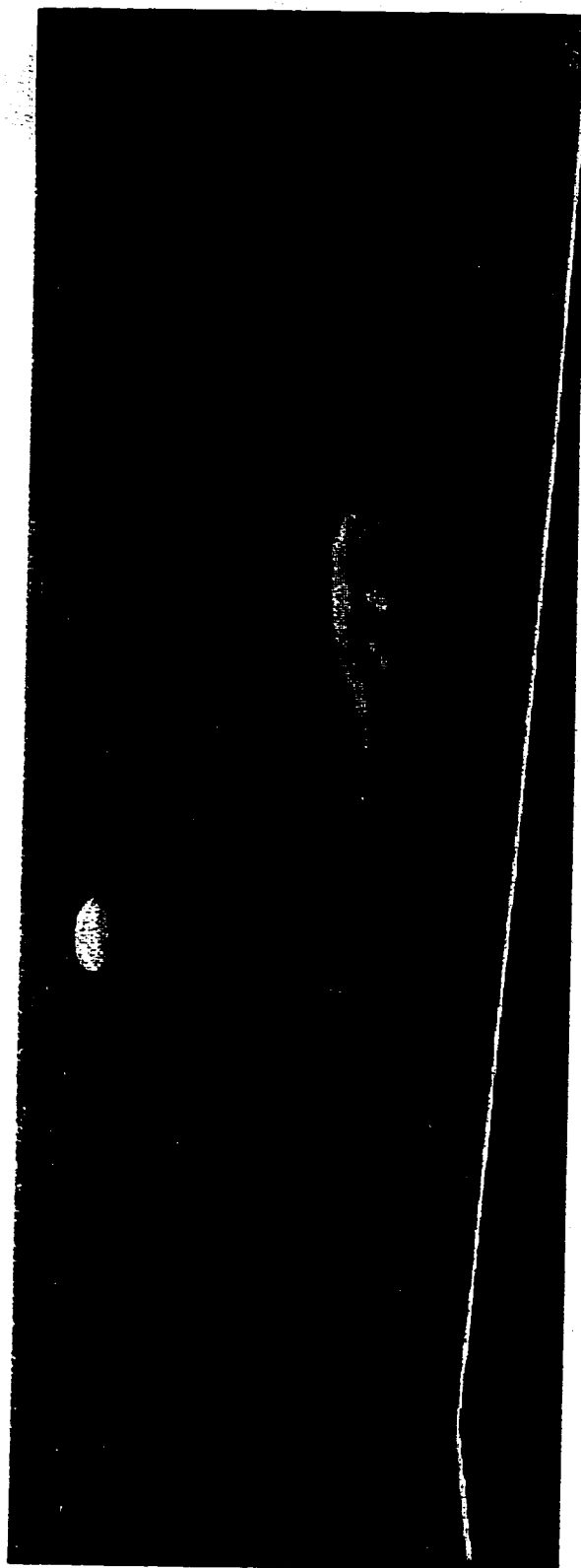
Figure 117. IIR - IIR Precombed and Separated Ping-Pong
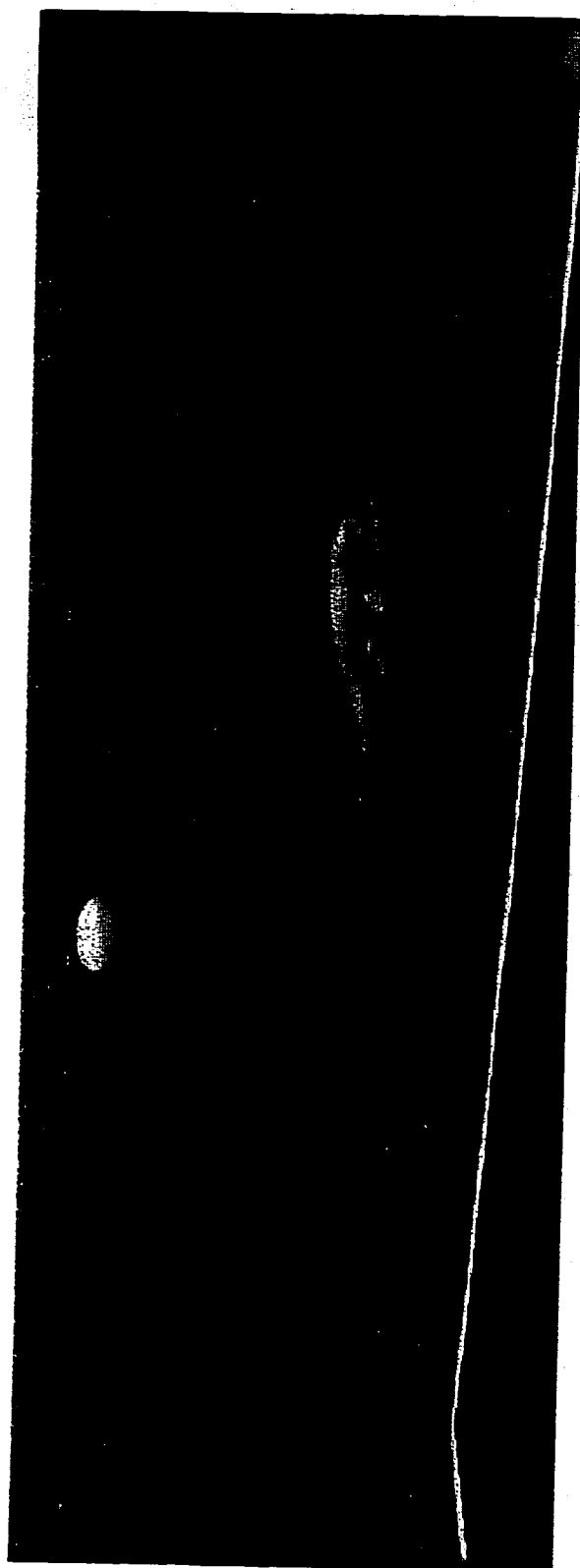
Figure 118. SVU - SVU Precombed and Separated Ping-Pong
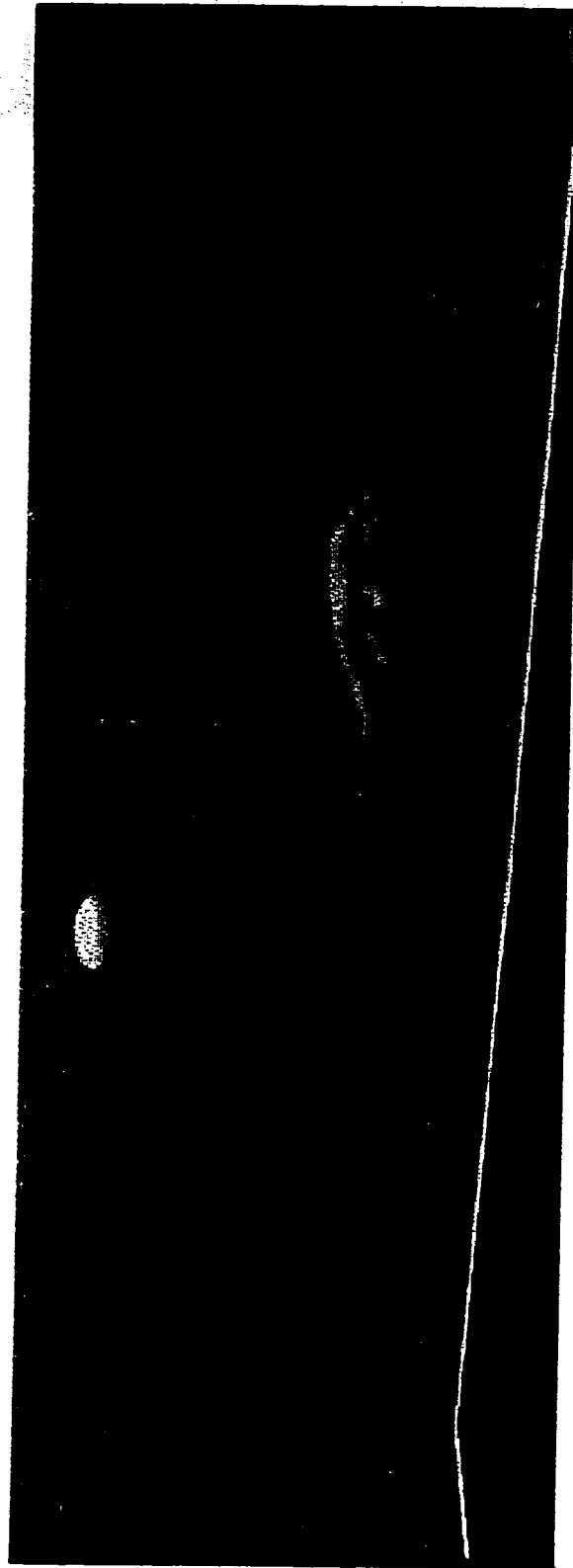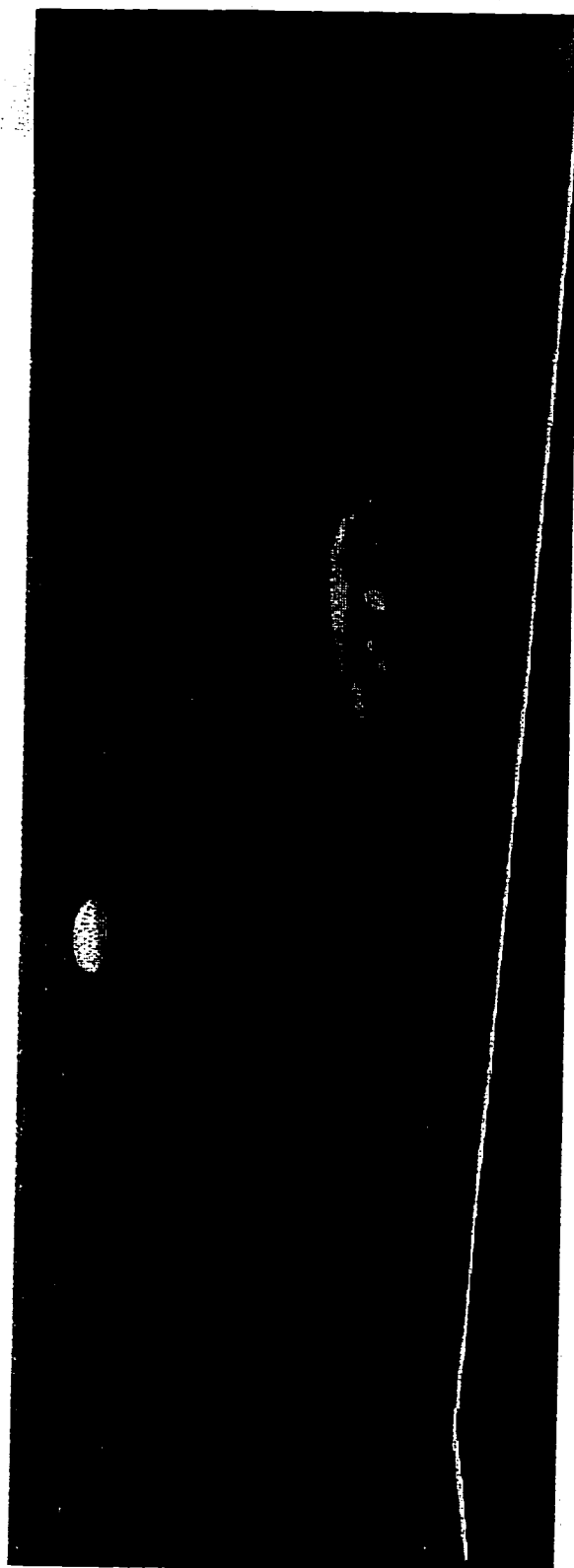
Figure 119. FIR - IIR Precombed and Separated Ping-Pong
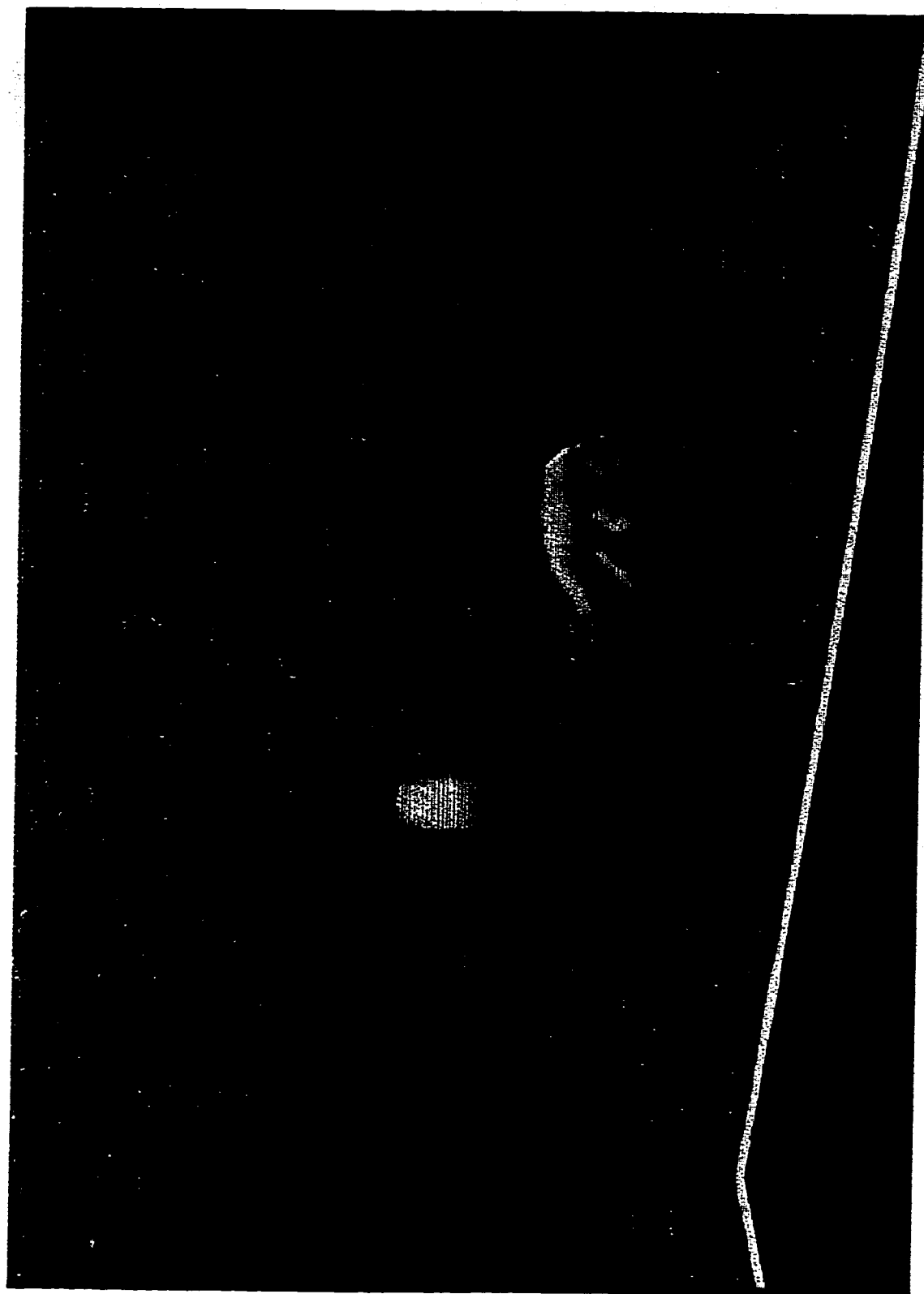
Figure 120. FIR - SVU Precombed and Separated Ping-Pong

141

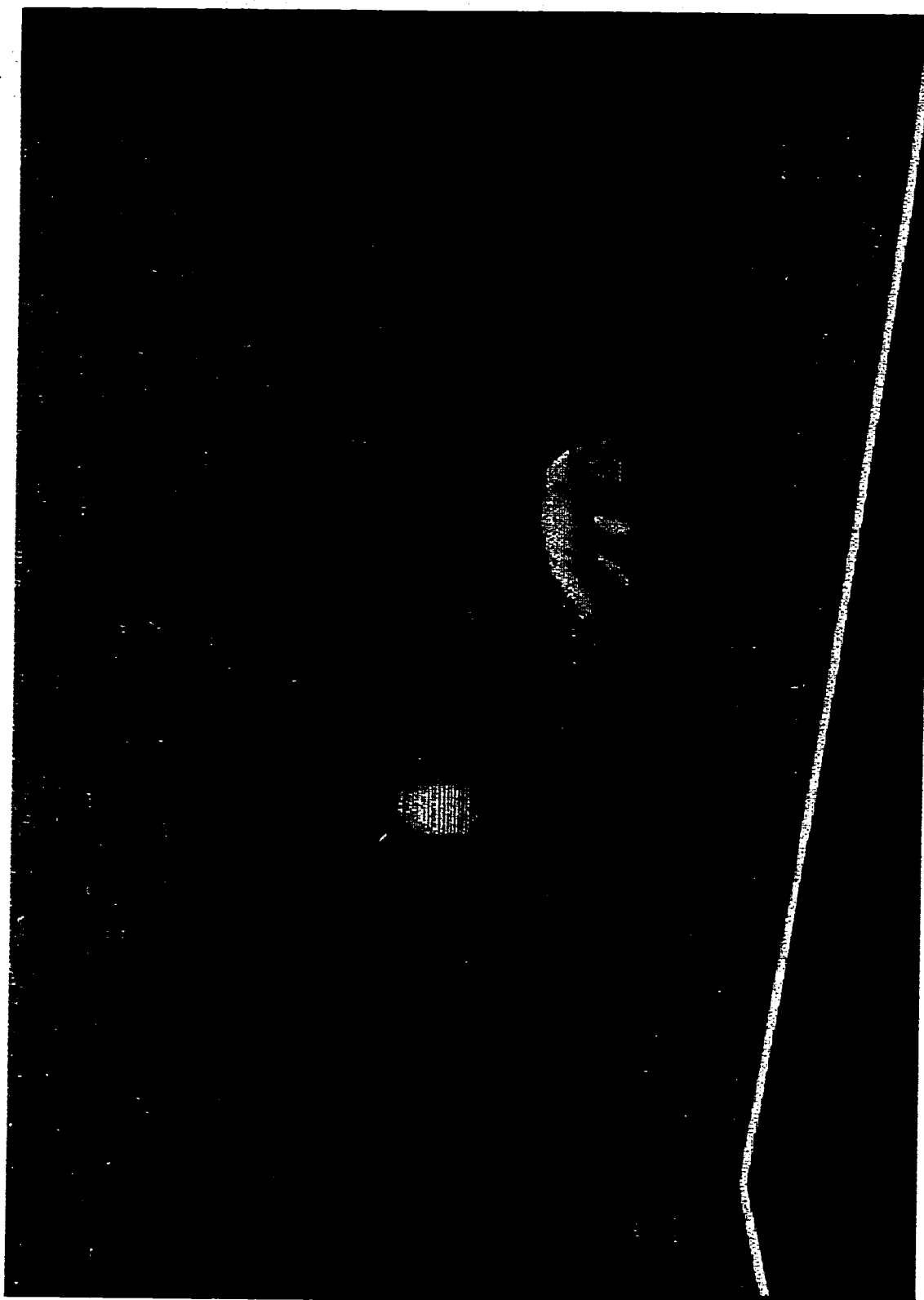Figure 121. FIR - IIR Precombed, Separated and IIR Deinterlaced Ping-Pong

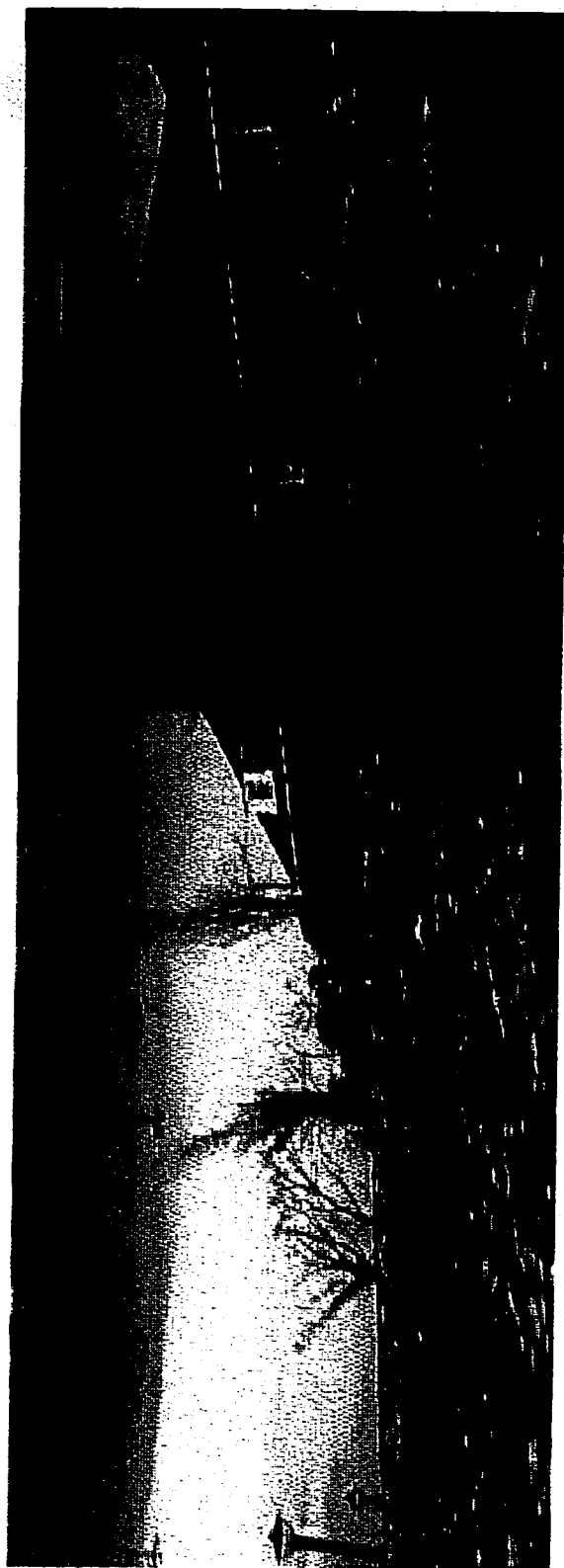Figure 122. FIR - SVU Precombed, Separated and SVU Deinterlaced Ping-Pong

143

Figure 123. FIR - FIR Precombed and Separated The House

Figure 124. IIR - IIR Precombed and Separated The House

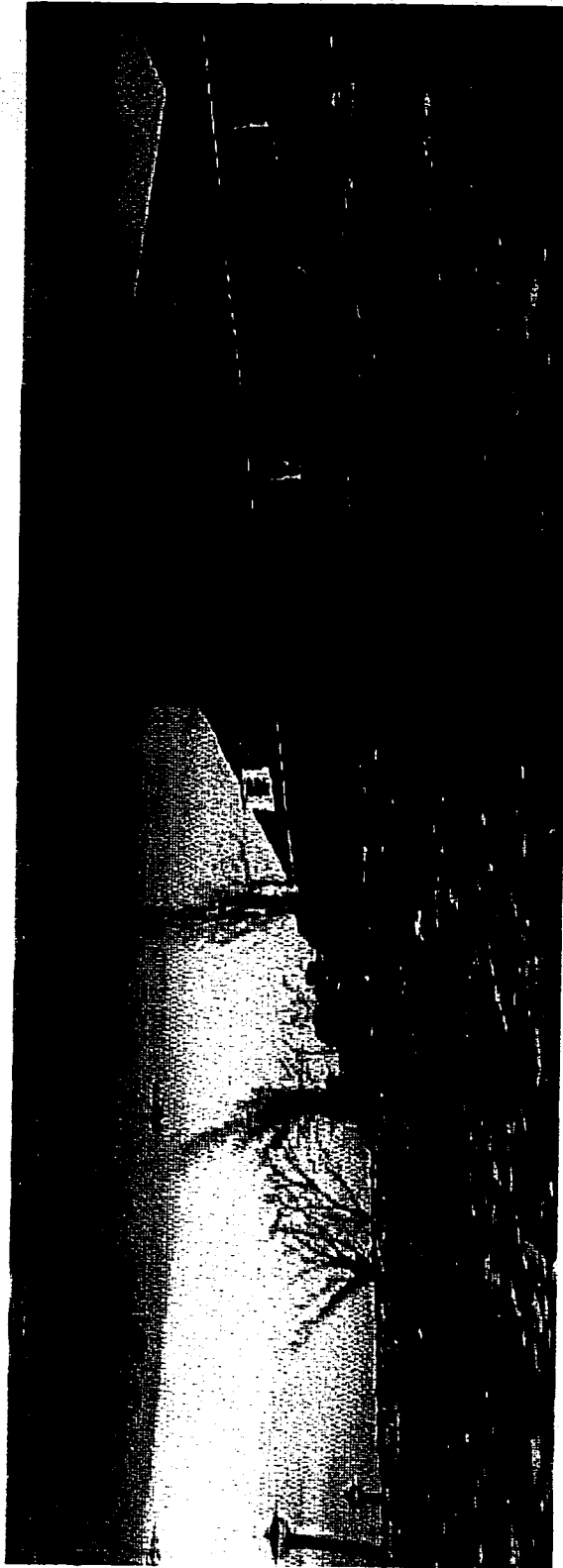Figure 125 SVU - SVU Precombed and Separated The House
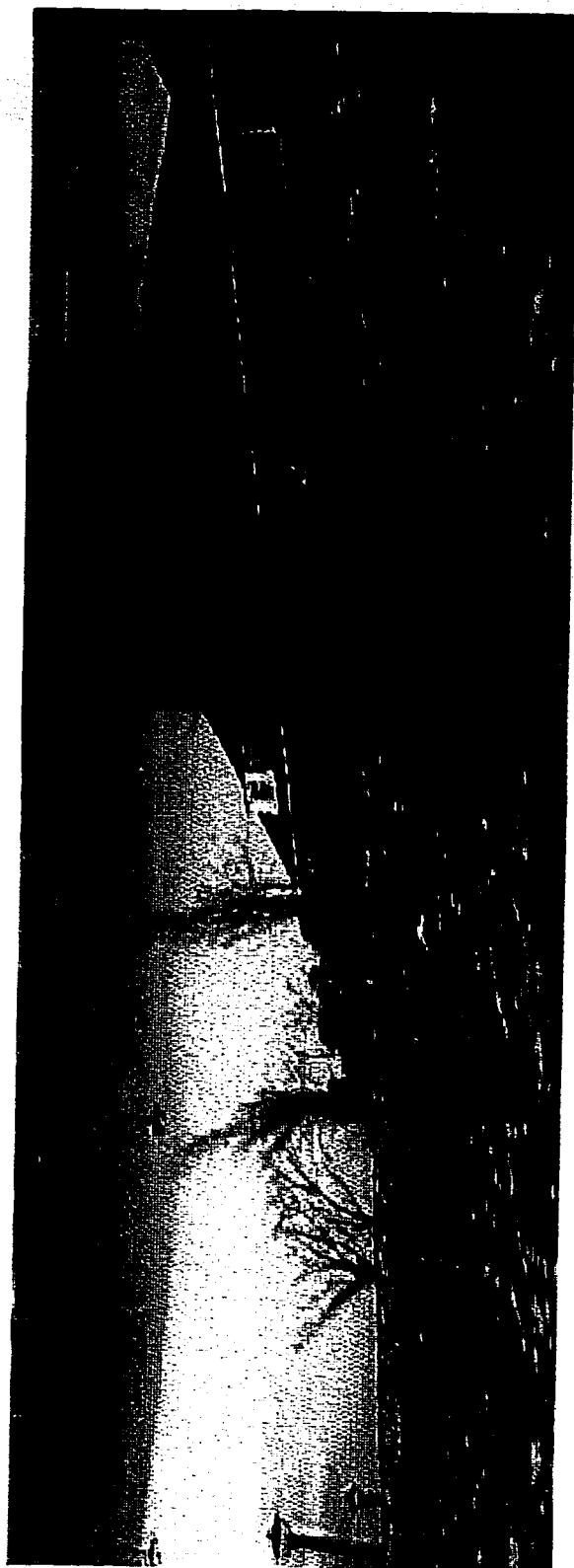
Figure 126. FIR - IIR Precombed and Separated The House
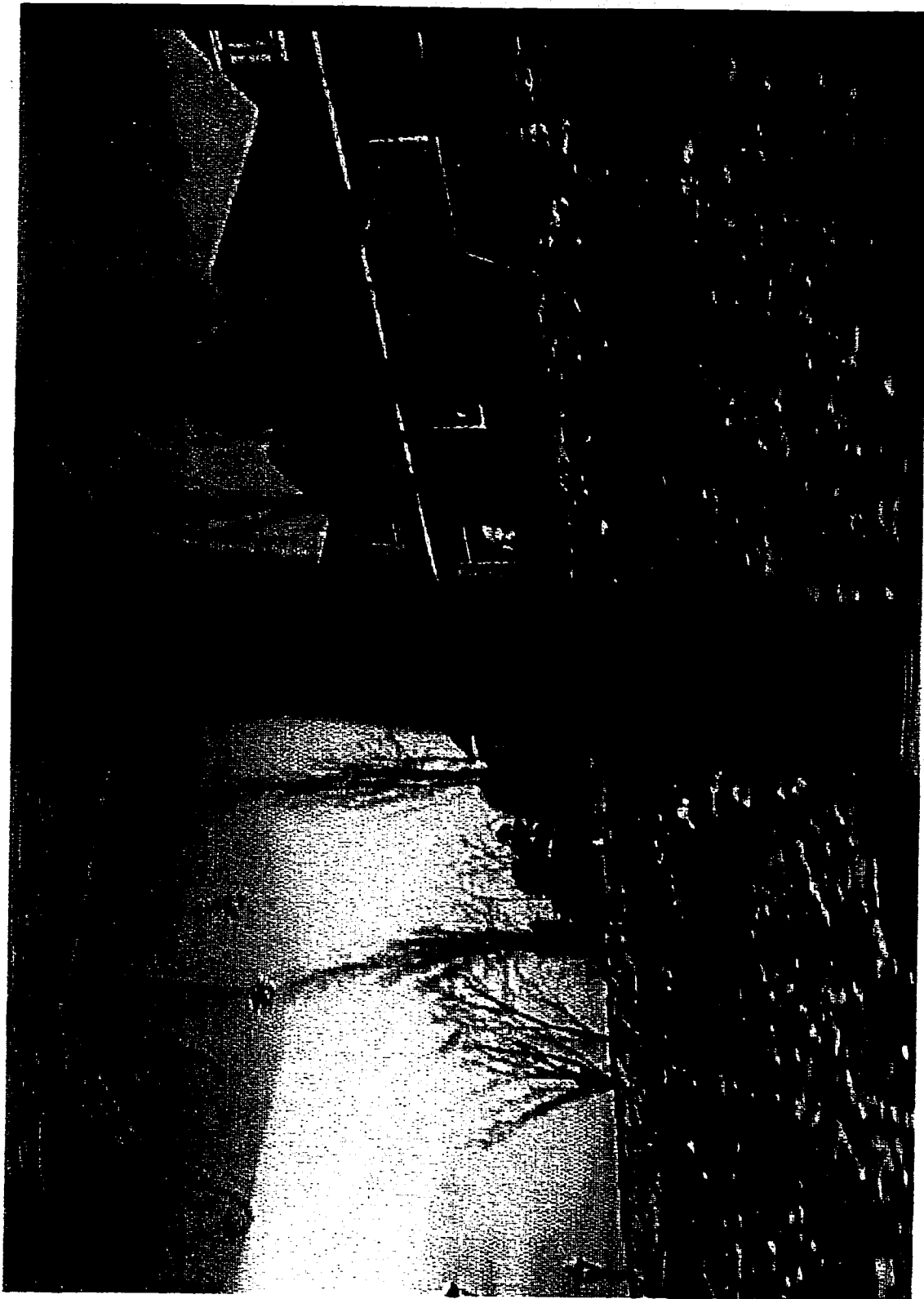
Figure 127. FIR - SVU Precombed and Separated The House

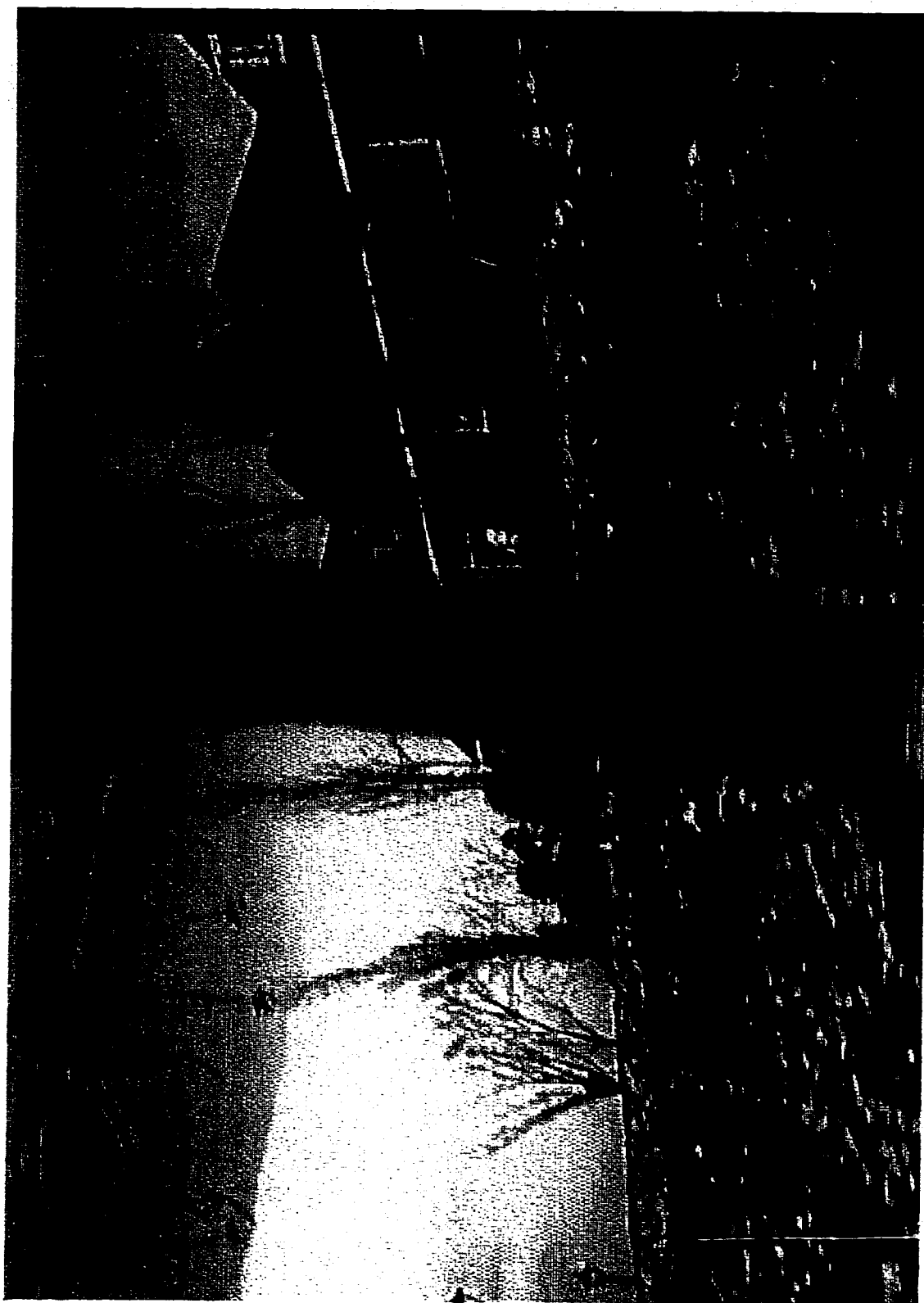Figure 128. FIR - IIR Precombed, Separated and IIR Deinterlaced The House

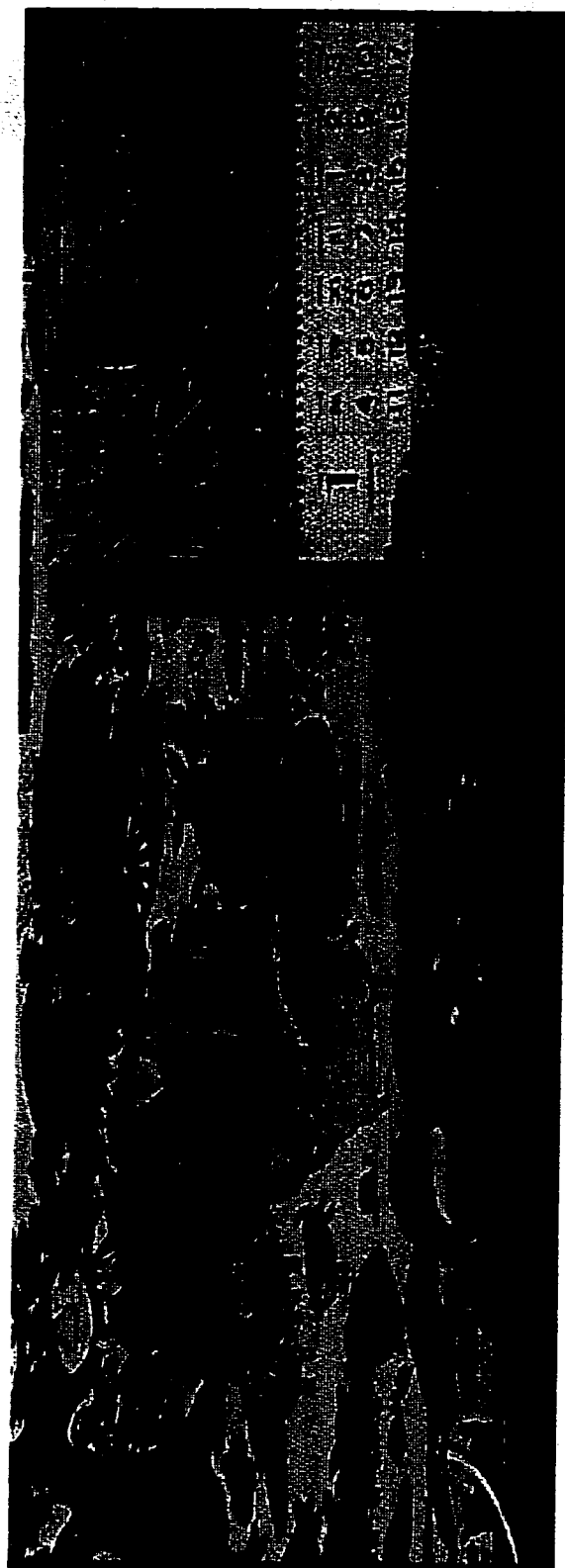Figure 129. FIR - SVU Precombed, Separated and SVU Deinterlaced The House
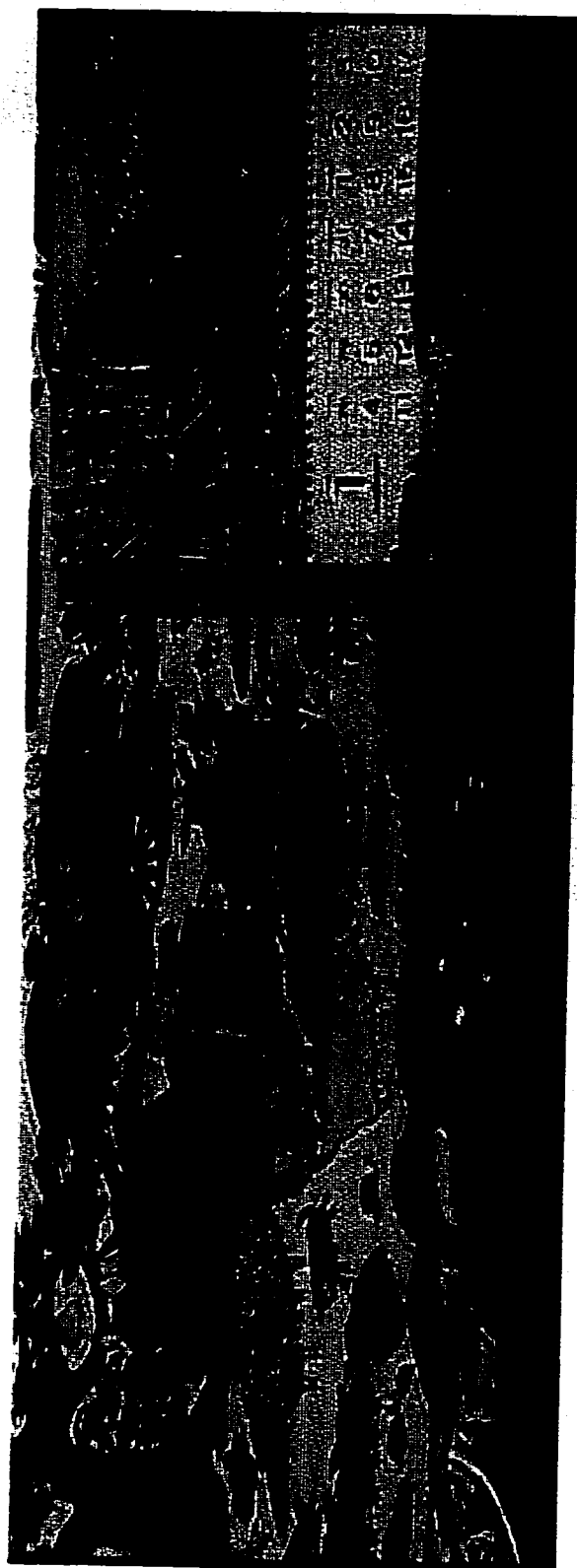
Figure 130. FIR - FIR Precombed and Separated The Train

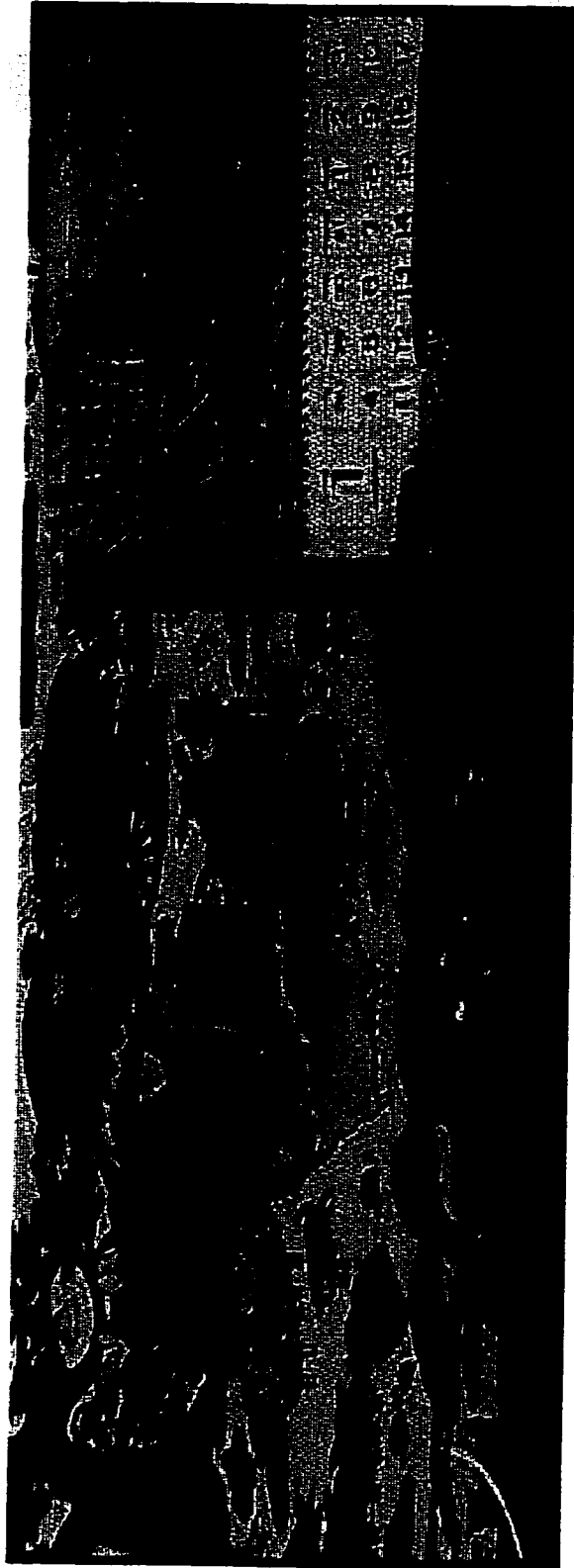Figure 131. IIR - IIR Precombed and Separated The Train

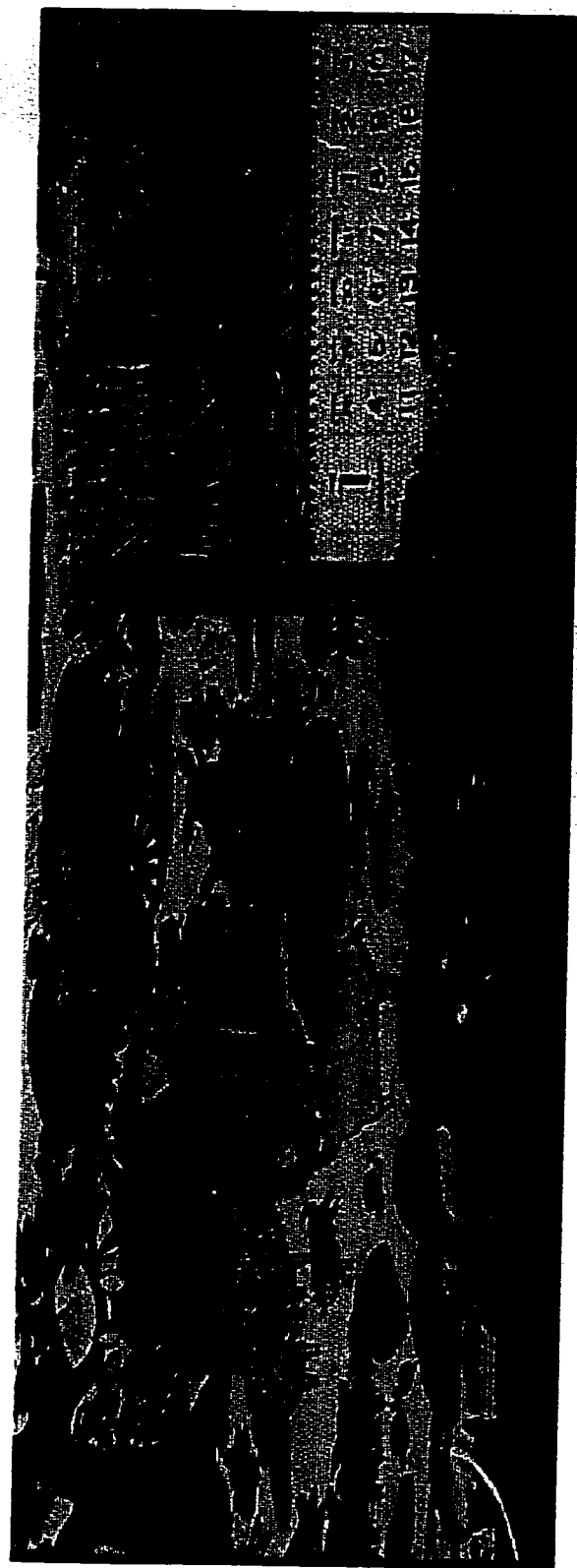Figure 132. SVU - SVU Precombed and Separated The Train

Figure 133. FIR - IIR Precombed and Separated The Train

154
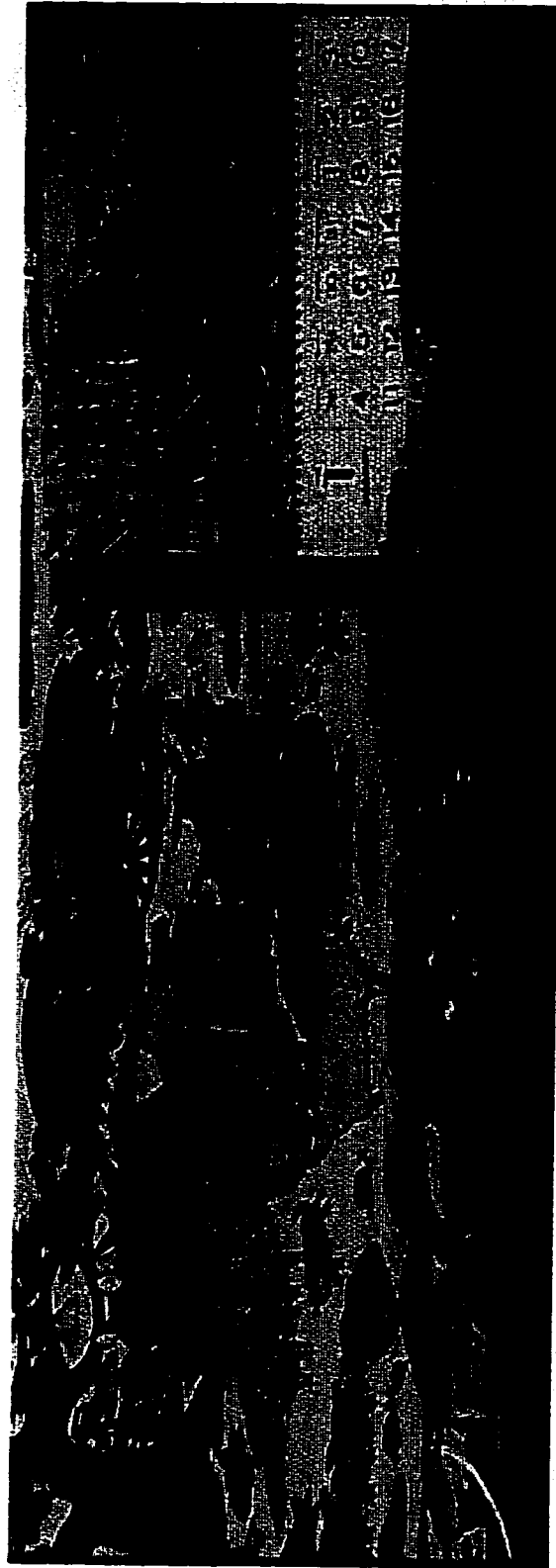
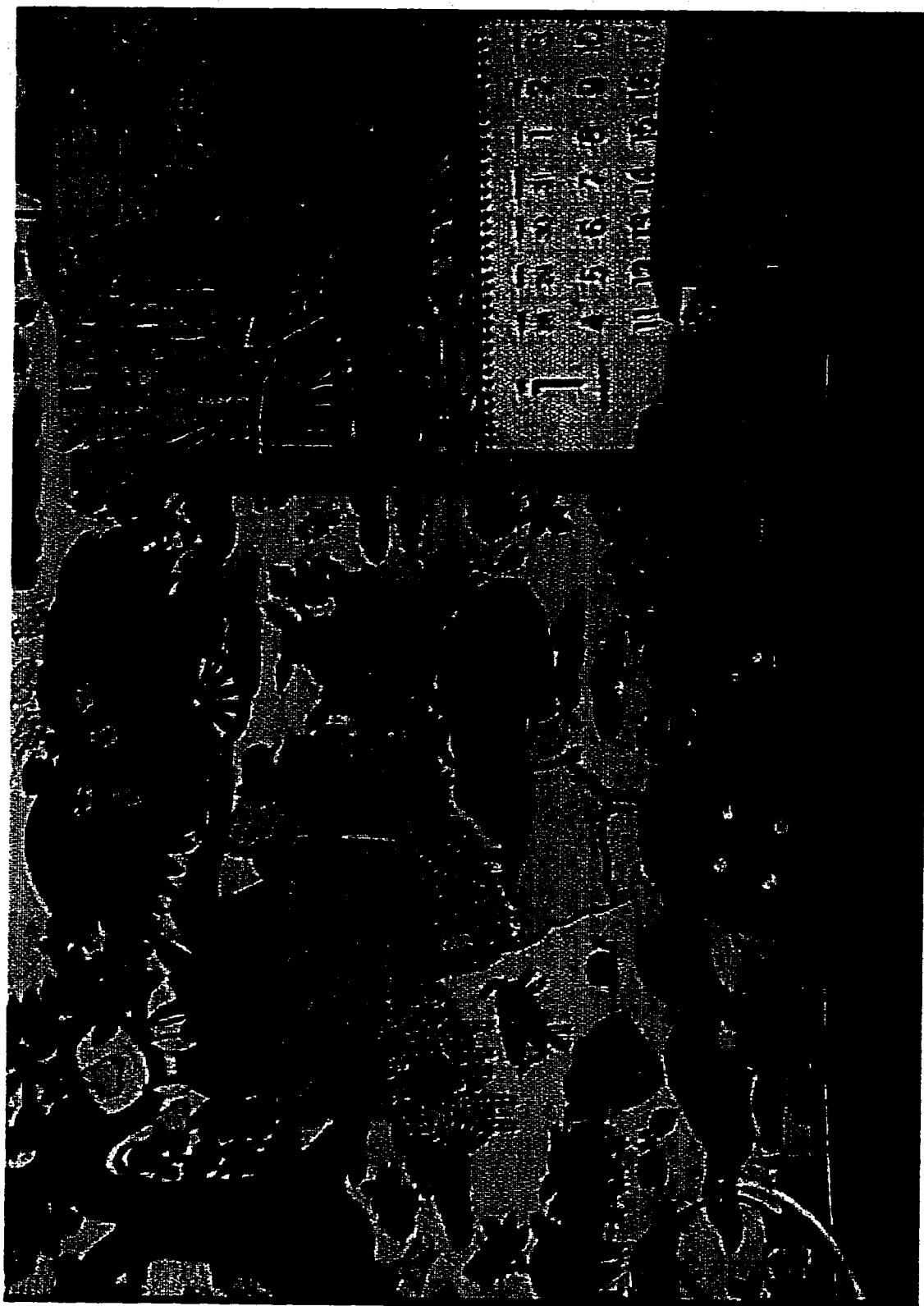**Figure 134. FIR - SVU Precombed and Separated The Train**

Figure 135. FIR - IIR Precombed, Separated and IIR Deinterlaced The Train

Figure 136. FIR - SVU Precombed, Separated and SVU Deinterlaced The Train

7 Conclusions and Possible Future Research Directions

7.1 Conclusion

This thesis has established a new filtering technique, namely State Value Updating, for recursive filtering. By combining SVU with a recursive filter, we have the efficiency of recursive filtering with only a minor phase distortion, the tradeoff being minor spectral leakage.

The SVU technique demonstrated in this thesis is based on the lattice WDF. It uses the steady-state condition as the reset state. The result is that ringing after a step function is suppressed. Although SVU is derived based on preserving the flat area after a step, it has been shown that SVU produces a reasonable filtering result for the common waveforms. To illustrate the practicality of the SVU, tests such as image sampling structure conversions, video deinterlacing, and 3-D Y/C separation were performed.

In Chapter 4, the test results of sampling structure conversion were compared with those generated by FIR and WDF filtered images. The results have shown that SVU filtered image is not as good as WDF with anticausal filtering. However, it is sharper than FIR filtered image and cleaner than WDF.

image is not as good as WDF with anticausal filtering. However, it is sharper than FIR filtered image and cleaner than WDF.

For the deinterlacing test in Chapter 5, the media filter using eleven points motion detector produced the best result. WDF filtered images suffered from serious ringing problem. SVU filtered has less ringing but suffers from minor resolution loss similar to those caused by field repetition, and minor interleaving line effect similar to those caused by field insertion.

For the last test Y/C separation in Chapter 6, we used FIR, SVU and WDF filtering on an FIR filtered composite signal. The Y/C separated signals were also deinterlaced to simulate a complete IDTV receiver. The filtered SVU images were comparable to those generated by FIR filtering, and are much cleaner than those generated by WDF filtering alone.

It has been shown that SVU will produce consistently better quality results than by using WDF alone, because of the reduction of ringing. When the results were compared with other known algorithms, such as the multiple median filtering method described in Chapter 5, SVU does not perform as well. However, due to the simple structure of SVU, it offers a better balance between cost and quality.

7.2   Possible Future Research Directions

The SVU technique is a method of controlling the recursive filter's behavior. There are still some aspects of SVU that have to be explored, such as:

State transition: The SVU technique resets the state of a filter to a steady state when a discontinuity is detected. The sudden change introduces extra high frequency components which lead to aliasing after downsampling. To improve SVU, one can find a better value or a sequence of values to transit to the reset state.

Decision Algorithm: The SVU technique uses a decision algorithm to control as to when to reset the filter's state. The suggested algorithm could handle the deterministic waveforms shown in Chapter 3. For random signals, it may cause too many resets and

may introduce excess high frequency. It may be possible to find a more robust algorithm that will function better under random signal condition.